LAPPEENRANTA-LAHTI UNIVERSITY OF TECHNOLOGY LUT
School of Energy Systems
Degree programme in Electrical engineering

Antti Holopainen

CONTROL OF EXCITATION CURRENT IN A BRUSHLESS SYNCHRONOUS MOTOR STARTED WITH LOAD COMMUTATING INVERTER

Examiners: Professor Pasi Peltoniemi
D.Sc. (Tech.) Markku Niemelä

Supervisor: M.Sc. (Tech.) Olli Liukkonen

ABSTRACT

Lappeenranta-Lahti University of Technology LUT
School of Energy Systems
Degree Programme in Electrical engineering

Antti Holopainen

Control of excitation current in a brushless synchronous motor started with load commutating inverter

Master's thesis
2021
111 pages, 58 figures, 24 tables and 5 appendices

Examiners: Professor Pasi Peltoniemi
D.Sc. (Tech.) Markku Niemelä

Keywords: AC/AC excitation, excitation control, brushless excitation, synchronous motor, asynchronous excitation machine

In this master's thesis, the control of the excitation current of direct online brushless synchronous motor has been studied when the motor is started with load commutating inverter. This thesis includes a general overview from the different starting and magnetization methods that are available for the synchronous motors. The more detailed and profound investigation is conducted to the AC/AC magnetization and different control methods which are used. Different control methods are studied with models build into Simulink® environment and by comparing outcome from the simulation to actual laboratory measurements. Based on the simulation results, control method is chosen and implemented to ACS880 low voltage frequency converter to evaluate the suitability for practical application.

From the literature-based overview, it was discovered that the soft starting with the variable frequency drive causes less strain to the motor and reduces the risk of failure during starting. Such a soft start requires an AC/AC magnetization to be used, which requires antiparallel thyristor or frequency converter supply for the magnetization machine. Simulation results showed that the control, where frequency of the magnetization machine supply could be changed, improves the capability to magnetize the synchronous motor at standstill. The practical part of this thesis was able to verify the results of the simulation. However, the validation also showed that the magnetization machine model is not able to reliably represent the dynamics of the system, especially when fast changes are simulated. As a final result of this thesis, constant frequency and constant slip frequency control methods based on the flux control, were successfully implemented to commercial ACS880 low voltage frequency converter for the purpose of controlling the magnetization current.

TIIVISTELMÄ

Lappeenrannan-Lahden teknillinen yliopisto LUT
School of Energy Systems
Sähkötekniikan koulutusohjelma

Antti Holopainen

Kuormakommutoivalla vaihtosuuntaajalla käynnistetyn tahtimoottorin magnetointivirran säätö

Diplomityö
2021
111 sivua, 58 kuvaa, 24 taulukkoa ja 5 liitettä

Tarkastajat: Professori Pasi Peltoniemi
TkT Markku Niemelä

Hakusanat: AC/AC-magnetointi, magnetoinnin säätö, harjaton magnetointi, tahtimoottori, asynkroninen magnetointikone

Tässä diplomityössä tutkitaan verkkoon liitettävän harjattoman tahtimoottorin AC/AC-magnetointia ja sen säätöä, kun moottori käynnistetään kuormakommutoitua vaihtosuuntaajaa käyttäen. Työssä tutustutaan yleisellä tasolla erilaisiin tahtimoottorin käynnistys- ja magnetointimenetelmiin. Työssä syvennytään AC/AC-magnetointiin ja eri säätötapoihin, joita voidaan käyttää magnetoinnin säädössä. Eri säätömenetelmiä tutkitaan Simulink®-ympäristöön luoduilla malleilla, sekä tutkitaan mallien toimivuutta vertaamalla tuloksia käytännön mittauksiin. Työssä rakennetaan simulaation tulosten perusteella säätö ACS880-pienjännitetaajuusmuuttajalle ja tutkitaan niiden soveltuvuutta käytännön sovellukseen.

Kirjallisuuteen perustuvan yleiskatsauksen perusteella huomattiin, että pehmokäynnistys taajuusmuuttajalla aiheuttaa moottorille vähemmän rasitusta ja pienentää käynnistyksen epäonnistumisen riskiä. Tällainen pehmokäynnistys vaatii kuitenkin AC/AC-magnetoinnin, mikä vaatii vastarinnankytketyn tyristorisillan tai taajuusmuuttajan syöttämään magnetointikonetta. Simuloinnin perusteella todettiin, että magnetoinnin säätö, missä magnetointikoneen syöttötaajuutta voidaan muuttaa, parantaa järjestelmän kykyä magnetoida tahtimoottoria nollanopeudella. Käytännön toteutuksessa simulaation tulokset pystyttiin todentamaan luotettaviksi. Kuitenkin simulointimallia todennettaessa päädyttiin lopputulokseen, ettei simulointimalli kykene esittämään järjestelmän dynamiikkaa luotettavasti, etenkään nopeissa muutoksissa. Työn lopputuloksena pystyttiin esittämään vuosäätön perustuvat vakiotaajuus- ja vakiojättämätaajuusmenetelmät, jotka voidaan toteuttaa kaupallisessa ACS880-pienjännitetaajuusmuuttajassa magnetointivirran säätämiseksi.

ACKNOWLEDGEMENTS

This thesis was done in collaboration with ABB Oy. I would like to thank M.Sc. (Tech.) Pekka Ketola for giving me this interesting and challenging topic. During this thesis, ABB experts from various fields provided me valuable information and I am grateful to them for that.

I would like to thank my supervisor M.Sc. (Tech.) Olli Liukkonen for guidance and feedback during this thesis. His advice, alternative perspectives, and corrections were valuable during this project. I would also like to thank the examiners Professor Pasi Peltoniemi and D.Sc. (Tech.) Markku Niemelä for their interest towards this topic as well as for their valuable comments and advice. I am also grateful for the help I received from the laboratory staff.

Especially I want to thank my family and friends who have been supporting and helping me during these past five years.

Lappeenranta, 15.07.2021
Antti Holopainen

TABLE OF CONTENT

1. INTRODUCTION 5

1.1. The objectives and outline of this thesis 6

1.2. Structure of the thesis 6

2. DIRECT ONLINE SYNCHRONOUS MOTOR 7

2.1. Field current and control of direct online synchronous motor 7

2.1.1. P/Q diagram 10

2.2. Starting methods for brushless synchronous motor 11

2.2.1. Direct online starting of brushless synchronous machine 13

2.2.2. Soft starting for the DOL synchronous motor 15

2.3. Dynamics of the field winding 18

2.4. Field-winding current supply methods for direct online machine 19

2.4.1. The static excitation 20

2.4.2. Brushless excitation 21

2.5. Standards and requirements related to the excitation systems. 23

3. CONTROL OF THE BRUSHLESS ASYNCHRONOUS EXCITER 26

3.1. Calculation of field current reference 27

3.1.1. Load commutating inverter 27

3.1.2. Automatic voltage regulator 28

3.2. Anti-parallel thyristor bridge 30

3.3. Variable frequency drive 35

3.3.1. Current control with constant frequency 36

3.3.2. Current control with constant slip frequency 37

3.3.3. Flux control with constant frequency 39

3.3.4. Slip control 41

3.4. Hardware limitations that control designer must take account 42

4. SIMULATION AND PERFORMANCE EVALUATION 44

4.1. Overview of the asynchronous excitation machine model 44

4.1.1. Per-unit values 46

4.2. Antiparallel thyristor supply model 47

4.3. Frequency converter models 50

4.3.1. Control unit with constant supply or slip frequency 51

4.3.2. Control unit with slip control 55

4.4. Simulation cases and results 56
4.4.1. Step response test *57*
4.4.2. Accuracy test *62*
4.4.3. Summary from the simulations *71*
5. MEASUREMENTS, RESULTS AND ANALYSIS 72
5.1. Test equipment and environment 72
5.1.1. Drive application programming (IEC 61131-3) *75*
5.2. Model verification 76
5.2.1. Verification of the asynchronous exciter model *76*
5.2.2. Verification with the frequency converter model *80*
5.3. Implementation of control methods with ACS880 84
5.3.1. Parameterization of ACS880 ..... *86*
5.4. Algorithm testing, results and analysis 88
5.4.1. Step response test: Flux control with constant frequency *89*
5.4.2. Accuracy test: Flux control with constant frequency *94*
5.4.3. Accuracy test: Flux and constant slip frequency control *100*
5.4.4. Summary from algorithm testing *105*
6. SUMMARY AND FINAL CONCLUSION 106
REFERENCES 107
APPENDICES

LIST OF SYMBOLS AND ABBREVIATIONS

Acronyms

AC	alternating current
ANSI	American National Standards Institute
API	American Petroleum Institute
DC	direct current
DIO	digital input/output
DEPs	Design and Engineering Practices
DOL	direct online
emf	electromotive force
IEC	International Electrotechnical Commission
LCI	load commutating inverter
NEMA	National Electrical Manufacturers Association
PI	Proportional-Integral controller
PLC	Programmable Logic Controller
VFD	variable frequency drive

Roman variables

E	electromagnetic force
U	voltage
I	current
I^*	current reference
L	inductance
P	real power
P	Proportional gain
I	Integrator
p	pole pair number
Q	reactive power

R	resistance

Greek variables

α	firing angle
α^*	firing angle reference
δ	load angle
φ	phase angle
φ^*	phase angle reference
τ'	transient time constant
ψ	flux linkage
$\boldsymbol{\psi}$	flux linkage vector
ψ^*	flux linkage reference

Subscripts

a	armature
act	actual
d	direct axis
df	mutual inductance between stator d-axis and field winding
d0	Open circuit
f	field winding
md	direct magnetizing inductance
meas	measured
q	quadrature-axis
r	rotor
s	stator

1. INTRODUCTION

Direct online synchronous motors and generators have been used in the industrial sectors for a long time. The field wound synchronous motor has been the most used machine type in the specialised high power motor applications. The excitation systems for synchronous machines have been studied a lot in the past 70 years and many topologies and methods have been proposed in the scientific community during these years. Due the development of power electronics and transitioning from analogue controllers to digital control technologies, brushless excitation systems have been developing a lot in these years due need of reliable excitation systems. (Nøland et al. 2018)

The development of variable frequency drives has been rapid and variable frequency drives can now be found from many applications where they have not been traditionally used. The study of synchronous motors and variable speed drives has mainly focused on the control and supply methods on the stator side of the synchronous motor. When large brushless direct online synchronous motors are used, the variable frequency drives can be found to assist in the starting of the synchronous machine. The use of frequency converter for the starting presents an additional requirement that asynchronous exciter machine and AC supply for the excitation machine should be used.

Currently the most widely used technology for the supply of asynchronous exciter in the brushless variable frequency drives has been antiparallel thyristor bridge. The use of frequency converter as a supply for the asynchronous exciter machine has not been studied extensively.

The possibility to use frequency converter as a supply for the asynchronous excitation machine is studied in this thesis. In this thesis the antiparallel thyristor bridge and frequency converter supply are studied in comparative manner to find out the main differences between the two. This study also includes an overview of different control methods that are developed for the frequency converter in earlier studies. The different control methods are studied using simulation models, as well as laboratory measurements.

1.1. The objectives and outline of this thesis

The aim of this thesis is to find and present a stable and dynamically sufficient control algorithm for the frequency converter supplying an asynchronous exciter so that it meets the key requirements of the industry. The second objective for this thesis is to find a way to implement and verify the algorithm with ABB ACS880 frequency converter. The framework for this thesis is large direct online synchronous motors over 1 MW, which are started with the help of load commutating inverter.

1.2. Structure of the thesis

The second chapter of this thesis is dedicated to short introduction into topic of control and starting of direct online synchronous motors. Chapter also investigates the magnetization systems which supply the field winding of the wound rotor synchronous motors and standards related to synchronous motors and the brushless excitation systems.

Chapter three takes a more detailed look into the excitation system which contains an asynchronous exciter with a three-phase converter. The differences between the antiparallel thyristor bridge and frequency converter supply are discussed and based on the literature some control algorithms that could be used with the frequency converter are introduced.

Fourth chapter is dedicated to the simulation of different algorithms used in frequency converter supply. The antiparallel thyristor bridge is used as the base for the performance comparison.

The chapter five contains the implementation of the control algorithm to the ACS880 and description of the measurement setup which is used to verify the algorithm.

Chapter six is dedicated to summary of this thesis with conclusions and thoughts about the future work and research that could be done related to topic of this thesis.

2. DIRECT ONLINE SYNCHRONOUS MOTOR

The wound rotor synchronous machines are traditional machine type used in the high-power applications where rotational speeds have been relatively low. The reason behind the popularity of synchronous machines in these applications is that synchronous machines pose five key qualities:

1. High efficiency
2. High reliability & robustness
3. High temporary overload capability
4. Rotational speed is dependent from the load torque
5. Ability to take a part into reactive power regulation in the grid

In this chapter the main principles related to the control of the direct online synchronous motors are discussed. The topic of this thesis is heavily linked to the starting of the synchronous motors which is the reason why the brief introduction to the different starting methods is also addressed. Final two sections of this chapter are dedicated to the different excitation methods and standards related to excitation systems and especially the control of excitation. As for the clarity, whenever the synchronous machine is mentioned in this thesis the salient pole synchronous machine is addressed unless otherwise specified.

2.1. Field current and control of direct online synchronous motor

The basis of understanding the principle of the operation and control of the synchronous machines relies on the understanding the vector diagram of synchronous machine in either motoring or generating operation. In the scope of this thesis the vector diagram of the synchronous motor is presented and discussed. The vector diagram can be seen from the figure 2.1. In the next discussion about the vector diagram and the operation principle of the direct online (DOL) synchronous motor, the steady state operation is assumed, to keep the discussion clear and simple. If the transient situations during operation are to be included in the discussion the effect of the damper windings should be added into the vector diagram and the discussion becomes a bit more complicated.

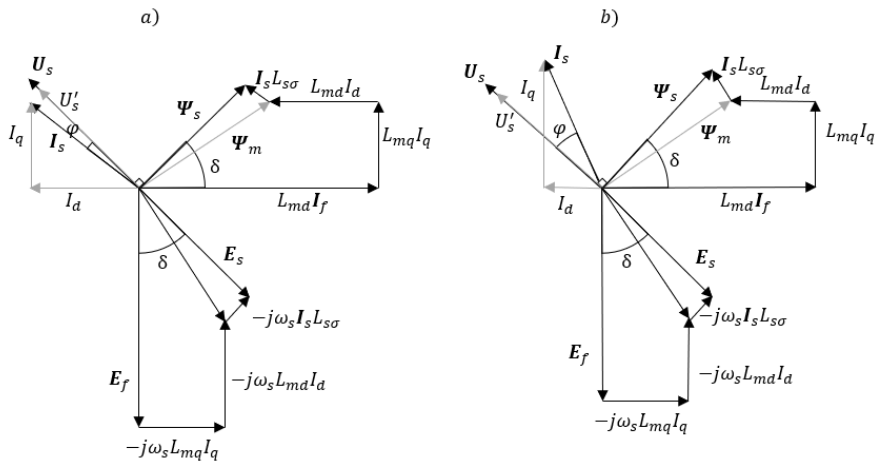

Figure 2.1 Simplified vector diagram from synchronous motor. The diagram a) illustrates motor in the state of over-excitation b) illustrates the motor in the state of under-excitation.

The length of the stator voltage vector $\boldsymbol{U}_s$ of the synchronous motor is fixed to the voltage of the grid which supplies the motor and could be treated as constant in this discussion, because of the steady state. From the stator voltage vector, the vector for the stator flux linkage is integrated $\boldsymbol{\psi}_s$. The relation between stator voltage and stator flux linkage means that the stator flux linkage must also stay constant if the grid voltage stays constant and angle between these two vectors can be treated as constant 90 degrees.

The control of the synchronous motor relies on the control of field winding current $\boldsymbol{I}_f$ in the direct online applications. When the current at the field winding increases or decreases the stator flux linkage stays constant. This means that the relation between direct axis I_d and quadrature axis I_q components of the stator current must alter to compensate the effect of change in $\boldsymbol{\psi}_f$. This rearrangement in the current components changes the phase angle φ between the current $\boldsymbol{I}_s$ and voltage $\boldsymbol{U}_s$. The changes in the phase angle φ between the phase current and stator voltage changes the power factor of the machine.

If the real power is kept constant the increase in the $\boldsymbol{I}_f$ will either reduce or increase the length of the $\boldsymbol{I}_s$ depending on the state of excitation inside the machine. Which is the situation in the motor application where the load stays constant and motor is connected into the rigid network. This relation between the stator current and field winding current is commonly presented with V-curve plot which is illustrated in figure 2.2. When unity power factor is

kept, the stator current gets its lowest value. If the field current is decreased the machine enters the state of under-excitation and if it is increased the machine enters the state of over-excitation, each of these cases leads into situation where motor draws more current from the supplying network. Hence the name V-curve plot.

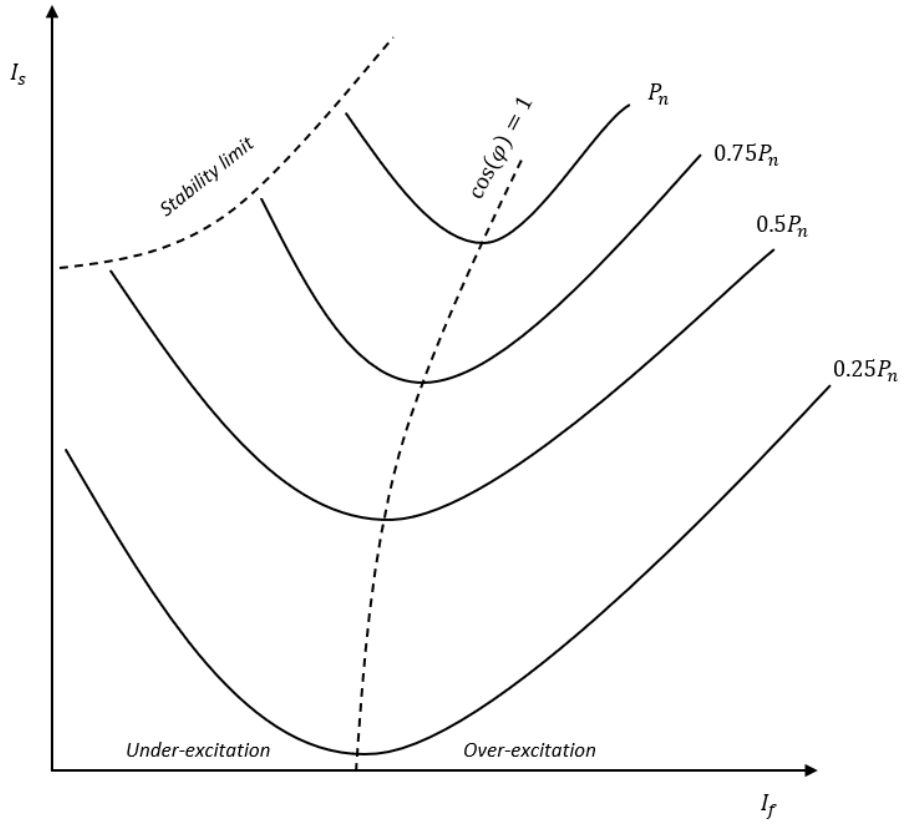

Figure 2.2 Illustrative presentation of the V-curves that would be determined for the synchronous machine. These curves are also called load curves in literature. The relation between the field current and stator current of the synchronous machine are illustrated with different power levels, the same curves could also be presented with different torque levels.

The change in the field winding current also affects into the torque production capability of the synchronous motor. The torque change comes from the change in the load angle δ between magnetomotive forces produced by the stator $\boldsymbol{E}_s$ and field winding $\boldsymbol{E}_f$ or from the perspective of the flux linkage vectors between $\boldsymbol{\psi}_s$ and $\boldsymbol{\psi}_f$. The load angle is at its highest at the state of under-excitation and lowest at the over-excitation if the load torque is constant. When the loading at the shaft of the synchronous motor increases the load angle also increases. To compensate the increase in the load angle, the field winding current should be increased. The maximum torque and power can be achieved when the load angle is near but

below 90 degrees in the salient pole synchronous motors (Pyrhönen et al. 2014). The machine loses its synchronism if the torque required by the load is more than pull out torque of the motor because the load angle increases further than 90 degrees. When synchronism is lost the rotor starts slowing down and oscillating which causes lots of vibration to the whole motor and could potentially damage the motor.

2.1.1. P/Q diagram

From the control engineering point of view, it is necessity to know the different excitation states and physical limitations of the machine which give the boundaries for the operation. A usual way to present the conditions and limitations at continuous operation for the direct online synchronous machine is to draw P/Q diagram presented in the figure 2.3. P/Q diagram illustrates the different operational points of the synchronous machine in the context of power flow between the supplying grid and the motor, with the physical boundaries which limit the operation of the machine. The international standards such as IEC 60034-3 requires that the manufacturer shall provide P/Q diagram which shows the limits of operation. The same diagram can either be used to describe generator or motor with only difference in the sign of real power.

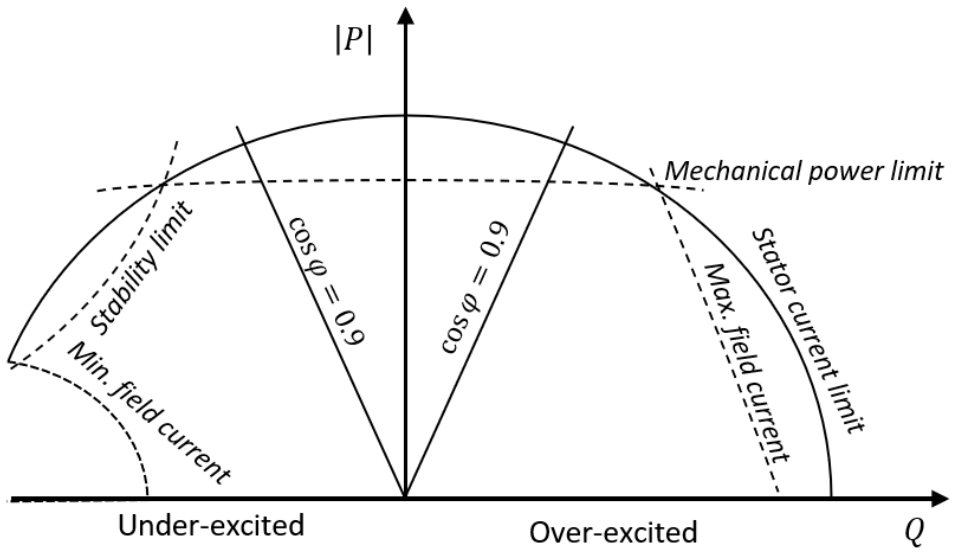

Figure 2.3 P/Q diagram of the synchronous machine, with the physical limitations which create the boundaries for the continuous operation of the machine. Stator and maximum field current limits protect the windings from overheating. The mechanical power limit is not always presented for synchronous motors. (Arnsten et al. 2018; Pyrhönen et al. 2016; Ilic et al. 2011)

At the unity power factor, the grid only supplies real power *P* to the motor from the grid. The motor looks like a resistive load from the grid point of view. The limiting factor which affects the loading capability of the synchronous motor at the unity power factor, are either the stator current or the mechanical power limit of the load. Mechanical power limit can be higher than the stator current limit in motoring applications.

Operating at the region of over-excitation means that the motor takes real power from the grid and supplies reactive power *Q* to grid. The real power supplied to the machine is still limited by the load or the stator current, but the amount of the reactive power motor can supply to the grid is limited by the current limit of the field winding. In the over-excited region, the motor looks like a capacitive load from the perspective of the grid.

When the machine is operated at the region of under-excitation the machine is supplied with both real and reactive power. The real power supplied to the machine is still limited by the load or the stator current, the amount of the reactive power which motor can draw from the network is limited by the minimum amount of field winding current required to keep the machine stable. In the under-excited region, the motor looks like an inductive load from the perspective of the grid. This unique characteristic of the machine appearing as different load, enables synchronous motors to be used in reactive power compensation of the grid of industrial plant if necessary.

2.2. Starting methods for brushless synchronous motor

The synchronous motor can be started with multiple different ways depending on the requirements given by the application, environment, and the grid which the synchronous motor is connected. The process of selecting the right starting method has many steps and different factors should be taken into account. Ristanovic et al. (2020) have summarised these in the six different factors:

1. Grid characteristics and the effect of starting motor to the supplying bus
2. Starting and breakdown torque characteristics of the synchronous motor
3. Torque characteristics of the load
4. Operating speed range of the load
5. Process which motor is part of

6. Cost and complexity

The starting method that will be chosen after carefully considering the factors above will eventually reveal the most suitable method to be chosen from the starting methods that are listed and illustrated in figure 2.4 below:

a) Direct online starting
b) Auto transformer starting
c) Reactor starting
d) Switched capacitor starting
e) Soft starter or variable frequency drive
f) With auxiliary starter motor

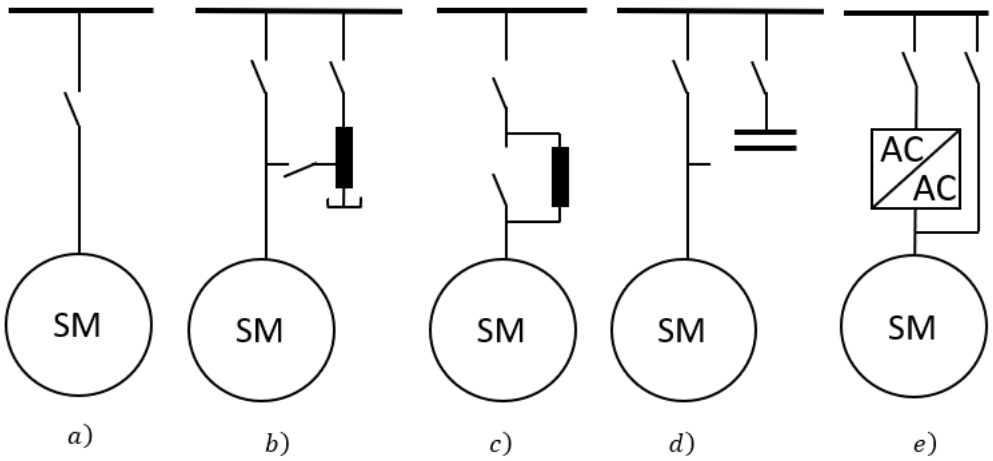

Figure 2.4 Single line diagram from different starting methods used with direct online synchronous motors a) Direct online b) Autotransformer c) Reactor starting d) Capacitor start e) soft start with traditional soft starter.

The direct online starting and other starting methods that have been introduced to reduce unwanted behaviour during start-up are discussed in the next two sections. The soft starting method, where both voltage and frequency can be adjusted, is introduced in the paragraph 2.2.2.

2.2.1. Direct online starting of brushless synchronous machine

In the direct online applications, each synchronous motor has been equipped with a damper winding at the surface of the rotor pole shoes which are shorted together with endplate. The main function of these dampers is to damp the effect of fluctuating rotational speeds when the load produces pulsating torques and counter react to the fast-transient phenomena that could happen in the power supply (Pyrhönen et al. 2014). When synchronous motor is started direct online, the damper windings act like a squirrel cage in asynchronous motor and enables the starting of the machine. The phenomenon resembles the starting of the asynchronous machine. The inrush current which is drawn from the network could be as large as 3.8-7.1 times the nominal current, depending on the size of the machine and the total reactance of the series connection with the motor and network (Nevelsteen & Argon 1989). Engineering guidelines from different companies such as Shell (2007) define the amount of inrush current which is allowed during asynchronous start at their facilities. Shell (2007) for example defines that inrush current cannot be over 6.5 times the rated current of the motor.

During start up the field winding of the machine should be shorted. If the field winding is supplied during the start up, it produces magnetic flux that opposes the stator and produces torque that would prevent the starting (Aura & Tonteri 1986). The starting torque of synchronous motor can be adjusted with the resistance which the field winding has been shorted to, but generally it should be as small as possible. The current is supplied to the field winding after the motor has been accelerated to the slip value which is around 5%.

In the brushless synchronous machines, one way to short the rotor circuit is to add special circuit to the shaft of the machine presented in the figure 2.5. This circuit shorts the rotor circuit through starting resistor during start up and protects the diode bridge supplying the field winding. Circuit contains traditionally three thyristors which are controlled with special control circuits which monitor the positive and negative half cycles of the induced voltage to the rotor during start up. When rotor circuit experiences the positive half cycle the thyristors 1, 2 and 3 are not conducting and the current flows through the starting resistor and diode bridge. During the negative half cycle the diodes must be protected, thyristors 1 and 2 start to conduct to redirect the negative current flow away from the diode bridge. When the synchronous machine has been accelerated almost to the synchronous speed the thyristor

1 starts to conduct to bypass the starting resistor before the excitation current is started to supply. (Tervaskanto 2018)

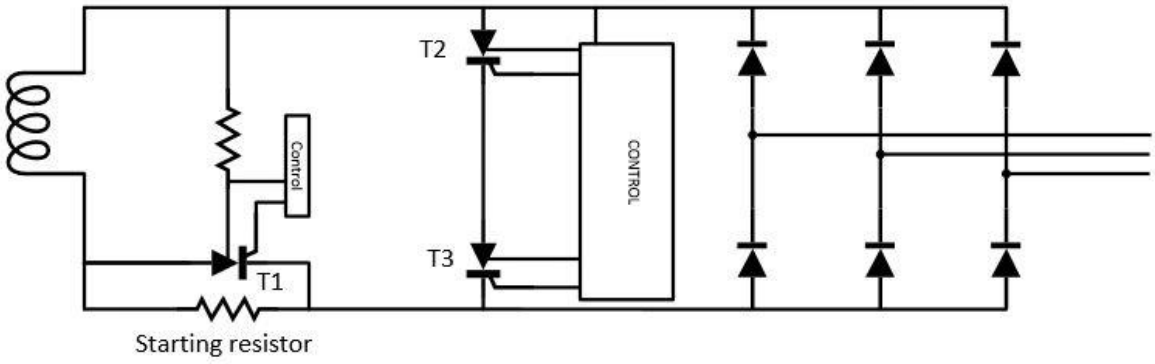

Figure 2.5 Illustrative presentation from the rotor circuit which contain thyristors to protect the diode bridge during direct online starting of synchronous motor.

The direct online starting is relatively easy and cost-effective way to start the synchronous motors because it does not need much of additional and costly components as for example start with an auxiliary motor would need as LeDoux et al. (2015) have found comparing different starting methods. The direct online method still has some drawbacks. There are two major drawbacks that would make it unusable for many applications where especially large synchronous motors are used. The first problem comes with the network where the machine will be connected. When the motor is connected into the grid, it introduces a large inductive load to the network which could cause voltage to drop significantly if the network is not rigid enough. Direct online start requires a lot of reactive power from the grid. If the short circuit capacity of the network is not sufficient, voltage in the grid and motor terminals will drop. This voltage drop could be significant enough that it violates the grid codes causing unwanted behaviour in the network such as flickering of lights or disturbs the operation of other devices connected to the same point of common coupling (LeDoux et al. 2015). In the worst-case scenario, the whole grid inside the facility could collapse and cause significant cost for the process owner as Ritter et al. (2007) explained based on observations taken from refinery where large motors were started directly online. To define when the grid could be classified as rigid, one can say that if the available short-circuit power is approximately 10 times the power of the motor, the grid can be assumed to be rigid (Pyrhönen et al. 2016).

The amount of inrush current and voltage drop during the start-up can be limited with certain methods. Such methods are the autotransformer, reactor and capacitor starting where extra components need to be connected to the supply side of the motor (Ristanovic et al. 2020; Aura & Tonteri 1986). After the synchronous speed has been reached the added components would be bypassed. The drawback in these methods is that because of the voltage drop has been reduced the starting torque has also been reduced by the square of the voltage reduced (Nevelsteen & Argon 1989). The starting capacitor is little different and is used for correcting the power factor of the supplying bus and support weak network during start (Nevelsteen & Argon 1989; LeDoux et al. 2015). Other methods introduced are not capable of supporting already weak network which means that other means like auxiliary motor or variable frequency drive start should be considered (Nevelsteen & Argon 1989).

The second problem related to the direct online starting of a synchronous motor is that it causes oscillating torques during start-up and thermal stresses. Oscillating torques introduce lots of mechanical stress to the motor. The thermal and mechanical stress to the damper windings, especially in the brazed joint between the endplate and damper bars is the concern (Barry & Hamidi 2015). Thermal stresses can lead into the cracking and breaking of the damper bars if the motor must be started multiple times and the time between consecutive starts is not sufficient to let the bars to cool down properly as Barry & Hamdi (2015) have been concluded in their study. This is especially concerning problem with large motors which are driving loads where the moment of inertia and breakaway torques are high. High level of inertia in the system leads into slower acceleration times, which increases the thermal stress that motor must endure. It is also studied that in the situation where start has been interrupted suddenly the insulation of the motor can be damaged by the overvoltage if proper measures of protection has not been used (Eichenberg et al. 1998). The significant time which is needed to let the rotor cool down means that the starting and synchronization should not fail multiple times because extra down time costs lots of money in lost production volumes (Ritter et al. 2007).

2.2.2. Soft starting for the DOL synchronous motor

As mentioned earlier if the network in the facility is too weak to endure direct online starting of the synchronous motor other means should be considered for example soft starting with

variable frequency drive. The term variable frequency drive (VFD) start contains both, starting with load commuted inverter (LCI) or with the ordinary voltage source inverter. This VFD method could be referred as a soft start for the synchronous motor although it can control both the voltage and frequency rather than just the voltage like traditional soft starters where reduced voltage is supplied with the grid frequency. It is also good to remember that the soft starting requirement could also come from the load if it cannot handle high torsional stresses or should not be accelerated too fast to name few possible reasons. (Nevelsteen & Argon 1989).

In case of soft starting with variable frequency drive, the synchronous machine is driven from zero to its nominal speed, synchronised to the frequency converter supply. After the synchronous motor has been accelerated into its nominal speed it is synchronised to the utility grid and VFD is then bypassed. VFD starting can utilize the general control principle of electrical machines. More commonly referred as a voltage-hertz control where stator flux of the machine is kept constant by fixing the ratio between voltage and frequency. In this soft starting method, the field winding of the machine should be energised right from the beginning at the zero speed. In case of brushless excitation system alternating current is fed to the excitation machine which is equipped with three phase winding at its stator to supply three phase winding in synchronous machine shaft which is connected to the rotating rectifier unit as presented in figure 2.8.

During starting, the voltage and frequency are increased gradually which means that the magnetic field of the stator and rotor are always rotating synchronously. Currents are not induced to the damper windings and the problems discussed at section 2.2.1 are eliminated. The reduced stress also increases the lifetime expectancy of the motor and other components in the system (Ritter et al. 2007). The soft start system has obvious benefits compared to the direct online starting but this system is rather complex and introduces lots of new components to the system which increases the total cost of the system (LeDoux et al. 2015).

The VFD soft start method enables nominal torque from the start and more controlled manner of starting for the motor, at the zero speed. The stator current of the motor is determined by the necessary load torque and stays constant during the acceleration if the loading and ratio between voltage and frequency stays constant. The slope of the ramp or the shape of the curve which is used to control the motor can be altered to be specifically

suited for different kind of loads for example IR compensated curve can be used with loads that need high torque from the start and quadratic voltage curves could be used in the blower applications (Pyrhönen et al. 2016). In the direct online methods, the slope of the ramp for the acceleration cannot be controlled it is entirely dependent on the load and the designed parameters of the synchronous motor and network.

If the industrial facility has multiple direct online synchronous machines, the same VFD can be used to accelerate one motor at the time to the network (Ritter et al. 2007). Figure 2.6 presents a network topology where multiple direct online motors are connected to the network and one converter is used to accelerate each of them. When the synchronous motor reaches the synchronous speed, the supply from the converter needs to be bypassed and grid connection should be established after the synchronization. There are two ways of doing that as presented in the ABB (2017) engineering guidelines:

- Close-before-open method where supply to the grid is established by closing motor breaker 1 of the figure 2.6. Before the VFD supply is to be disconnected by opening breaker 2 from the VFD supply.
- Open-before-close other method where VFD supply is disconnected before the connection to the grid has been established.

The preferred method for the bypassing is the close-before-open because the open-before-close method causes speed and voltage drop together with difference of phase angle between machine terminals and network. Which increases the risk of failure in the starting and synchronization.

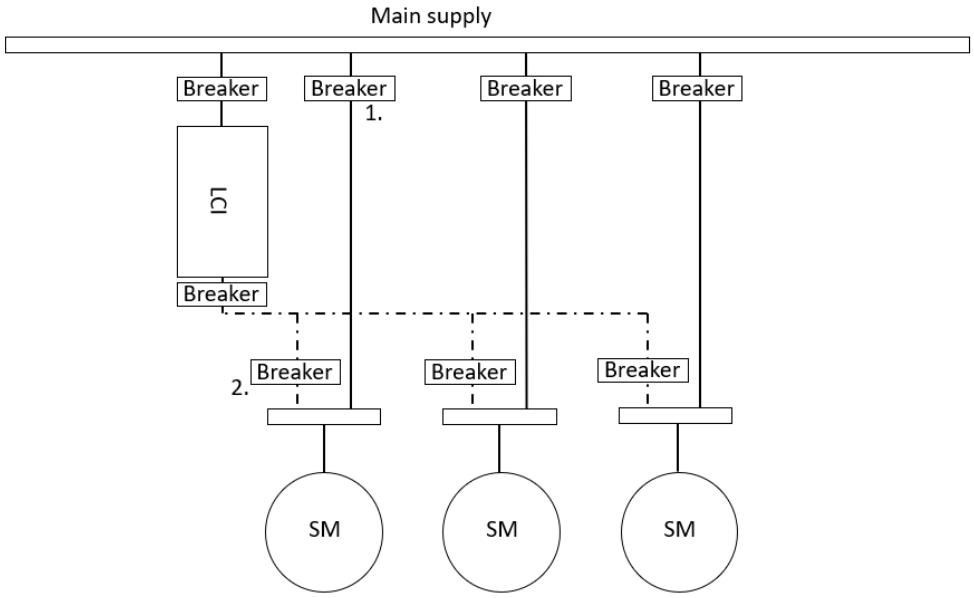

Figure 2.6 Illustrative figure from the LCI soft start system with multiple DOL synchronous machines and breakers to bypass the LCI supply.

2.3. Dynamics of the field winding

The field winding of the synchronous machine and the stator winding together create the magnetic flux to the air gap of the machine as described in section 2.1. The excitation method used in the synchronous machine drive has a significant impact to the stability and dynamical performance of the drive system. The one common nominator between all the excitation systems in direct online applications is that the magnetic state of the synchronous machine cannot be changed faster than the time constant of the field winding. The time constant which is used to describe the change in the field winding current at no load is the d-axis open circuited time constant τ'_{d0}. The field winding can be described in its simplest form as a common *RL* circuit which yields a dynamic performance of first order system. The time constant is produced as a ratio between inductance L_{f} and resistance R_{f} of the field winding is presented in the equation 2.1 (Nøland et al. 2018; Platero et al. 2015).

$$\tau'_{\mathrm{d0}} = \frac{L_{\mathrm{f}}}{R_{\mathrm{f}}} \tag{2.1}$$

When the machine is loaded the time constant changes and can be described with time constant τ'_f which is the rotor time constant during loading (Platero et al. 2015). The damper

windings of the synchronous machine have an effect only at the subtransient situations. From this expression the effect of the damper winding can be neglected because the subtransient situations are happening in smaller time frames (Nøland et al. 2018; Pyrhönen et al. 2016). The time constant can be solved using equation 2.2 where the effect of the direct-axis stator inductance L_{d} and mutual inductance L_{df} between the stator winding and field winding is subtracted from the L_{f}. The mutual inductance is in the practice direct-axis magnetizing inductance L_{md} when mutual inductance between field winding and damper winding has been neglected which could be described with Canay inductance (Pyrhönen et al. 2016; Luomi 1982).

$$\tau'_{\mathrm{f}} = \frac{L_{\mathrm{f}} - \frac{{L_{\mathrm{df}}}^2}{L_{\mathrm{d}}}}{R_{\mathrm{f}}} = \frac{L_{\mathrm{f}} - \frac{L_{\mathrm{md}}^2}{L_{\mathrm{d}}}}{R_{\mathrm{f}}} \tag{2.2}$$

The response time that field winding has for the step like increase of the voltage is dependent to the available ceiling voltage according to Nøland et al. (2018) and Pyrhönen et al. (2016). Ceiling voltage has been defined by IEC 60034-16-1 (2011) as a maximum direct voltage that the excitation system can supply at certain conditions for example no-load and under load. Visualization from the effect of available ceiling voltage to the time constant can be found from Nøland et al. (2018).

2.4. Field-winding current supply methods for direct online machine

There are numerous excitation methods that have been introduced, studied and presented in the literature such as Pyrhönen et al. (2016) and scientific articles like Nøland et al. (2018, 2019), for the purpose of supplying the necessary DC current to the field winding of the wound rotor synchronous machine. The excitation systems used in the direct online applications can be divided in to three main categories which are:

- Static excitation
- Brushless excitation
- Harmonic excitation

In this paragraph a brief introduction from different excitation methods is given before the control of the asynchronous excitation system is introduced in more detailed manner in

chapter 3. The harmonic excitation systems have been studied a lot recently and many topologies have been introduced in literature and journals (Nøland et al. 2018, 2019). These topologies unfortunately are not worth of discussion in the framework of this thesis. The static and brushless excitation systems are the main systems used in the industry today and that is why these two are introduced and compared in the framework of this thesis.

2.4.1. The static excitation

The static excitation system consists of a static controllable rectifier circuit which rectifies the ac supply from the grid supplying the excitation unit of producing correct amount of direct current that needs to be supplied to the field winding of the synchronous machine, while it is operated. The supply is arranged via brushes and slip rings as illustrated in the figure 2.7. The capability to keep the field winding energized at zero speed makes it well suited for both direct online and VFD drives. Static excitation topologies are commonly used in applications which have more demanding requirements for the dynamical performance of the drive system (Nøland et al. 2018; Pyrhönen et al. 2014). Such demanding applications are for example hot rolling mills and hoists.

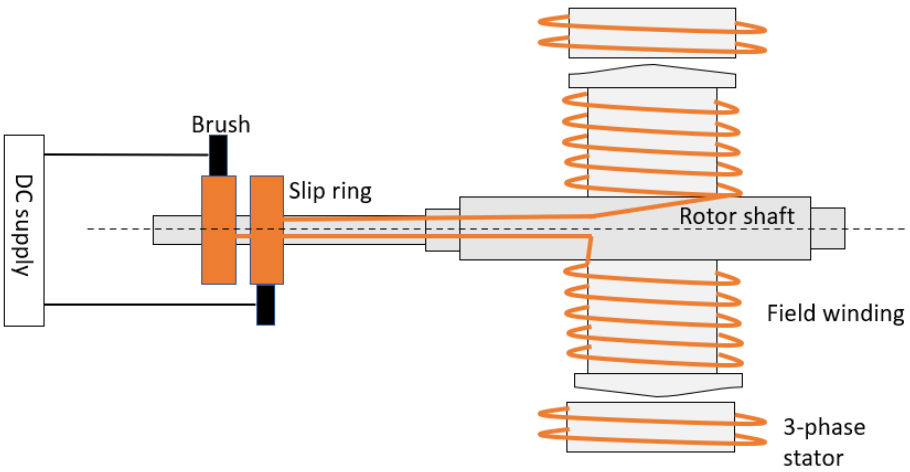

Figure 2.7 Field current supply of synchronous machine with brushes and slip rings.

The benefit of the static excitation system is that it allows direct monitoring and measuring of the parameters I_f, R_f and L_f of the synchronous motor, which in turn helps to control the

whole system. The fast response is achieved by capability to supply higher voltages that force the step response of excitation current without any extra time constants in the system in addition to the field winding time constant. There is also possibility to supply negative current to the rotor circuit which improves the de-excitation capabilities (Nøland et al. 2018). The de-excitation capabilities are specially in the point of interest at generator applications.

Static excitation systems have also some drawbacks. This system requires regular maintenance because of the brushes and slip rings, which wear down during operation. This has an effect to the reliability of the system which limits the usage of this system at certain applications where reliability is one of the key requirements when choosing a drive system for example marine drives. The static excitation systems are not for example allowed in some applications where sparking is not allowed based on ATEX and IECEx certifications which are required. Static excitation requires also more power than brushless excitation because all the power to the field winding should be supplied by excitation unit (Tervaskanto 2018).

2.4.2. Brushless excitation

Brushless excitation systems have been traditionally used in applications where the loading profile is continuous, and reliability of the excitation system is important (Nøland et al. 2018; Pyrhönen et al. 2014). Brushless excitation system does not have brushes or slip rings to supply the field winding. The machine is more maintenance free and the risk of sparking is reduced considerably. Without brushes and slip rings the excitation current must be supplied through electromagnetic energy conversion. One common aspect for all brushless excitation systems is that rotor faces alternating flux that creates an alternating current opposite to change in flux linkage to the rotor circuit. The direct current is created and supplied to the field winding of the synchronous machine through rotating rectifier unit which is mounted to the same shaft as the field winding. There is different methods that are introduced and used in the brushless excitation systems two are illustration is presented in figure 2.8. The exciter machines can be summarised into three categories:

- Outer pole synchronous exciters
- Rotating brushless permanent magnet exciters
- Three-phase wound-rotor, wound-stator exciters

The traditional outer pole synchronous exciters have DC winding at the stator side of the excitation machine and polyphase winding at the rotor side which is connected to the rotating rectifier. The stator side can be supplied with same kind of system which is used in the static systems where DC has been created with thyristor bridge. The power rating of the supply unit can be reduced because this kind of excitation system takes most of the energy needed from the rotational energy of the synchronous machine which means that less ampers needs to be supplied to the stator side of the exciter (Tervaskanto 2018). The outer pole excitation systems are simple and traditionally used in the high-power generators and direct online applications (Pyrhönen et al. 2016; Nøland et al. 2019). This system is not capable of supplying the field winding at zero speed, because it needs the rotor to rotate to induce voltage and current to the field winding.

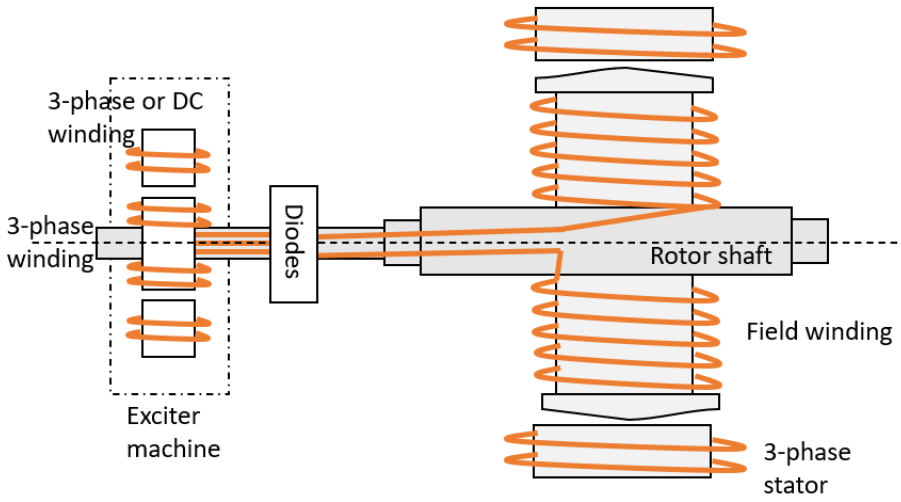

Figure 2.8 Brushless excitation supply for the synchronous machine with DC/AC or AC/AC excitation machine.

In variable frequency drives the excitation system must be able to supply current to the field winding at the zero speed. Because of that variable frequency drives utilize asynchronous exciters where stator and rotor side are made of poly phase windings. Asynchronous exciter can be described to be fundamentally like rotating transformer where the secondary side is connected into diode rectifier (Nøland et al. 2019; Kjaer et al. 2005). Common solution to supply AC in the stator side of the asynchronous exciter is to use anti-parallel thyristor bridge

but it could be also fed with frequency converter. The main idea behind feeding the field winding through the asynchronous exciter is that it allows the energization of field winding at zero speed and makes brushless synchronous machines viable option for frequency converter drives.

There are still some drawbacks. The dynamical performance of drives equipped with brushless excitation is reduced due extra time constant between magnetization machine and rotor circuit (Pyrhönen et al. 2016). The de-excitation capability of the brushless excitation relays on the natural time constant because negative current cannot be supplied to the field winding. De-excitation capabilities can be nowadays enhanced with discharge resistor and controllable rotating rectifier circuitry but its control ads extra complexity to the system (Nøland et al. 2019).

2.5. Standards and requirements related to the excitation systems.

There are many different standardisation organizations which are creating technical requirements for the manufacturing industry. The main standardization organizations which create the overall boundaries for electrical machines and excitation systems are:

- The International Electrotechnical Commission (IEC)
- American National Standards Institute (ANSI)
- National Electrical Manufacturers Association (NEMA)

There are also many industry specific standards, which are usually based on IEC or ANSI standards, but which specify those guidelines more specifically to certain applications for example American Petroleum Institute (API) which specifies the framework created by other standards more specific for the petroleum industry. Then there are technical specifications for design and engineering practices (DEPs) which are specific for customer company for example Shell (2007).

The IEC 60034-1 (2017) and ANSI/NEMA MG 1 (2016) defines the basic requirements and guidelines for the features related to the synchronous motor ratings and performance. The synchronous motor if connected to the utility grid must withstand voltage and frequency variations during operation. Figure 2.9 from IEC 60034-1 (2017) presents the different zones

where synchronous motor shall be capable of producing rated torque and the excitation system must be able to maintain either rated power factor or rated field current.

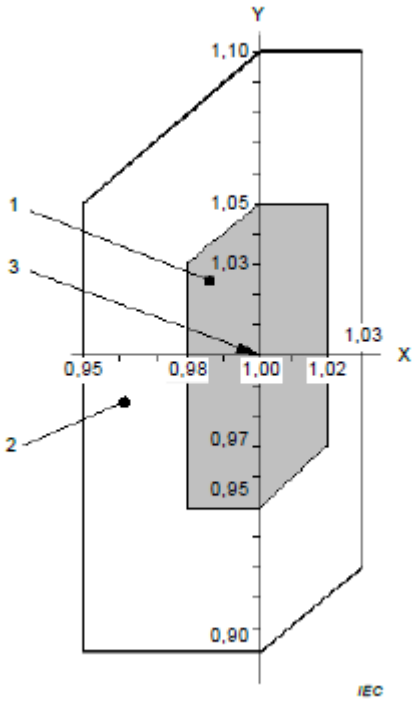

Figure 2.9 Zones of variable voltage and frequency for AC machines. Pointer 1 points to zone A, pointer 2 to zone B and pointer 3 to rated point. X axis is the frequency and Y axis is the voltage presented in per-unit values. (IEC 60034-1 2017)

In the figure 2.9 at the zone A motor should be able to perform continuously. The zone B is area where the performance can deviate more than in zone A, but it is not recommended to operate extensively at this area. The ANSI/NEMA MG 1 (2016) has a similar requirement, but the variation range is a bit different.

IEC 60034-1 (2017) has also specified that the synchronous motor should be capable of withstanding 50 % momentary excess torque for 15 seconds without losing the synchronism and the excitation system must be able to keep the excitation corresponding to the value of rated load, when automatic excitation is used.

The API 546 (2008) gives more detailed definitions which amendment and supplement IEC and ANSI standards on what are the requirements for the exciter machine design and rotating diode bridge and protective devices for brushless machines. For the control system API 546

(2008) defines that in motor applications the system should be able to automatically control the power factor or reactive power. The power supply for the exciter should also be arranged in such a way that it can maintain at least 95% of the rated voltage if the primary voltage supply decreases as low as 50% from the normal voltage.

The DEPs of Shell (2007) are not defined just for brushless machines, but the DEPs also take a stand on design features related to the excitor machine, protective devices and functionalities that should be taken into account. For example, machines connected to the grid should be able to continuously supply their rated output power at rated values during 10% voltage variation during operation. The control system should contain automatic power factor controller which can keep the power factor in the variation margin of 2.5%. The DEPs also specify that the excitation should be brushless type with ac exciter and rotating exciter for motoring application. (Shell 2007)

The dynamical performance related to the control of the excitation system in the direct online motoring applications is not as thoroughly standardised as generator applications. The main requirements come from the end-user and their applications. Usually, these requirements are loose because applications where DOL synchronous motors are used does not require high dynamical performance. In generator applications there are more requirements which come from national grid codes defined by transmission grid operators. Which are for example specified from European network codes. (ABB 2021)

In this study, the rise time of 0.2-0.5 seconds is chosen as a dynamical objective for 0.1 p.u step. This objective comes from Fingrid (2018) grid codes for generators equipped with brushless excitation, operating at no-load and disconnected from grid. The requirement for generators is chosen because it is clearly defined, and special requirements for motor application are not clearly defined. In this study the rise time is calculate from the field winding current instead of the terminal voltage of the synchronous machine.

The end-user demands towards the verification of the machine performance and accuracy of the simulation models has increased. The end-user requires models and parameters which describe the system when they are considering the different options from manufacturers. The end-users are also interested about the accuracy of the models and are comparing the results from simulation and actual tests. This is the case especially in generator applications where grid codes are defining the performance. (ABB 2021a)

3. CONTROL OF THE BRUSHLESS ASYNCHRONOUS EXCITER

The control of asynchronous exciter is addressed in this chapter in the context of industrial drive where direct online synchronous motor is accelerated into the synchronous speed with the help of LCI. The main things that affect to the excitation current in the field winding of the synchronous machine and should be noted in the design of the asynchronous exciter and its control system are:

- Characteristics of the asynchronous exciter machine
- Voltage produced by the converter supplying asynchronous exciter
- Characteristics of the rotating rectifier unit
- The impedance of the field winding.

The control of an asynchronous exciter is a part of excitation control system illustrated in the figure 3.1. The IEC 60034-16-1 (2011) definition of the excitation control system includes all the elements which regulate and control the supply of the field winding and synchronous machine and the exciter machine itself. These parts produce the feedback control system for the whole operation. For this reason, it is briefly explained in this chapter, how the field current reference for the control system is created at the higher-level control systems based on the parameters measured from the motor stator side.

After that, the inner loop of the control system which act upon the current reference created by the higher-level control has been studied and discussed in more detailed manner. This inner loop has been denoted as excitation supply in the figure 3.1 it contains converter supplying the exciter machine. The supply methods and their control systems addressed in this chapter are the antiparallel thyristor bridge and frequency converter supply.

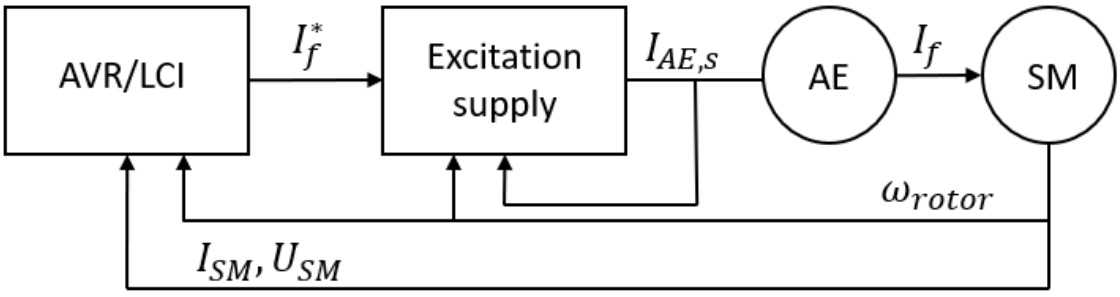

Figure 3.1 Excitation control system of synchronous machine where the higher-level control system is load commutating inverter or automatic voltage regulator.

3.1. Calculation of field current reference

The direct online synchronous motor has two different systems which create the field current reference in the different situations. During the starting phase, the field current reference, which is fed to the controller of the exciter, comes from the load commutating inverter itself. After the machine has been accelerated and synchronized to the grid, field current reference is generated by automatic voltage regulator. During continuous operation, automatic voltage regulator is the main control device producing reference signal to excitation supply unit.

3.1.1. Load commutating inverter

The control of the load commutating inverter is based on controlling the natural commutation of the thyristors in the inverter bridge and dc link through the control of rectifying unit. The back electromotive force (emf) created by the over-magnetized synchronous machine is normally used to supply the necessary reactive power for the inverter bridge and to make commutation possible. While the synchronous motor is at standstill and needs to be started, the machine will not produce electromotive force needed for normal operation. The starting of the synchronous machine is then executed by controlling rectifier unit and the inverter bridge is commutating freely (Stemmler 1994). There are also special circuits available which allow the force-commutating of inverter bridge (Steigerwald & Lipo 1974). The field current reference, which is created for the excitation system, is based on the reference values of the direct axis current, stator flux reference and phase angle. Figure 3.2 contains block diagram from the excitation control of load commutating inverter when constant margin angle is used.

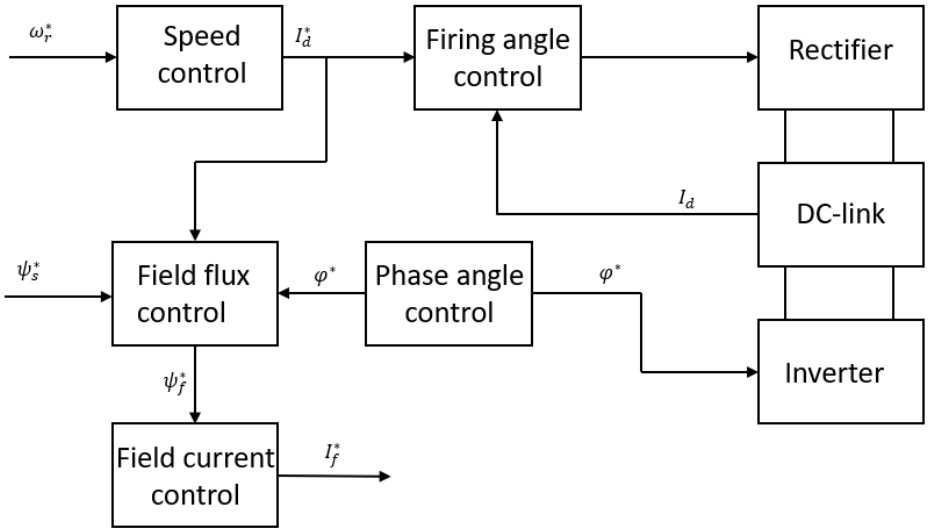

Figure 3.2 Illustrative block diagram from the control system which creates field current reference for the exciter of the synchronous machine.

The calculation procedure of field flux controller and field current controller can be described for example with equations 3.1 and 3.2 presented in Bose (1986)

$$\psi_{\mathrm{f}}^* = \sqrt{\psi_{\mathrm{s}}^{*2} + \psi_{\mathrm{a}}^{*2} + 2\psi_{\mathrm{s}}^*\psi_{\mathrm{a}}^* \sin(90 + \varphi^*)}, \tag{3.1}$$

where ψ_{f}^* is the stator flux reference ψ_{a}^* is the armature reaction based on the direct axis current reference and φ^* is the phase angle reference. The current reference for the field winding can be calculated by multiplying field current reference with gain K_{f}.

$$I_{\mathrm{f}}^* = K_{\mathrm{f}}\psi_{\mathrm{f}}^*, \tag{3.2}$$

While the load commutating inverter is used to start the synchronous motor, the field winding current reference should be large enough to keep the power factor of the machine at unity at least in the beginning of the start when the stator current of the main machine is recovering from the value which create enough pull-out torque as can be seen from example case presented in Ritter et al. (2007).

3.1.2. Automatic voltage regulator

Automatic voltage regulator (AVR) is one of the key devices in the excitation control system of the synchronous machine in direct online applications. The main function of the automatic

voltage regulator is to operate and regulate the magnetic state of the synchronous machine by monitoring the stator side of the grid where synchronous machine has been connected. Based on the machine voltage and current measured with the help of potential and current transformers the regulator calculates current reference which is given for the field current controller.

The control which AVR performs is usually described in the P/Q frame. The active voltage regulator usually contains four basic principles as ABB (2020) depicts. AVR can be used to control the field current of the synchronous machine with:

- Automatic control
- Power factor control (PF)
- Reactive power (VAr)
- Manual control

The Automatic control function means that the controller monitors the voltage from the stator side of the synchronous machine and regulates the excitation current feed to the field winding with the intent to keep voltage of the synchronous machine terminals at defined set point value.

When the power factor control mode is selected the AVR monitors the phase difference between the measured current and voltages from machine terminals and keeps the phase angle between them at the set value, regardless of the voltage in the machine terminals by increasing or decreasing the excitation current. The real and reactive power are the input variables in this control mode. The reactive power control differs from the power factor control in the manner that the reactive power is kept constant at set value every situation by altering the power factor of the machine and the real power. In the figure 3.3 the power factor and reactive power control are illustrated. Regardless of the control mode, which has been chosen, the same limiting factors create the framework for the operation as described in the section 2.1.

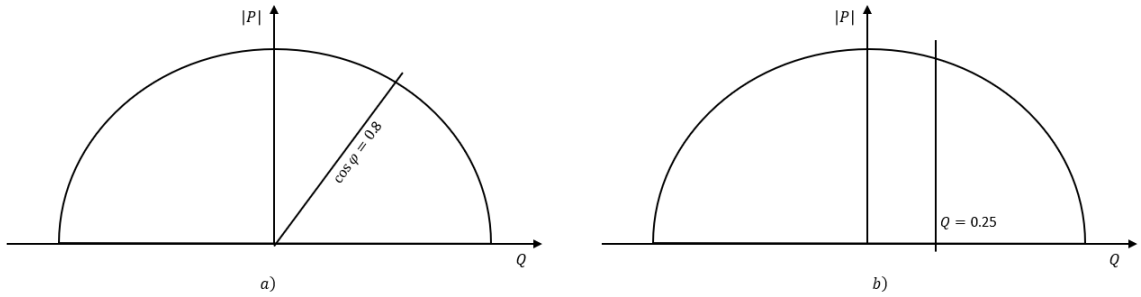

Figure 3.3 a) Illustrates the line where the machine operates if power factor control is used and b) when reactive power control is used.

3.2. Anti-parallel thyristor bridge

The asynchronous exciter needs a controlled three-phase power supply to the stator side for the purpose of controlling the field current of the synchronous machine. The simplest method of supplying the stator with controlled three phase alternating current, is to use the antiparallel thyristor bridge at high power applications. The use of antiparallel thyristors as illustrated in the figure 3.4 allows the control of voltage supplied to the exciter with a constant frequency. The RMS voltage output of antiparallel thyristors is controlled as an ordinary thyristor which is used to rectify alternating current to the direct current with a firing angle α. The major difference is that during the negative half cycle the line voltage commutation happens through extra thyristor which has been connected parallel and reverse direction compared to the conducting thyristor.

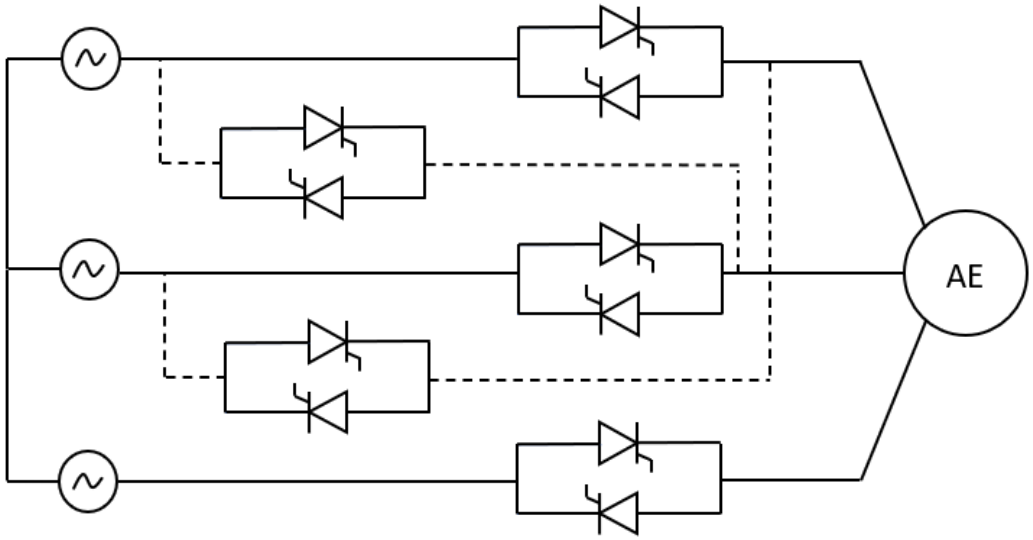

Figure 3.4 Antiparallel thyristor bridge supply for the asynchronous exciter. Bridge contains four extra thyristor which could be used for the change of the direction of stator field rotation.

When thyristor bridge is supplying resistive load, the commutation is based on the voltage waveform. The current stops flowing through the thyristor when the voltage waveform reaches zero. The three phase outputs and currents supplied to the resistive load are illustrated in the figure 3.5.

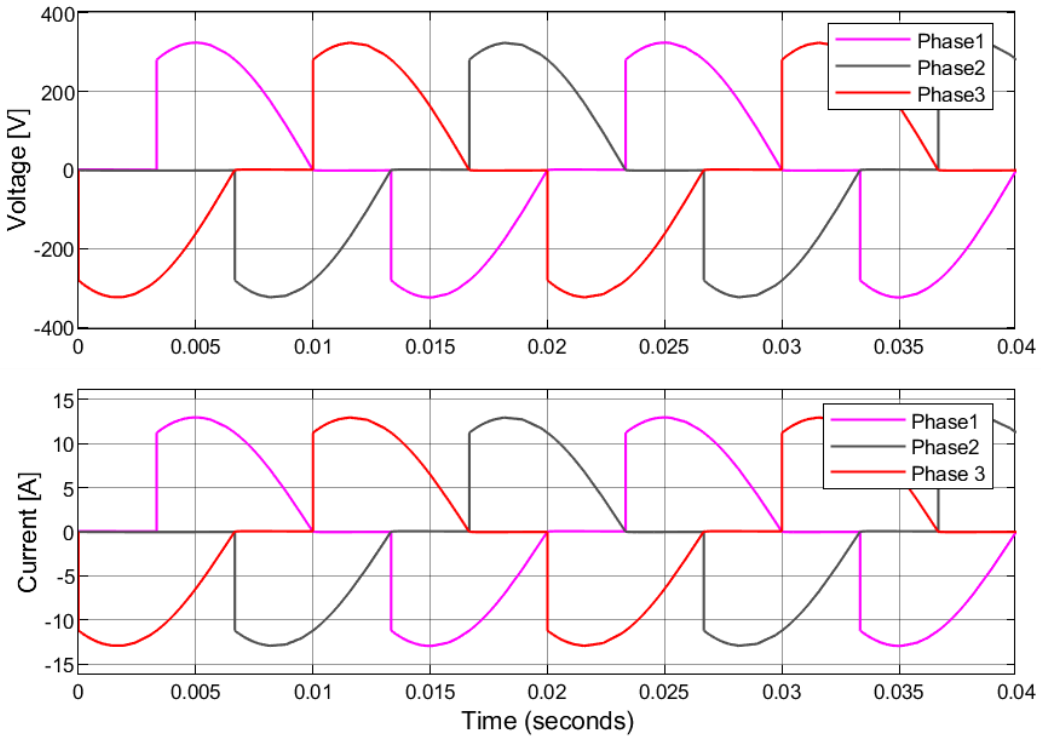

Figure 3.5 Simulation based waveforms of three phase antiparallel thyristor supply which is used to control the voltage of resistive load from 50 Hz and 230 V RMS line supply with firing angle $\pi/3$.

The asynchronous exciter however is not a purely resistive load. The whole system has reactance that is mainly inductive, which leads into the situation where the commutation of thyristor does not stop at the point when the voltage waveform reaches zero due the phase difference between voltage and current. The voltage across the thyristor follows the voltage waveform of the supply until the current reaches zero and blocking state can be achieved as can be seen from figure 3.6.

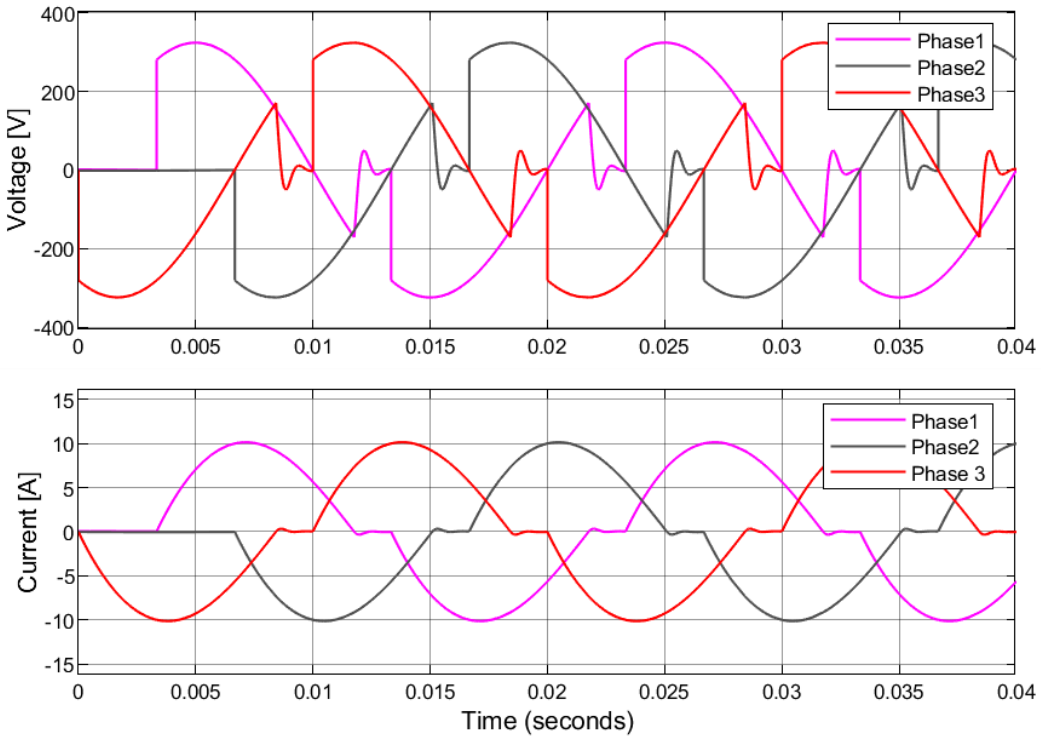

Figure 3.6 Simulation based waveforms of three-phase antiparallel thyristor supply which is used to control the voltage of *RL* load from 50 Hz and 230 V RMS line supply with firing angle π/3.

The structure of the control loop for the antiparallel thyristor bridge can be illustrated with figure 3.7. The current reference which comes from higher level control system is fed to the field current controller which can be implemented as a simple PI-controller. The PI-controller forms a firing angle reference α^* for the firing angle control which produces six different pulses for the thyristors at phase difference of 60 degrees. In the figure 3.7 the two pulses per phase are presented with one phase specific signal. The firing angle reference and phase specific signals can be created based on the measured phase current supplied to the asynchronous exciter.

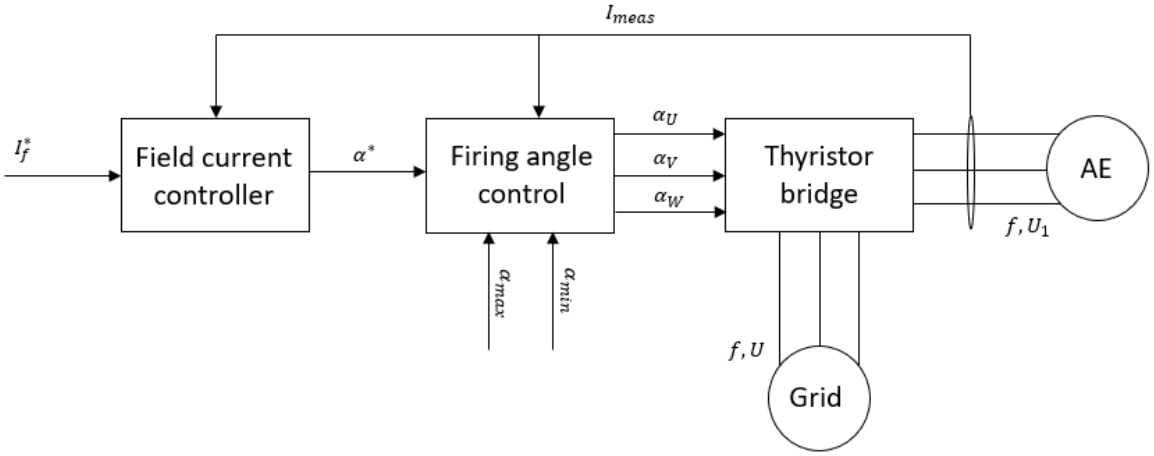

Figure 3.7 Simple structure of asynchronous exciter control system with antiparallel thyristor supply.

In the system presented in figure 3.7 the field current reference I_f^* is in the rotor coordinate system of the main machine. I_f^* is first multiplied with the ratio between nominal field current and nominal current of the converter. The field current reference is multiplied with the ratio to reduce the field current reference into the stator coordinate system of the exciter machine. The measured stator current of the exciter machine is first scaled to correspond the field current with predetermined coefficient so that the field current reference, which is reduced to the stator coordinate system and actual measured stator current, are proportional to each other in per-unit basis. After the coordinate transformation the error between I_f^* and I_{meas} is calculated and fed to PI-controller which creates voltage reference that is used to calculate the firing angle reference for the firing angle control.

The determination of minimum and maximum firing angle limitations are important parameters to ensure reliability of the supply. When antiparallel thyristor bridge is used to control heavily inductive loads, in the process of determining the firing angles it is important to keep in mind that the firing angle cannot be too small. If the firing angle is too small the phase current becomes continuous because thyristor starts to conduct straight after the zero has been reached.

The firing angle determined for the antiparallel thyristor supply cannot be infinitely large either. As Rashid (2018) has pointed out the supply unit is a part of balanced three phase system without the line zero. This means that there should be at least two phases which are conducting at the same time to ensure path for the current to flow. If firing angle is too large

there comes a situation when only one phase is conducting at the time and the current has no path to flow which interrupts the power flow to the excitation machine.

The drawback related to the anti-parallel thyristor bridge is that it introduces lots of harmonics to the supply of the asynchronous exciter because the output is far from sinusoidal signal. Many studies based on simulations and measurements have been done and it is a well-known fact in the literature such as Trzynadlowski (2016) and Qasmi et al. (2019) that with larger firing angles the voltage and current waveforms going to the load are more distorted. Especially 5th and 7th harmonic components are potentially harmful as they are well known to produce pulsating torque components. The harmonic content in the current waveform also increases the losses of the excitation machine. The harmonic content is also introduced to the supplying grid and for this reason each three-phase antiparallel thyristor bridge should be connected to the network via own transformer (Qasmi et al. 2019). These extra transformers will add expenses to excitation system.

The antiparallel thyristor is matured and proven technology but if it is compared with frequency converter supply, it does not have the capability to control the frequency of the supply which would give extra degree of freedom to the control and machine design. The constant supply frequency means that the slip frequency changes according to the rotational speed of the main machine. Constant frequency also introduces a problem in drives where synchronous machine must rotate in both directions. In these drives the rotational direction of the asynchronous exciter should also be changed and it requires extra thyristors as in the figure 3.4 and adds complexity to the control. Even if the rotational direction is not changing during operation the constant frequency guides the design of the magnetic circuit in asynchronous exciter because at zero speed the frequency should be high enough to keep machine sufficiently magnetised.

3.3. Variable frequency drive

The use of frequency converter brings to the control system one extra controllable variable which is the frequency of the supplied voltage and current. Zhang et al. (2016) and Ahonen et al. (2013) have studied the effects of frequency into the magnitude of the field current of the synchronous motor. From both studies it can be concluded that frequency supplied to the

asynchronous exciter can be used to affect the field winding current. This effect comes partly from the capability to adjust the slip between exciter and main machine stator fields.

The study of Zhang et al. (2016) found out that there is a trade-off between the optimal minimum voltage and apparent power required by the exciter. The optimal apparent power requires higher frequency to be supplied in exciter machine stator than the minimum voltage. While the rotational speed of the main machine rotor increases, the voltage increase required to supply required field current decreases if the frequency of the asynchronous exciter has been kept constant and the stator field of exciter rotates to opposite direction. Which in turn means that while the slip between the asynchronous exciter and main machines rotor increases, the ratio between excitation voltage and field current decreases as was found in the study of Ahonen et al. (2013).

Benefits of using frequency converter is that the current, which frequency converter can supply to the asynchronous exciter, is more sinusoidal compared to the thyristor bridge. When the switching frequency of the semiconductors, like IGBT, is increased, the current is more sinusoidal and total harmonic distortion becomes lower in both voltage and current waveforms. The use of IGBT or other fast semiconductor switch-based frequency converter also introduces some drawbacks from the machine insulation point of view. Extra stress is introduced to the insulation of the machine due short voltage rise times and overshoots (Pyrhönen et al. 2016). To eliminate the effects the output of the frequency converter may need to be filtered. The frequency converter also introduces a possibility to use an energy storage to ensure the excitation during faulty supply in the grid. The asynchronous excitation systems and their supply have not been studied extensively but in this part of the thesis a few methods, that can be found from different scientific studies and publications, are introduced.

3.3.1. Current control with constant frequency

The simplest method of using the frequency converter is to use the frequency converter to simulate a thyristor bridge. LeDeux et al. (2015) described the exciter controller where commercial low-voltage variable speed drive was used with modified software to produce output with fixed frequency and adjustable voltage in the range of the nominal range of the frequency converter.

In this method the closed loop current control can be implemented by adjusting the voltage so that the difference between measured phase current output of the frequency converter and field current reference is as small as possible. The field current reference should be reduced to the exciter stator reference frame to make the variables comparable. The control can be implemented using a PI-controller. Commercial low voltage frequency converter could be parametrised so that it uses a scalar control with modified U/f curve where the converter nominal voltage range has been fitted to very narrow frequency range. Ultimately leading in great change in the supply voltage without affecting the frequency of the exciter machine significantly. (ABB 2021b)

3.3.2. Current control with constant slip frequency

The vector control of brushless asynchronous exciter has been under research and development in the field of aviation where wound rotor synchronous machines have been used as starter motors and generators. Zhang et al. (2017) proposed closed loop control principle for three phase asynchronous exciter and Jiao et al. (2019) have studied the similar closed loop method for two-phase excitation machine. The simplified closed loop control scheme presented in the articles can be illustrated as in the figure 3.8.

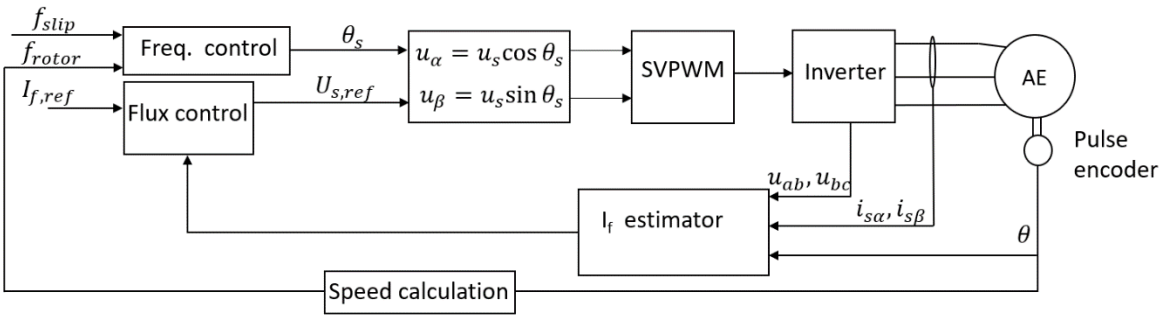

Figure 3.8 Simplified block diagram of the closed loop control presented in the articles of Zhang et al. (2017).

The control presented in the figure 3.8 is based on keeping the frequency of the magnetic field in the rotor circuit constant at whole speed range of the main machine. This frequency of the magnetic field can also be described as constant slip frequency. The fundamental frequency of the stator field in the asynchronous exciter is determined by the equation 3.3

when rotational direction of exciter machine stator field and main machine stator fields oppose each other.

$$f_s = f_{slip} - pf_{rotor}, \tag{3.3}$$

$$f_s = f_{slip} + pf_{rotor}, \tag{3.4}$$

where f_{slip} is the constant frequency difference between stator field and frequency of the main machine rotor f_{rotor} and p is the number of pole pairs in the asynchronous exciter. While the main machine accelerates the frequency in the exciter stator decreases, until it reaches zero and the phase sequence of the asynchronous machine should be changed so that both magnetic fields rotate at the same direction. Frequency of the asynchronous exciter stator field should then be increased into certain frequency which corresponds the constant slip and it is determined by the equation 3.4. From the calculated necessary stator frequency, the angle between voltage components can be determined by integrating the frequency reference calculated by the frequency controller.

The current reference and estimated field current of the synchronous motor are used to produce voltage reference for the control. The flux controller can be implemented with PI-controller. The current of the field winding cannot be measured directly which means that it must be estimated to achieve closed loop control. Because there is diode rectifier, the rotor circuit includes lots of nonlinearity to the system and makes the estimation of the field current more difficult. Kjaer et al. (2005) presented two methods for the field current estimation: current method and voltage method. From these, the voltage method was considerably better when used to estimate the field current of the synchronous machine because the error between measured and estimated was under 5% in most of the test points whereas the current method leads constantly errors over 11%. The models which Kjaer et al. (2005) presented did not take into account the nonlinearities in the rotating rectifiers in the rotor circuit which has resulted into inaccuracy also the results suffer from inaccuracies of the machine parameters used in the estimation.

To address the issue of nonlinearities of the diode bridge Jatskevich et al. (2006) presented parametric average value model for the diode rectifier system of synchronous machine. Jiao et al. (2017) developed the parametric average model further for the asynchronous exciter where asynchronous exciter was modelled in stationary reference frame. The estimation method presented by Jiao et al. (2017) was more accurate compared to the voltage model

presented by Kjaer et al. (2005) with accuracy of 2 %. The estimation method however relies on determining the impedance of the diode bridge at different operation points. The analytical determination of the impedance is difficult and relies on accurate simulation model from the system to determine the impedance as a function of loading of the diode bridge.

3.3.3. Flux control with constant frequency

The constant slip control can be beneficial if both machines are driven at the same direction. Ahonen et al. (2013) found out that if the asynchronous exciter and main machine are driven in opposite directions, the constant slip does not provide any significant benefits for the control of the machine excitation current. Ahonen et al. (2013) developed a method where the supply frequency of the exciter machine was kept constant and the slip between the main machine rotor was allowed to change freely as main machine rotational speed changed. In this method the machines are driven to opposite directions.

This control is based on the fact that the excitation current of the main machine field winding increases almost linearly while the voltage supplied to the exciter machine is kept constant and the slip increases naturally while the main machine accelerates. Ahonen et al. (2013) also determined that the same linear relation could be found as the slip is kept constant and the voltage supplied to the exciter machine is increased. These same relations were also found and confirmed in preliminary tests done by the author presented in the figures 3.9 and 3.10.

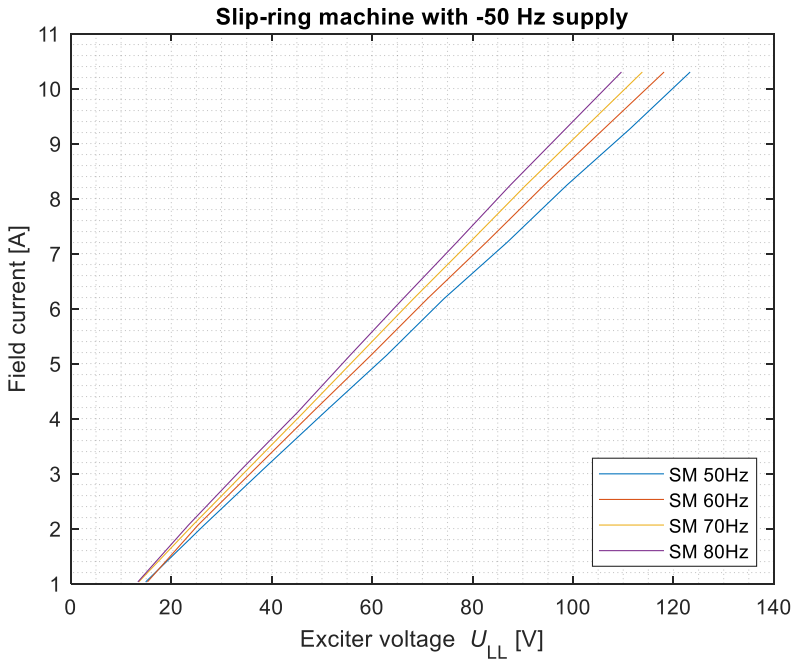

Figure 3.9 The field current of the emulated synchronous machine as a function of voltage fed to the exciter machine with stator of the exciter machine at constant frequency and different rotational speeds for synchronous machine. Negative sign in front of slip ring motor (-50 Hz) means that the main machine is driven opposite direction.

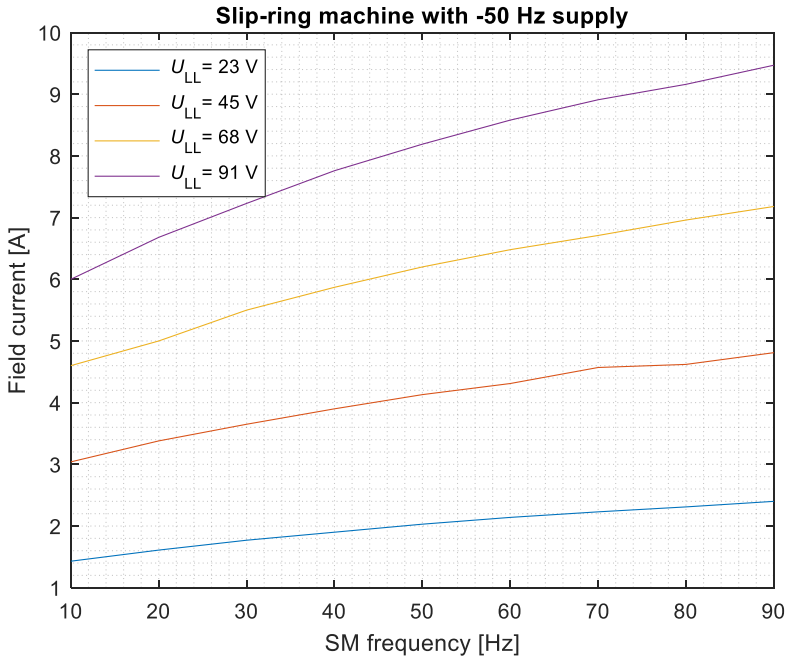

Figure 3.10 The field current of the emulated synchronous machine as a function of rotational frequency when stator frequency of the exciter is kept at constant -50 Hz. The increase in the field current is chancing linearly after the slip is over 2 (50 Hz) and nonlinearly before this point.

The control principle developed by Ahonen et al. (2013) is based on the mathematical model of the excitation machine where the relation *K* between excitation current and voltage at different slip values are determined. When the factor *K* is plotted as a function of slip and linearized the information about the present slip can be used to determine the voltage needed for the required excitation current. This relation can be used to transfer the field current reference into the voltage reference of the asynchronous exciter.

This method, where exciter machine was modelled with function that describes the ratio between voltage and field current, was found to work sufficiently when it was used to magnetize the synchronous machine with varying load and with constant load. When larger loads were introduced to the synchronous machine, excitation current reacted to that with an overshoot as can be expected and reached the continuous state without significant oscillation. When the load was disconnected the magnetizing current oscillated more and it took more time to reach a new steady state. With smaller loads the overshoot was negligible but when load was taken away the oscillation in excitation current increased notably.

Ahonen et al. (2013) also used the same basic idea of keeping frequency of the asynchronous exciter stator constant and tested a control principle where the current transfer coefficient was predetermined and averaged at multiple voltage reference values. In this method the measured phase current of the asynchronous exciter was reduced to the rotor coordinate system of the exciter machine with this predetermined transformation coefficient. The PI-controller was then used to create the flux reference. In this control method the reaction was similar than with the earlier method. However, the overshoot which resulted from big load connected to the synchronous machine was much smaller. Also, in the situation where the load was disconnected the reaction was significantly smaller and oscillation in the excitation current was greatly reduced. The step response times from the control systems developed and tested by Ahonen et al. (2013) varied from 40 to 60 milliseconds without major difference regardless of what control principle was used.

3.3.4. Slip control

The control methods presented in sections 3.3.2 and 3.3.3 are based on the principle that the voltage of the machine is the main variable which is controlled with current feedback to create necessary flux while slip is kept constant or let to vary freely. There is however

another option which is to intentionally control the slip between the main machine and the excitation machine stator with supply frequency of the exciter machine while the voltage of the exciter machine is kept at constant or varied at the same time. The relation between slip and field current is linear at constant voltage if the slip frequency is two or more times larger than the exciter stator frequency as can be seen from figure 3.10. If the slip frequency is less than two times greater, the relation between slip and excitation current is not linear at constant voltage and the slope of the field current curve starts decreasing faster. Ahonen et al. (2013) based one of the presented control methods on the relation ratio between the excitation current and flux as a function of slip and they used the slip as an input which determined the flux reference that should be used.

In theory it should be also possible to use the measured relation between the field current or exciter machine stator current and slip as a base for the control. If the slip frequency bandwidth is limited multiple voltage levels could be created so that the whole field current range could be utilized.

3.4. Hardware limitations that control designer must take account

There are certain limitations that should be taken into account when designing the control system and limiter functions should be built to protect the hardware.

The limitations related to the frequency converter:

- Current limit: The semiconductor switching devices such as IGBT has a maximum current rating which cannot be exceeded for continuous operation without significant risk to damaging the component. This limit is based on the thermal time constant and maximum junction temperature of the device.

- Voltage limit: Maximum voltage that frequency converter can supply for the excitatory machine is dependent on the line-to-line voltage of the grid supplying the frequency converter. The characteristics in the rectifier components are though the limiting factor. Generally, it is 83% of the line-to-line voltage if overmodulation is not used. With overmodulation the output voltage can be

increased little bit higher than line-to-line voltage but overmodulation leads into square wave, which contains harmonic components effecting to torque pulsation.

- Frequency limit: The maximum frequency of the frequency converter like ACS880 is limited to 500 hertz.

- Rated field current of main machine: The field current cannot exceed the nominal current rating of the field winding except momentarily for example in situation where over-magnetization is needed or step like response introduces some overshoot. Control should have some way to implement thermal protection of the rotor circuit.

- Minimum excitation current: The synchronous machine needs an excitation current large enough to stay at synchronism and to eliminate effect of possible AC components at the DC part of the field supply. The control should have function which monitors the minimum current.

The asynchronous exciter also has some limiting factors that should be taken into account:

- Stator current limit: Stator current limit is the maximum current that can be fed to the stator of the exciter machine during continuous operation without the risk of overheating the exciter. This value can be exceeded momentarily but continuous operation increases the risk of damaging the machine.

- Rotor current: The rotor of the exciter machine cannot withstand currents greater than the nominal value continuously without risking to damaging the rotor winding due thermal stresses.

4. SIMULATION AND PERFORMANCE EVALUATION

In this chapter, the different supply and control methods that have been discussed in the chapter 3, are studied and evaluated based on simulation models created into the MATLAB® Simulink® environment. Brushless asynchronous exciter system has been previously modelled and simulated with state machine model developed by Ruuskanen et al. (2008). In this study the model is created with Simscape™ electrical blocks.

The created simulation models take into account the main principles of the presented control methods. The performance of the antiparallel thyristor-based control system and PWM modulation-based frequency converter are studied in this chapter using step response test to evaluate if there is significant performance benefit when frequency converter is used to the supply the asynchronous exciter. The different control methods are also evaluated by simulating acceleration ramp that simulates the start-up of the actual synchronous motor. This study is done to evaluate the accuracy of the control systems. On all the simulation models the ratio between the exciter stator current and field current is used to estimate the field current.

4.1. Overview of the asynchronous excitation machine model

The asynchronous excitation machine was modelled with wound rotor induction machine block from Simscape™ electrical electromechanical library in MATLAB® 2021a. Machine was modelled using SI parameters of the equivalent circuit. Parameters which were used in the simulation model are taken from actual slip ring induction machine which is used in the laboratory measurements described in the chapter 5 of this thesis.

The slip ring machine was the same which was used in the study performed by Ruuskanen et al. (2008) to verify the state machine model of the asynchronous excitation machine for the brushless excitation system. The equivalent circuit parameters for the slip ring machine are presented in the study of Ruuskanen et al. (2008). The name plate values of the star connected machine can be found from the Appendix I and equivalent circuit parameters referred to the stator side are presented in the table 4-1. The rotor circuit of the wound rotor induction machine has been connected to the six-pulse diode rectifier which is used to create the direct current for the field winding. Series *RL* circuit depicts the field winding of the

synchronous machine. Figure 4.1 presents the circuit which is created to the Simulink® environment.

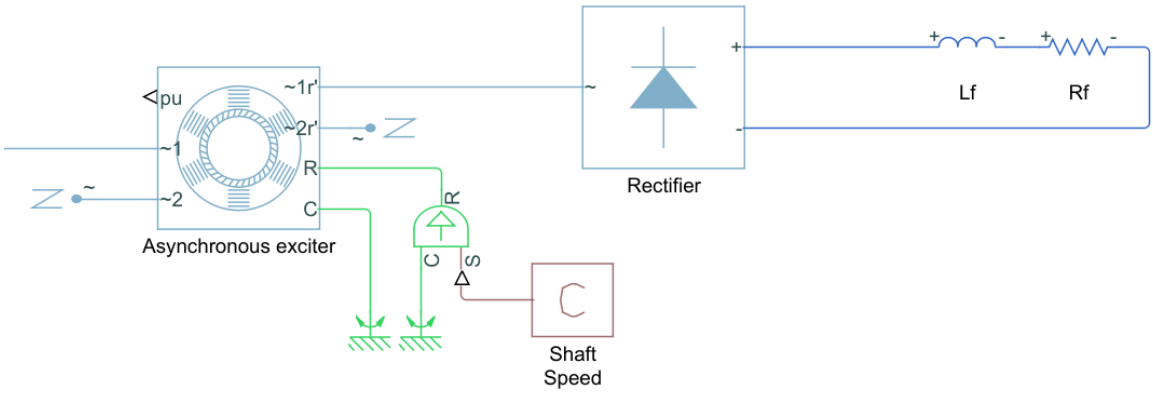

Figure 4.1 Asynchronous exciter machine and rotor circuit of the synchronous motor with ideal angular velocity source which is used to simulate the rotation of the synchronous machine shaft.

Parameters for the components connected to the rotor circuit have also been transferred to the stator reference frame of the asynchronous exciter. Parameters of the rectifier and field winding are also presented in the table 4-1. The ideal angular velocity source is used to simulate the rotating shaft of the synchronous machine. The angular velocity of the shaft is typed with negative value to simulate the opposite rotating direction of the rotating magnetic field of the main machine to the field of the asynchronous exciter.

Table 4-1 Parameters of the components used in the simulation.

Parameter	Symbol	
Nominal power	P_n	1.8 kW
Nominal voltage	U_n	380 V
Nominal current	I_n	4.5 A
Nominal frequency	f_n	50 Hz
Pole pairs	p	2
Stator resistance	R_s	2.2 Ω
Rotor resistance	R'_r	5.4 Ω
Magnetizing inductance	L_m	0.271 H
Stator stray inductance	$L'_{s\sigma}$	12 mH
Rotor stray inductance	$L'_{r\sigma}$	27 mH
Reduction factor	μ	2.3
Nominal field winding voltage	$U_{f,n}$	86 V
Nominal field winding current	$I_{f,n}$	10.3 A
Field winding inductance	L'_f	3.75 H
Field winding resistance	R'_f	31.37 Ω
Diode bridge resistance	R'_D	43 mΩ

4.1.1. Per-unit values

The common way of presenting the electrical parameters in control systems and studies is to use per-unit values. Per-unit values are presenting variables such as resistance or current in the relation to the certain base value that can be determined based on the nominal values given by the name plate of the electrical machine. The use of the per-unit values makes the solutions and parameters more easily comparable and usable in the context of different machines. There are multiple ways to form the per-unit values and it is vital to know how the per-unit values have been formed. In this section the per-unit system used in this study has been presented. The parameters for which base values are defined are simply converted to the per-unit by dividing with the base value presented in equations 4.1-4.5. In the case of voltage and current the peak values of those measured values are divided with base value.

The base value for the current I_{base} is formed based on the equation 4.1.

$$I_{base} = \sqrt{2} I_n, \tag{4.1}$$

where I_n is the nominal current of the machine. The base value for the voltage is created based on the equation 4.2.

$$U_{\text{base}} = \sqrt{2}\frac{U_n}{\sqrt{3}}, \tag{4.2}$$

where the U_n is the nominal line to line voltage of the machine found from the name plate. The base value for the angular velocity is calculated based on the equation 4.3.

$$\omega_{\text{base}} = 2\pi f_n, \tag{4.3}$$

where the f_n is the nominal frequency of the machine. The base value for the inductance comes from the equation 4.4

$$L_{\text{base}} = \frac{U_{\text{base}}}{\omega_{\text{base}} I_{\text{base}}}. \tag{4.4}$$

The per-unit values for the resistance can be calculated using equation 4.5

$$R_{\text{p.u}} = R\frac{I_{\text{base}}}{U_{\text{base}}}. \tag{4.5}$$

4.2. Antiparallel thyristor supply model

The antiparallel thyristor supply model build to the MATLAB® Simulink® has been built from Simscape™ electrical piecewise linear thyristor blocks and capacitor which are used to implement *RC* snubber circuit for each individual thyristor. The model is presented in the figure 4.2

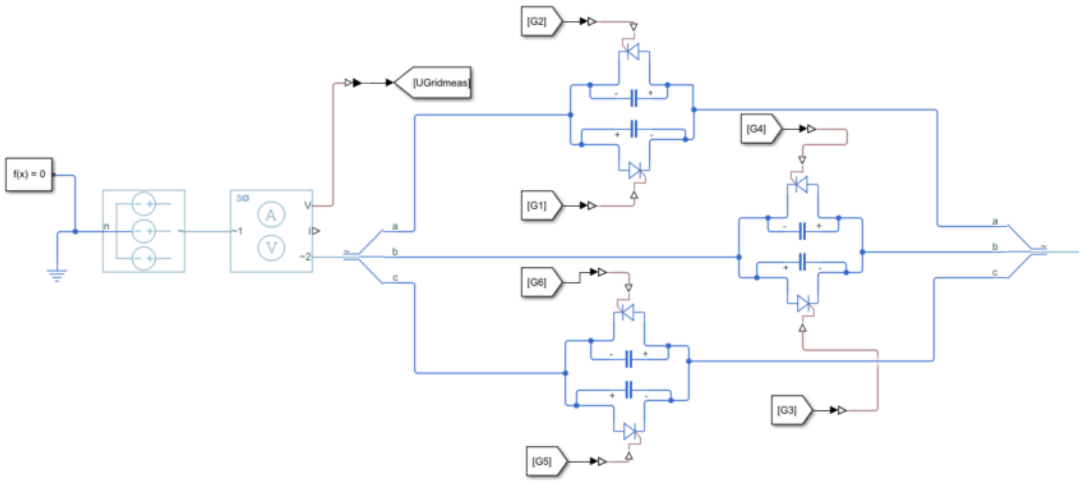

Figure 4.2 Antiparallel thyristor converter with *RC* snubber circuits of each thyristor. The *RC* snubber circuit has capacitance of 0.54 nF and resistance of 89 ohms. The grid which the thyristor converter is connected has frequency of 50 Hz and line to line voltage of 400 V.

To control the firing of the thyristors a simple pulse generator as presented in figure 4.3 was created. The pulse generator is build using sinusoidal measurement blocks which are estimating the angle of the measured voltage of each individual phase. The estimated angle is then compared to π to determine whether the signal is at its positive or negative part of the cycle. If the angle is greater than π the thyristor which is connected antiparallel is conducting. When pulse generator has determined the phase of the cycle, the angle is compared to the firing angle α calculated by the controller. If the firing angle α is smaller than the angle of the phase voltage the thyristor gets firing signal. In the figure 4.2 such antiparallel thyristors are thyristors with the control signals named G2, G4 and G6.

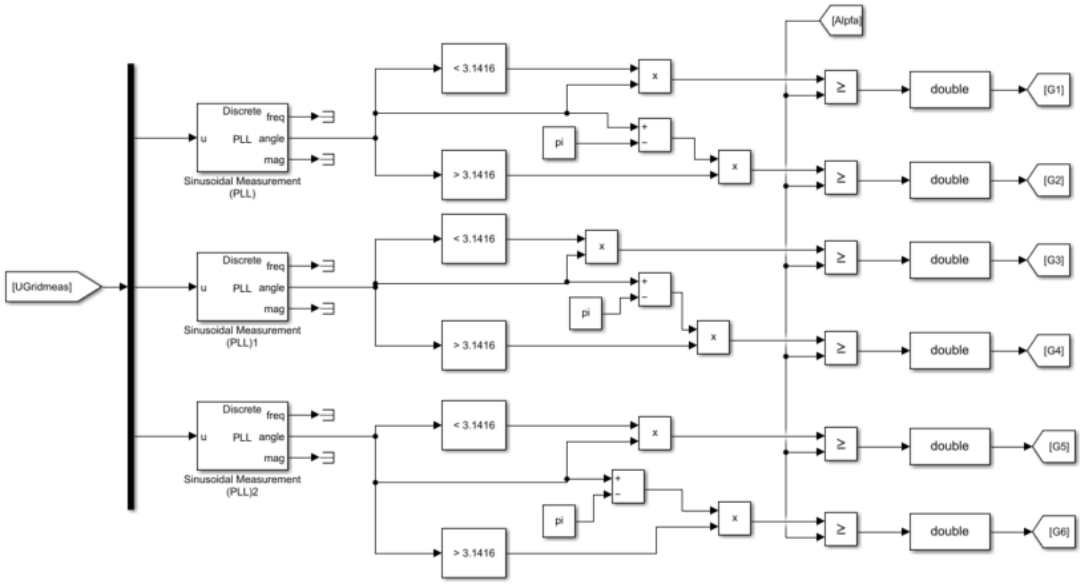

Figure 4.3 The firing unit for the thyristor converter build from sinusoidal measurement blocks and basic Simulink® blocks. Parameters of sinusoidal measurement block can be found from Appendix II.

The control unit created to determine the needed firing angle for the necessary field current is presented at the figure 4.4. The control unit takes the RMS value of phase current as an input. The phase current is then scaled to present the field current with predetermined function which gives the relation of the phase current and field current. Predetermined function is used to convert I_f reference to I_s because this system is non-linear and simple constant is not accurate enough to create the estimate. The value is then converted into per-unit value which is used to calculate the error. The reference coming from the higher-level control system is done created with the step generator which creates outputs between 0-10.3 amperes.

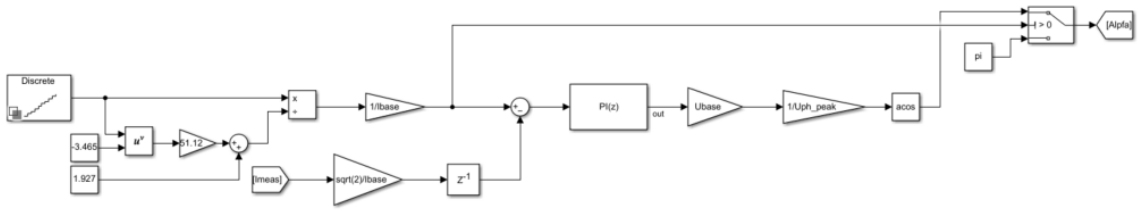

Figure 4.4 Thyristor control unit based on the stator current feedback. The field current reference has been transferred to stator current with predetermined function.

The PI-controller is used to calculate the necessary voltage to generate the field current defined by the reference. This voltage reference is then divided with the peak value of the voltage of the electrical grid which limits the maximum voltage that can be supplied to the excitation machine. Firing angle is calculated using arcus function of the cosine. Because the firing angle is limited during normal operation the firing angle cannot be equal to π which means that the supply current cannot be zero. To get around this problem the switch is used to bypass the control system during situation where the current must be zero.

4.3. Frequency converter models

The frequency converter, which is compared to the antiparallel thyristor supply, was build using Simscape™ electrical three-phase converter block. The converter was specified to use IGBT switches with integrated diodes without dynamics. The frequency converter part of the model is presented in the figure 4.5.

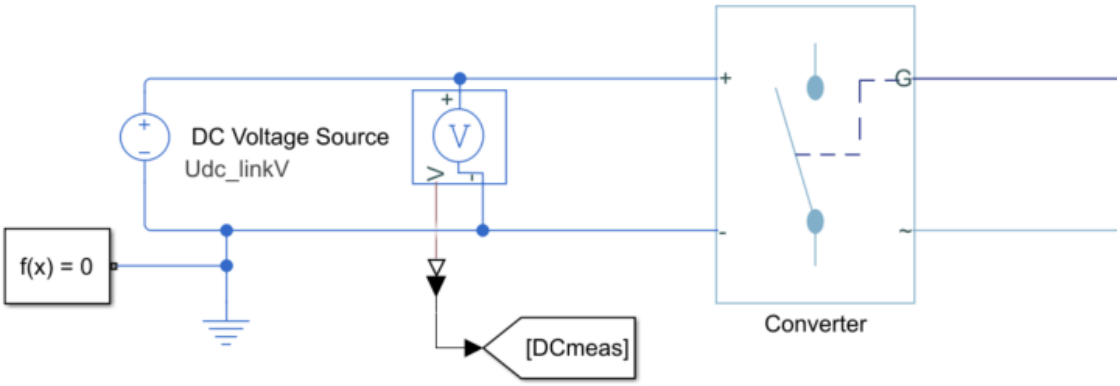

Figure 4.5 Frequency converter model build for the frequency converter supply.

The DC-link for the frequency converter is modelled with DC voltage source which is dimensioned based on equation 4.6.

$$U_{\mathrm{DC}} = \sqrt{2}U_{\mathrm{LL}} = \sqrt{2} * 400\ V_{\mathrm{AC}} = 565.685\ V, \tag{4.6}$$

where U_{LL} is the line-to-line voltage where frequency converter would be connected if the grid side would be modelled. In this study three different control methods are used when evaluating frequency converter supply:

- Current control with constant frequency
- Current control with constant slip frequency
- Slip control

The frequency converter model stays the same during simulation and the control unit is changed. Control units are described in the next section.

4.3.1. Control unit with constant supply or slip frequency

The control unit presented in the figure 4.6 contains the current control unit, waveform generator and modulation block. The current control unit uses PI-controller which takes the error between current reference and current feedback. The current control unit calculates the peak value for the voltage which corresponds field current reference. After the peak value is

calculated, three sinewaves created by the waveform generator are multiplied with the peak value to produce three reference signals for the voltage.

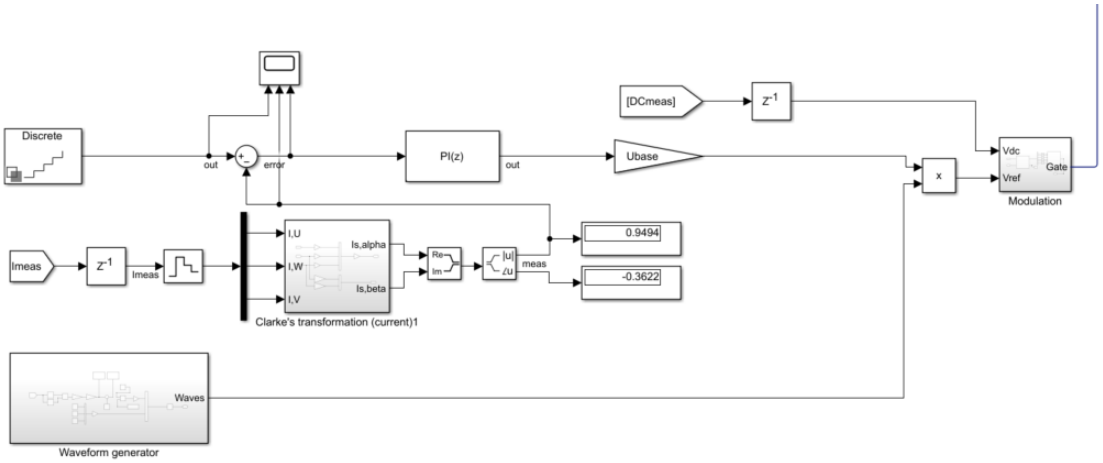

Figure 4.6 Overview from the control unit build to the frequency converter model. Both current and position sensor feedback can be used in this model.

The current feedback is created from measured phase currents of the supply to the asynchronous exciter. From these measured currents the amplitude of the current vector in the stationary reference frame is calculated and fed to the sum block as per-unit value. The Clarkes transformation block is presented in the figure 4.7 The Clarke transformation is used to form a two-phase presentation from the three phase currents supplied to the machine. The Clarkes transformation is based on three equations 4.7, 4.8 and 4.9. The equation 4.9, which gives the zero-sequence current, is usually neglected as is done in this study.

$$i_\alpha = \frac{2}{3}\left[i_{s,U} - \frac{1}{2}\left(i_{s,V} + i_{s,W}\right)\right] \tag{4.7}$$

$$i_\beta = \frac{1}{\sqrt{3}}\left[i_{s,V} - i_{s,W}\right] \tag{4.8}$$

$$i_{s,0} = \frac{1}{3}\left[i_{s,U} + i_{s,V} + i_{s,w}\right] \tag{4.9}$$

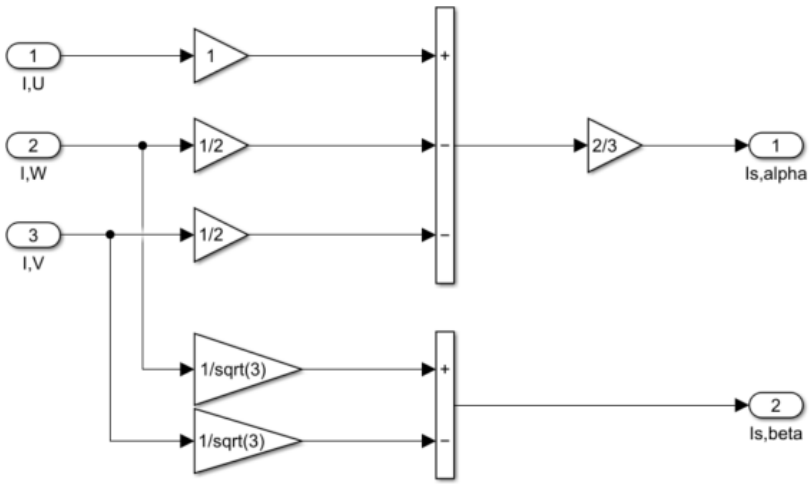

Figure 4.7 Clarke's transformation implemented into Simulink® from basic blocks.

The waveform generator presented in the figure 4.6 creates the frequency reference for the modulation unit controlling the IGBTs of the frequency converter. The waveform generator contains blocks for two different control methods that are used in this study. If the synchronous machine is keeping constant rotational speed the frequency reference created by the waveform generator is constant. The frequency can be set to constant 50 hertz or the frequency reference can be set to be calculated based on the rotational speed of the main machine and fixed slip frequency. The method can be chosen using a manual switch as in figure 4.9. The necessary frequency to keep the frequency of the magnetic field of the rotor constant is calculated based on equation 4.10. The position feedback from the Hall-effect rotary encoder block presented in the figure 4.8 is converter to radians with the PS-Simulink converter before it enters the waveform generator.

$$f(k) = \frac{\theta(k-1) - \theta(k-2)}{T_s} \frac{p}{2\pi} \tag{4.10}$$

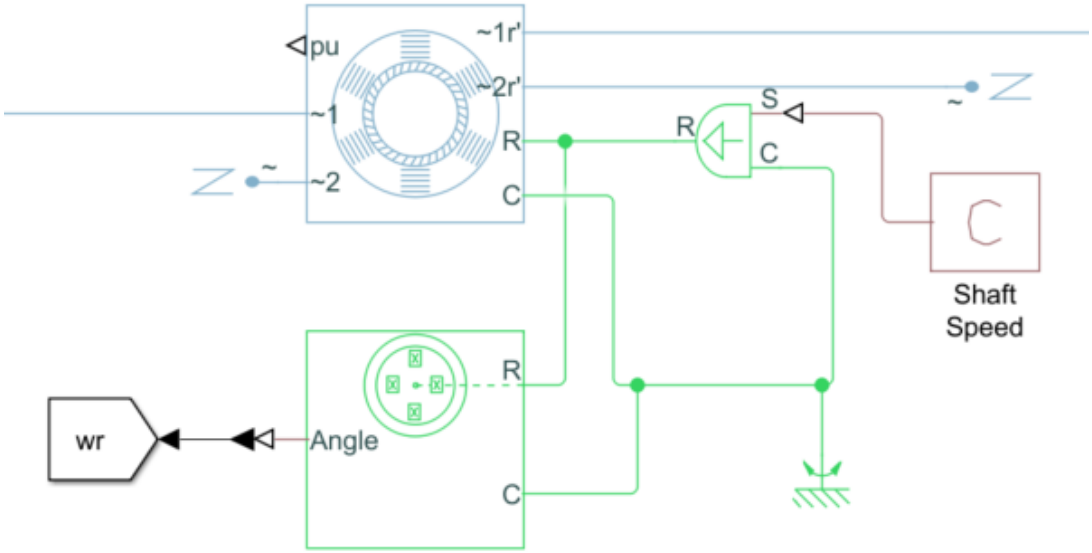

Figure 4.8 The hall sensor used to measure rotor position. The angle output produced by hall sensor block is converted to radians with PS-Simulink converter before it is sent to the control unit.

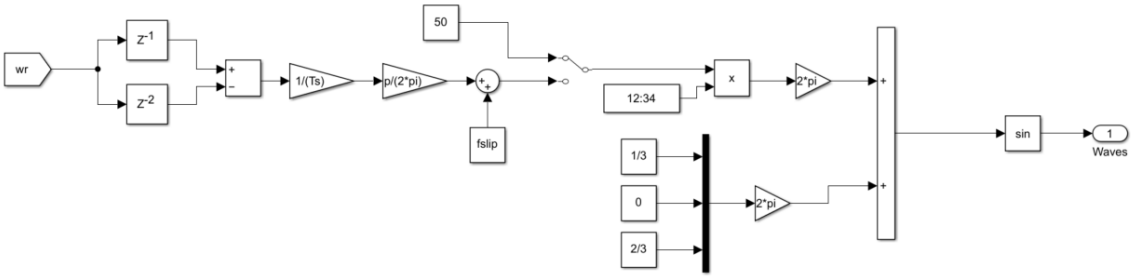

Figure 4.9 Frequency control unit. The frequency of the supply can be switched to constant 50 Hz or the position feedback can be used to calculate the necessary supply frequency.

Whether either of the possible methods are chosen the frequency waveform needs to be created and it is done by multiplying the frequency with time which is taken from the simulation. Next three different waves with phase difference of 120 degrees is created by summing the time varying angular frequency with the phase difference and supplying those signals through sine function.

The third part of the control unit is the modulation subsystem which is presented in the figure 4.10. Modulation subsystem takes as an input the three voltage waveforms produced by the product block and the voltage of the DC-link. The control signals for the switches are generated with three-phase two-level PWM generator block. The six-pulse gate multiplexer is used to multiplexes gate signals generated by the PWM generator so that the signals are in the form which the converter block can use them.

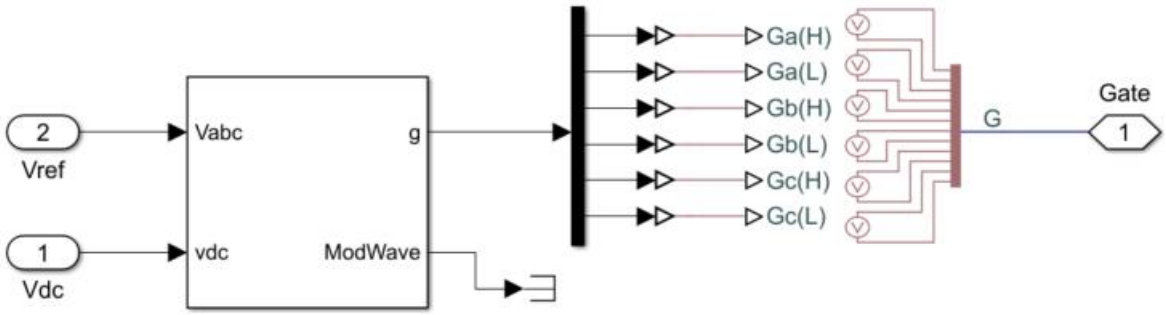

Figure 4.10 Modulation unit to control the switching of the IGBT switches at converter model. The parameters of the PWM generator block are shown in Appendix II.

4.3.2. Control unit with slip control

The control unit for the model, where the frequency of the supply changes based on the current reference, is like the control system presented above. The major difference is the creation of the voltage waveform reference as can be seen from figure 4.11.

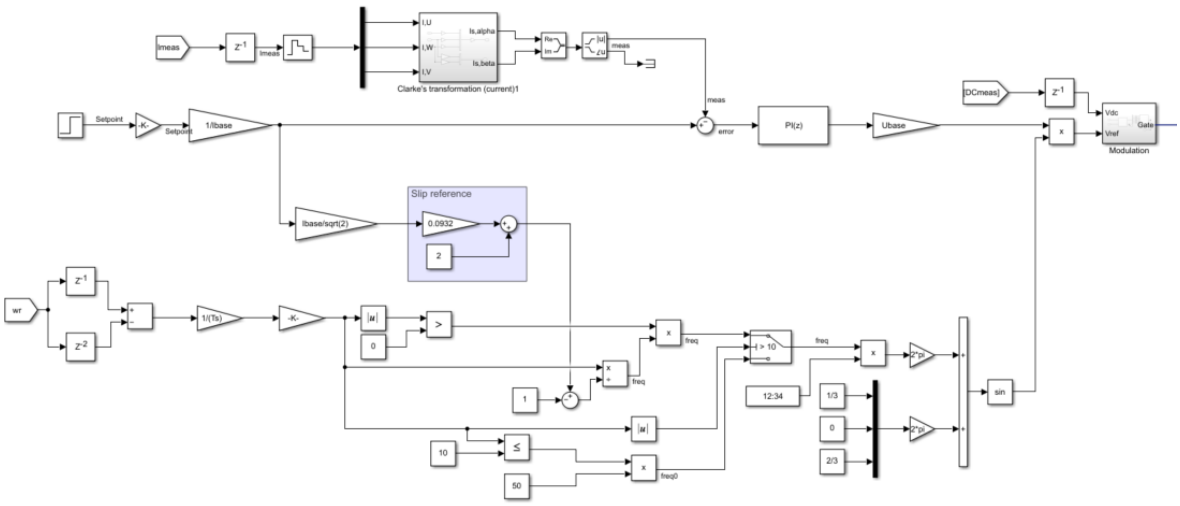

Figure 4.11 Control unit implementation from the slip control to control voltage and frequency simultaneously. The blue box contains the function creating the slip reference, which is used to determine the frequency of the waveform reference.

The voltage reference is created with PI-controller as is done with the other control principles. The frequency of the supplied voltage waveform is created by linearised slip curve. The linearised slip curve is created based on preliminary measurements which are done to the excitation machine, in this case simulation. In these measurements the field winding current and the stator current is measured as a function of slip with multiple values of supply voltage. Slip as a function of stator current is linearised so that each stator current reference has own corresponding slip value which is to be created. Based on that slip value the need frequency for the supply is created based on the feedback from the rotational encoder.

4.4. Simulation cases and results

The different simulation models that are simulated are classified in four different cases. The cases are:

1. Frequency converter with constant frequency
2. Frequency converter with constant slip frequency
3. Frequency converter with current specific slip
4. Antiparallel thyristor supply.

The step response tests are performed for the cases 1, 3 and 4. The case 2 is not tested because it is basically the same as case 1 in the step response test. The acceleration tests are done for all four cases. The field current values, which are presented as a result from the simulations, are transferred from stationary reference frame back to the rotor reference frame.

4.4.1. Step response test

In the step response test, there should not be major difference between frequency converter and thyristor bridge converter supply when control is based on similar stator current feedback. Step response test is also done to the frequency converter model where certain current reference has specified slip value. In this case both frequency of the supply and voltage are altered at the same time.

The rotational direction of the main machine during the step response test is set to opposite direction than the field of the asynchronous exciter. The rotational speed of the rotor is set to nominal of the main machine, which is 1500 rpm. The time step for the simulation must be less or equal to inverse of 10 times the switching frequency. During the step response test time step was set to inverse of 100 times the 16 kHz switching frequency. Time step was 0.625 µs to ensure accurate simulation results. In the control units the cycle time of the PI-controller is set to 1 millisecond for all models and parametrised to have proportional gain (P) 2.1 and Integral gain (I) 40.

The test is conducted so that the field current reference is increased from zero to nominal with 10 % steps every half a second. The rise time and time constant of the field current response are calculated from each step. The step response from 0 to 0.1 p.u has been neglected because in a real situation the field winding is already energised before the machine starts to rotate. In this simulation the machine is rotating from the start. Also, the situation where field current is between 0 and 0.1 can be neglected because current is so small that the minimum excitation current needed to keep the machine stable would be higher. It is debatable where the line should be drawn because it is machine specific.

The figure 4.12 presents the step responses from all the three cases which were simulated. In the figure 4.12 there is two notable differences between frequency converter models and thyristor model. The thyristor model which has limited range of control cannot be used to

supply field current references with small current reference values without going into the discontinuous region. Based on the simulation results it was determined that the thyristor supply was near the critical firing angle between step from 0.4 p.u to 0.5 p.u. From this reason it is feasible to neglect the results from steps below 0.4 p.u. The other distinct difference is that when the excitation is started the inrush current from thyristor supply is significant compared to the frequency converter.

The scaling factor between the stator current and field current did not stay constant with the thyristor bridge model which led to error between reference and result. Scaling factor was estimated with predetermined function from the relation of stator and field current. Even though the function for the scaling factor was determined, there was still some error with reference and actual value even though the magnitude of the step was correct. This was taken into account when calculating rise times and time constants. The scaling factor of I_f to I_s between each frequency converter case was not the same between all the models, the differences between them were small.

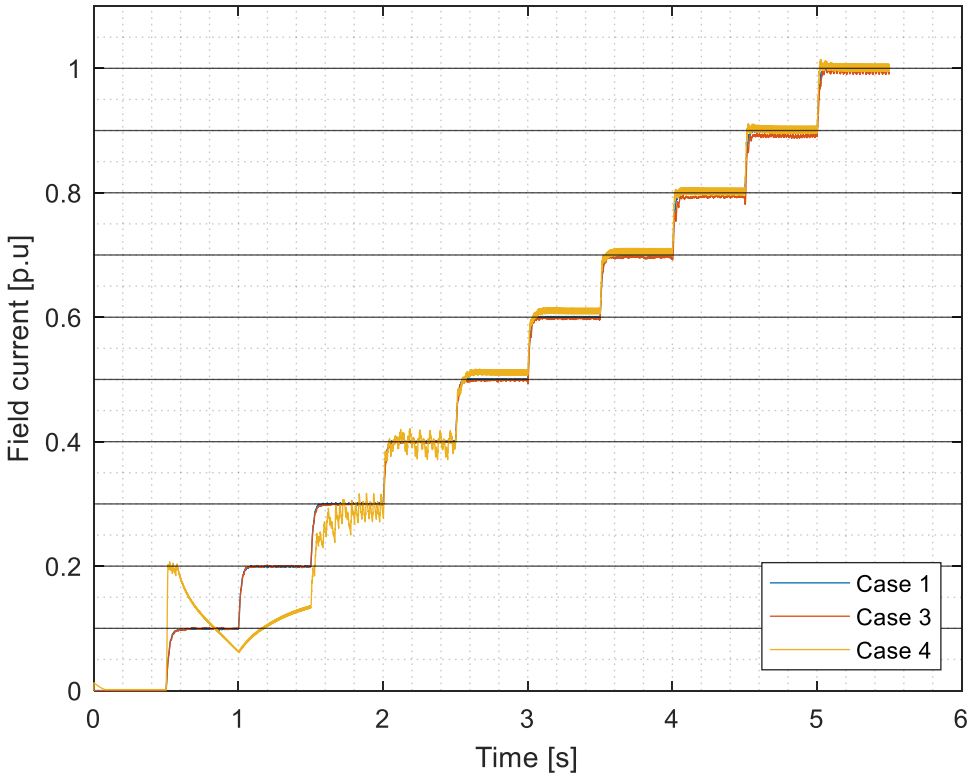

Figure 4.12 Simulation results from multiple step responses. The yellow graph represents the antiparallel thyristor bridge supply, the blue represents frequency converter system where frequency is kept constant, and the red is the frequency converter system where slip is controlled based on the field current reference.

The first simulation case 1 is the frequency converter model imitating the antiparallel thyristor bridge. When the supply frequency of the asynchronous exciter is kept constant and the supply voltage is controlled based on the phase current feedback, the average rise time from 9 steps is in the range of 28 milliseconds as can be seen from the table 4-2. The rise time does vary a little during simulation. The time constant of the excitation system, which includes the frequency converter, asynchronous exciter, and field winding, is 14.5 milliseconds based on the average of the measurements. Some variation to the results can be achieved by tuning the PI-controller so that it allows more overshoot. The effect of overshoot can be minimized by proper tuning of PI-controller.

Table 4-2 Computed rise times and time constants, based on simulation results from step response test of case 1.

Step [p.u]	Rise time [ms]	τ'_{d0} [ms]
0.1 to 0.2	35.35	17.74
0.2 to0.3	30.73	16.33
0.3 to 0.4	30.9	15.14
0.4 to 0.5	27.53	14.55
0.5 to 0.6	27.59	14.43
0.6 to 0.7	25.54	13.3
0.7 to 0.8	25.88	13.15
0.8 to 0.9	24.66	13.08
0.9 to 1	24.15	12.9
Avg.	28.0367	14.5133

The second simulation case was the case 3. The frequency converter model which has a current and a position feedback to control both the voltage and supply frequency. Based on the simulation results presented in the table 4-3 the average rise time for the excitation system with this control is around 32 milliseconds. The average rise time is around 4 milliseconds slower than in the simulation case 1. This result suggest that the control of the slip does not bring additional value to the excitation control in the perspective of dynamic response. The average time constant for the system is around 15 milliseconds, as in the case 1. Differences between case 1 and case 3 are small, and it could be feasible to say that the difference between results could come from either inaccuracy in the calculation during data processing or some inaccuracy during the simulation. The inaccuracy of the simulation can come from the change in frequency, which is the major difference between case 1 and case 3.

Table 4-3 Computed rise times and time constants, based on simulation results from step response test of case 3.

Step [p.u]	Rise time [ms]	τ'_{d0} [ms]
0.1 to 0.2	36.89	17.96
0.2 to0.3	37.31	15.36
0.3 to 0.4	29.9	16.77
0.4 to 0.5	27.85	14.42
0.5 to 0.6	26.66	14.64
0.6 to 0.7	38.78	13.52
0.7 to 0.8	44.32	14.78
0.8 to 0.9	25.83	16.08
0.9 to 1	27.81	16.86
Avg.	32.8167	15.5989

The antiparallel thyristor model was the last method to be simulated. The results in the table 4-4 suggest that when thyristor supply is used with the similar control than in case 1, the rise time is in the same range and bit quicker. Based on this result, it can be said that the use of a frequency converter does not significantly improve the dynamic response of the excitation system. The time constant of the excitation system with antiparallel thyristor bridge is around 10 milliseconds.

Table 4-4 Computed rise times and time constants, based on simulation results from step response test of case 4.

Step	Rise time [ms]	τ'_{d0} [ms]
0.4 to 0.5	36.81	12.98
0.5 to 0.6	31	10.18
0.6 to 0.7	34.04	10.12
0.7 to 0.8	10.79	9.46
0.8 to 0.9	10.5	9.43
0.9 to 1	10.49	9.4
Avg.	22.2717	10.2617

Inside the control loop the parameters that have the most significant impact to the rise time are the integral and proportional parts of the controller. In table 4-5 the effects of increasing P or I part is demonstrated. The parameters PI-controllers are the same between different models to eliminate the impact of the controller parameters.

Table 4-5 The effect of proportional gain P and integral gain I for the system response.

Parameter	Rise time	Overshoot	Settling time	Steady state error
P (Kp)	Decrease	Increase	Small change	Decrease
I (1/Ti)	Decrease	Increase	Increase	Decrease

The only model that significantly differs from others is the slip control model where slip and frequency are adjusted based on the current reference. Simulation results suggest that slip control has no effect. The supply with the antiparallel thyristor bridge was severely distorted. This could explain the difference between frequency converter and thyristor model.

Based on the step response tests it seems that the machine model is consistent without major difference between different control methods used. The average taken from each control system time constants has no more than around 4 millisecond differences, which is small. The average rise times are also close to each other with almost negligible difference under 10 milliseconds. In the context of this thesis the synchronous motor does not need fast response times from the excitation system which makes 10 millisecond differences in the response times negligible. If the difference would be in the range of 50 to 100 milliseconds the situation would be totally different.

The results are somewhat odd because the rise times of the system are in the same range as in the study of Ahonen et al. (2013), which was done with similar machines. The simulation model does not include the stator of synchronous machine which would cause reduction of the time constant at the field winding as equation 2.2 suggest, if energized. In the Ahonen et al. (2013) the stator was energized. Because the simulation results of this study and the study of Ahonen et al. (2013) are similar it raises the question if this model can deal with the transient situations correctly. Ahonen et al. (2013) did not study just the dynamics of field winding and did not specify the step size during step response test, which also rises some questions if comparison to those results can be justified.

4.4.2. Accuracy test

In the accuracy test the rotor of the asynchronous exciter is accelerated into 1500 rpm with 250 second ramp, which is close to actual ramp used to accelerate large synchronous motors in real applications using load commutating inverter soft start. In this test the value of the

field current is taken at predetermined angular velocities and compared to the reference value. The rotor rotates in the opposite direction than the field of the asynchronous exciter.

The simulation time step is increased because fast phenomena is not studied. Time step is still small because simulated system is rather complex, and errors in the calculation of differential equations describing components easily accumulate and affect the results, if time step is too long. The simulation time step for accuracy test is 2.5 µs for frequency converter models and for the antiparallel thyristor bridge the simulation time step is 1.25 µs. When the time step was 2.5 µs the system was not stable according to simulation results. This may be result of cumulative errors in calculations. The PI-controllers had same parameters as in the step response test. The switching frequency for frequency converters was set to 4 kHz.

The simulation results from the frequency converter model case 1 are presented in the table 4-6 and illustrated in the figure 4.13. The results from the simulation clearly indicate that this control method is accurate during acceleration and can keep the field current within 6 % of the desired value if the current reference is around the 0.5 p.u or higher. This method can also keep the current reference accurately with smaller values, but there seems to be larger variation in the accuracy during entire ramp. This current control loop does not have any method of measuring the effect of external disturbance such as the change in slip and slip frequency. From this reason the effects from disturbance cannot be compensated and error always occurs.

When the machine is at standstill the error between reference and actual field current value is highest around 5-6 % at current reference 1 p.u. When the machine starts to accelerate the error starts to decrease as the excitation starts to gain some energy from the rotation of the shaft and slip starts to increase. The maximum error is at 13.7 % with low excitation current and low speed.

Table 4-6 Results from the accuracy test of simulation case 1. Actual value and error between reference and actual vale are presented.

ω [rad/s]	$I_{f,ref}$ [p.u]					
	0.2 p.u		0.5 p.u		1 p.u	
	Actual [p.u]	Error [%]	Actual [p.u]	Error [%]	Actual [p.u]	Error [%]
0	0.1967	1.65	0.4842	3.16	0.9445	5.55
26.1	0.1998	0.1	0.4875	2.5	0.965	3.5
52.36	0.1735	13.25	0.4806	3.88	0.9785	2.15
78.54	0.19	5	0.4889	2.22	0.9872	1.28
104.72	0.1726	13.7	0.4863	2.74	0.9896	1.04
130.9	0.1794	10.3	0.499	0.2	0.9915	0.85
157.08	0.1924	3.8	0.4997	0.06	0.9973	0.27

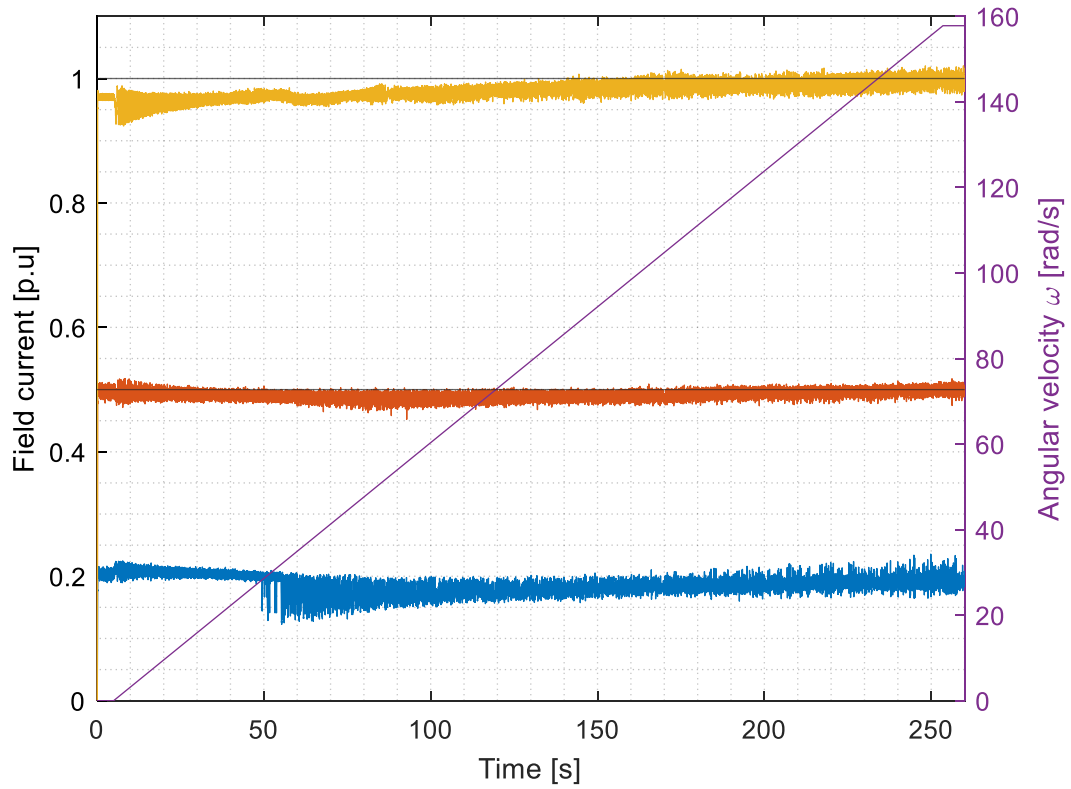

Figure 4.13 Results from the acceleration test with the frequency converter case 1. The field current and angular velocity at three different current reference 0.2 p.u, 0.5 p.u and 1 p.u as a function of time. The angular velocity presented is the absolute value.

The simulation results from the case 2 are presented in the table 4-7 and illustrated in figure 4.14. This control method keeps the slip frequency at constant 100 Hz. At small field current references this control system behaves similarly than the control system of case 1 where the

slip frequency is let to vary freely. The 0.5 p.u curve also seems almost identical to the case 1 except that the error between asked reference and actual field current value are almost negligible lower at some points.

Based on the results it could be said that the difference is almost negligible. The most obvious difference between case 1 and case 2 is noticeable from results of 0.5 p.u. and 1 p.u. In case 2, if the slip frequency is kept constant the field current tends to decrease as the machine accelerates and slip increases. In case 2 the field current reference can reach the wanted reference at zero speed before it gradually decreases while the machine accelerates. The frequency control and current control loops are independent which means that the current controller cannot adjust the field current more accurately than in case 1 and some error always occurs.

The decrease of field current in simulation during the acceleration can be explained by the fact that the frequency of the rotor does not stay constant 100 Hz which it is set. The frequency stays at constant value near the 100 Hz from 0 to 40 rad/s and starts to decrease linearly as a function of rotor speed. The smallest value from the 0.5 and 1 p.u simulations is near 50 Hz. When the acceleration is completed the frequency of the rotor moves back to the reference value 100 Hz. This may indicate the fact that this simulation model is not capable of coping with situations that include some form of transient situation.

Table 4-7 Results from the accuracy test of simulation case 2. Actual value and error between reference and actual vale are presented.

	$I_{f,ref}$ [p.u]					
ω [rad/s]	0.2 p.u		0.5 p.u		1 p.u	
	Actual [p.u]	Error [%]	Actual [p.u]	Error [%]	Actual [p.u]	Error [%]
0	0.199	0.5	0.4968	0.64	0.9687	3.13
26.1	0.2094	-4.7	0.5061	-1.22	1.0041	-0.41
52.36	0.1647	17.65	0.4901	1.98	0.9881	1.19
78.54	0.1727	13.65	0.4831	3.38	0.9713	2.87
104.72	0.1966	1.7	0.4869	2.62	0.9726	2.74
130.9	0.1971	1.45	0.4848	3.04	0.9622	3.78
157.08	0.1923	3.85	0.4964	0.72	0.9918	0.82

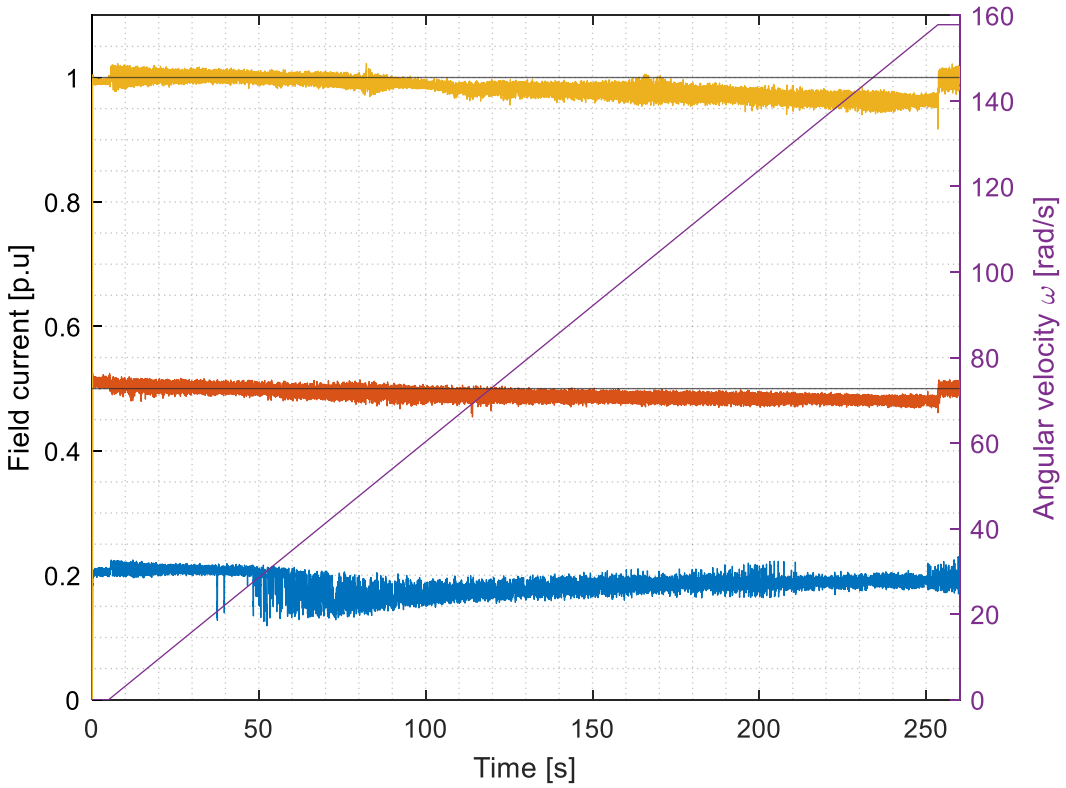

Figure 4.14 Results from the accuracy test of simulation case 2. The field current and angular velocity at three different current reference 0.2 p.u, 0.5 p.u and 1 p.u as a function of time. The angular velocity presented is the absolute value.

The results from accuracy test of the case 3 are presented in the table 4-8 and figure 4.15. The results on the table 4-8 suggest that the control of slip according to the field current reference does not have significant benefits compared to the case 1 where supply frequency is kept constant during acceleration.

There are however few notable problems with this control method during acceleration. The supply frequency of the asynchronous exciter should be at some predetermined constant at zero speed. The slip control should be switched on after machine has accelerated above some predetermined threshold frequency. In this simulation the frequency at zero speed was constant 50 Hz. Otherwise, the system would not be able to supply the exciter machine at zero speed. Second problem with the slip-based control is clearly visible at figure 4.15. When the slip control is switched on the frequency of the supply slumps and so does the field current. This happens because the current control loop cannot compensate the disturbance

from the change in slip and supply frequency. The unnecessary drop in the field current during acceleration is not an accepted feature and therefore this control method is not suitable for starting synchronous machines.

Table 4-8 Results from the accuracy test of simulation case 3. Actual value and error between reference and actual vale are presented.

	$I_{f,ref}$ [p.u]					
ω [rad/s]	0.2 p.u		0.5 p.u		1 p.u	
	Actual [p.u]	Error [%]	Actual [p.u]	Error [%]	Actual [p.u]	Error [%]
0	0.1908	4.6	0.4821	3.58	0.949	5.1
26.1	0.1178	41.1	0.4908	1.84	0.9672	3.28
52.36	0.183	8.5	0.4701	5.98	0.9435	5.65
78.54	0.1867	6.65	0.4867	2.66	0.9745	2.55
104.72	0.1817	9.15	0.4946	1.08	0.9859	1.41
130.9	0.1818	9.1	0.4898	2.04	1.0092	-0.92
157.08	0.1912	4.4	0.4974	0.52	0.9974	0.26

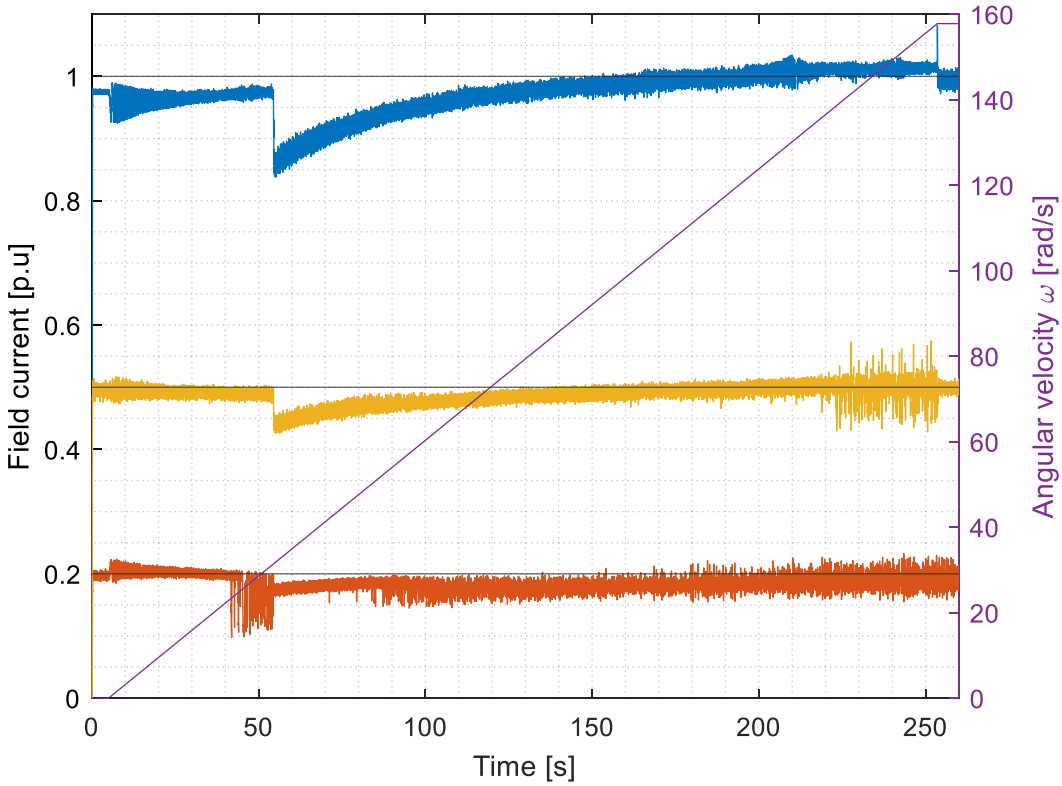

Figure 4.15 Simulation results from the frequency converter case 3. The field current and angular velocity at three different current reference 0.2 p.u, 0.5 p.u and 1 p.u as a function of time. The angular velocity presented is the absolute value.

The slump is a result of decreasing supply frequency. The relation between the supply frequency and the field current can be explained with equations 4.11-4.15 which are used to describe the peak of the rotor current in asynchronous motors. The amplitude of the back emf induced to the rotor circuit as a function of slip can be described with the equation 4.11. The equation 4.11 clearly depicts that the back emf is dependent on the frequency supplied to the stator of the asynchronous exciter. Back emf is also dependent on the amplitude of the rotor flux linkage which depends on the rotor and stator currents as equation 4.12 describes. The amplitude of the rotor flux linkage is not frequency dependent.

$$\hat{e_{\mathrm{r}}}(s) = s\omega_{\mathrm{s}}\widehat{\boldsymbol{\psi}_{\mathrm{r}}} \tag{4.11}$$

$$\boldsymbol{\psi}_{\mathrm{r}} = L_{\mathrm{r}}\boldsymbol{i}_{\mathrm{r}} + L_{\mathrm{m}}\boldsymbol{i}_{\mathrm{s}} \tag{4.12}$$

In the equation 4.13 the impedance of the rotor circuit is described without the impedance introduced by the diode bridge and field circuit. The diode bridge and field circuit are neglected to simplify the discussion and because those components are not affected by the stator frequency directly. If more detailed analysis would be done those components should be included.

$$Z_{\mathrm{r}}(s) = R_{\mathrm{r}} + js\omega_{\mathrm{s}}L_{\mathrm{r}\sigma} \tag{4.13}$$

By combining the equations 4.11, 4.13 and knowledge of the ohms law the equation 4.14 can be derived for the rotor current as a function of slip. Equation 4.14 can be arranged in the form of equation 4.15 by dividing with slip.

$$\hat{i}_{\mathrm{r}}(s) = \frac{\hat{e_{\mathrm{r}}}(s)}{Z_{\mathrm{r}}(s)} = \frac{s\omega_{\mathrm{s}}\widehat{\boldsymbol{\psi}_{\mathrm{r}}}}{R_{\mathrm{r}} + js\omega_{\mathrm{s}}L_{\mathrm{r}\sigma}} \tag{4.14}$$

$$\hat{i}_{\mathrm{r}}(s) = \frac{\hat{e_{\mathrm{r}}}(s)}{Z_{\mathrm{r}}(s)} = \frac{\omega_{\mathrm{s}}\widehat{\boldsymbol{\psi}_{\mathrm{r}}}}{\frac{R_{\mathrm{r}}}{s} + j\omega_{\mathrm{s}}L_{\mathrm{r}\sigma}} \tag{4.15}$$

The equation 4.15 notes clearly that both numerator and denominator are dependent on the supply frequency. In the case 3 the supply frequency at the start is 50 Hz which results into similar behaviour as in the case 1. When the rotor has reached 10 Hz margin, the slip control is activated and the supply frequency drops to 7.41 Hz in the case where reference is equal to 1 p.u. The slip is calculated based on the function

$$0.0932 I_s^* + 2,$$

which is the linearised function of the stator current and slip, the slip gets value 2.35. The drop in the frequency has an effect to the back emf and impedance of the rotor, which results in drop of rotor current. To compensate this drop, stator current of the asynchronous exciter should be raised significantly to raise the rotor flux. Because the current control loop does not take into account this disturbance, it cannot be compensated.

While the rotor accelerates the supply frequency also increases which means that the field current increases after the slump. In case 2 the supply frequency is at its highest at zero speed and smallest at nominal speed. The drop in the frequency supply happens gradually so this kind of slump is not visible. In the simulation case 1 in figure 4.13, the frequency stays constant, and the slump does not happen.

The antiparallel thyristor bridge supply is presented in figure 4.16 and the results can be seen from the table 4-9. The results are similar as in the case 1 because the supply frequency is kept constant and voltage is controlled based on similar current control loop. The control system has similar problem as in the case 1 to accurately follow the current reference while the machine is at standstill. While the machine starts to accelerate, this error starts to vanish and the error is gradually reducing while the machine accelerates towards nominal angular velocity.

Table 4-9 Results from the accuracy test of simulation case 4. Actual value and error between reference and actual vale are presented.

	$I_{f,ref}$ [p.u]			
ω [rad/s]	0.5 p.u		1 p.u	
	Actual [p.u]	Error [%]	Actual [p.u]	Error [%]
0	0.4591	8.18	0.9004	9.96
26.1	0.4917	1.66	0.9667	3.33
52.36	0.4948	1.04	0.977	2.3
78.54	0.5035	-0.7	0.9971	0.29
104.72	0.4912	1.76	0.9781	2.19
130.9	0.5111	-2.22	1.0064	-0.64
157.08	0.5063	-1.26	1.0042	-0.42

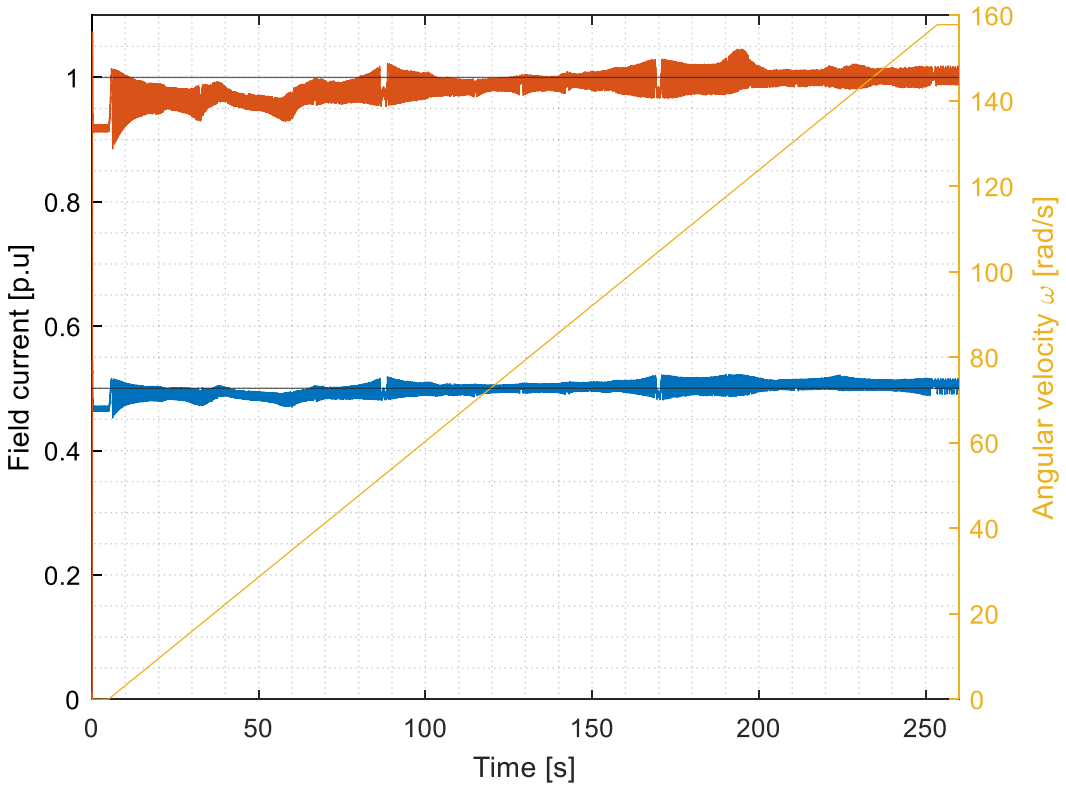

Figure 4.16 Simulation result from antiparallel thyristor model with two different field current reference values. The angular velocity of the rotor illustrated in the figure is absolute value.

The simulation models built to test different ways of controlling the asynchronous exciter work as expected and phenomenon described with equation 4.15 is clearly observable. From the accuracy point of view, there is not a huge difference between frequency converter supply and antiparallel thyristor supply. The ability to control supply frequency is beneficial with zero speed, but the difference is small. The real system is connected with the higher-level automation system which also makes adjustments to the field current reference based on the feedback from synchronous machine stator side. This means that the minor inaccuracies will be compensated by that control so the minor differences in the accuracy could be negligible.

4.4.3. Summary from the simulations

The main observations and results from the simulation part of the thesis can be listed as follows:

- The use of frequency converter does not bring additional benefit to the response of the system based on the step responses. The frequency converter offers a wider range to control the field current, because there is not critical firing angle limiting the output.

- The results from all the step responses are questionable. Results suggest that the machine model used, may not be able to cope with dynamical simulations accurately.

- The slip control does not give any benefits to the control since the supply frequency is dominant component. Especially if current control loop does not take into account the effects of changes in slip frequency.

- The control methods in case 1 and case 2 are the most promising control methods for implementation. These methods are implemented with the actual frequency converter that controls the asynchronous excitation machine.

5. MEASUREMENTS, RESULTS AND ANALYSIS

In this chapter the asynchronous exciter simulation model developed in the chapter 4 is verified with sinusoidal and variable frequency drive supply. The antiparallel thyristor supply is not verified because there is not such system available. This chapter also studies the possibility of implementing current control with constant frequency and constant slip frequency to an actual ACS880 frequency converter. First the measurement setup is introduced and discussed in general manner. After introduction to the measurement system, verification of the asynchronous exciter model is carried out with transformer with adjustable secondary voltage and frequency converter supply and results between measurement and simulation are discussed. Final part of this chapter is dedicated to implementation and testing of the chosen control method with ACS880 frequency converter.

5.1. Test equipment and environment

The measurement system has been built in the facilities of LUT Laboratory of electrical machines. The measurement system contains three electrical machines which are presented in the figure 5.1. The slip ring machine, which is the asynchronous excitation machine, is rotated with another asynchronous motor. This motor emulates the synchronous machine which has asynchronous exciter connected at the same shaft. The rotor of the synchronous machine is used as a load for the slip ring machine. In this study, the synchronous machine itself is not used to rotate the asynchronous exciter because the purpose is just to use the rotor circuit as a reactive load, without the stator side of the synchronous motor affecting on the behaviour of the field winding. The synchronous motor was chosen because its rotor offered the best ratio between the L_f and R_f from the components which were available, compared to real size synchronous motor. The drawback is that the synchronous machine has brushes between the diode bridge and the rotor circuit which increases the resistance compared to the actual system.

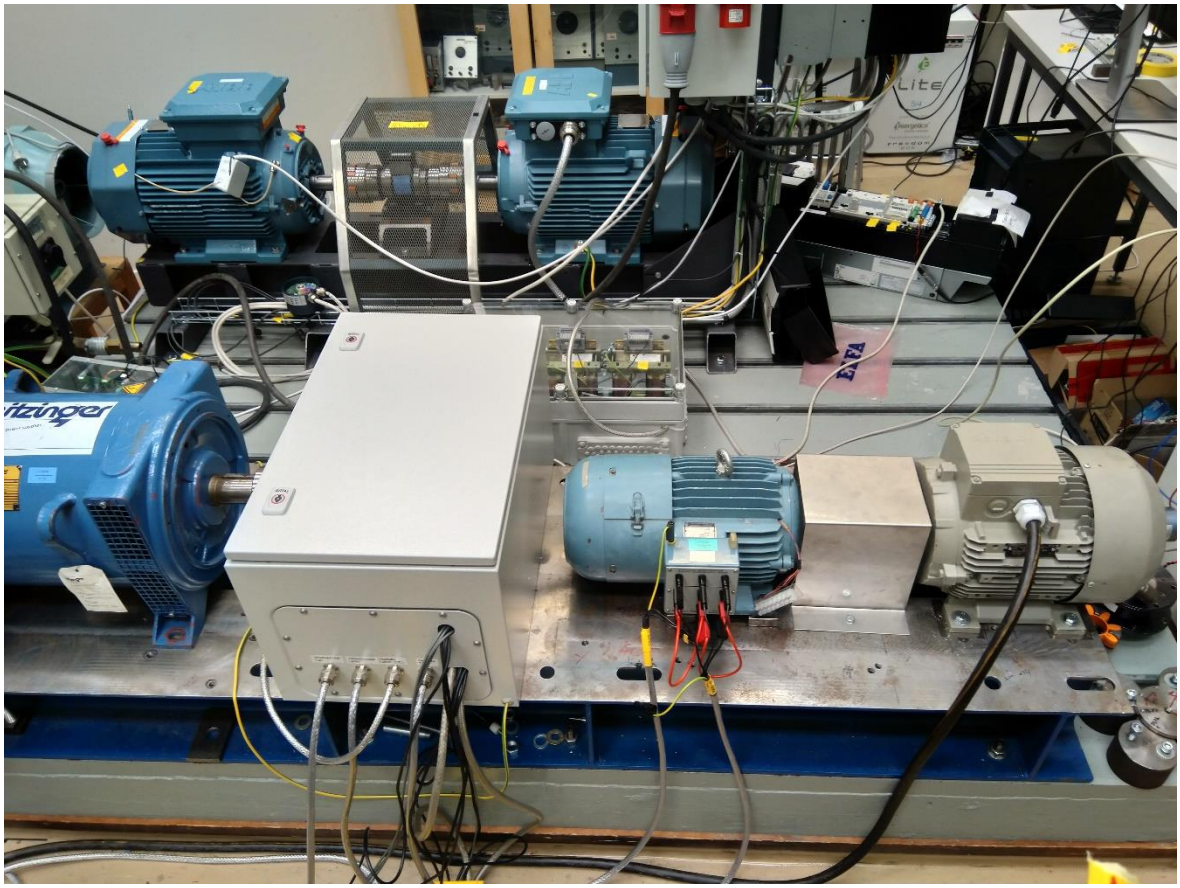

Figure 5.1 The testbed and electrical machines used in the study. The brown asynchronous machine is used to emulate the synchronous machine rotor. Light blue machine is the slip ring asynchronous machine used as an asynchronous exciter. The grey box between blue synchronous machine and SR machine contains the diode bridge, clamps and current transformers used in this study. In the left side is the blue synchronous machine, the stator side is open circuit.

During the verification of the machine model the slip ring machine has been supplied by transformer with adjustable voltage although in other cases the machine is supplied with other ACS880 frequency converter. The supply for the emulating asynchronous motor is arranged with ACS880 frequency converter in all the tests performed at this thesis.

The test setup is illustrated in the figure 5.2 and 5.3. The test setup contains AC500 PM583 programmable logic controller (PLC) which is used to emulate the higher-level control system which could be either the LCI or AVR as discussed in the chapter 3. The AC500 has been equipped with CM579 EtherCAT module which has been used to give the field current reference for the ACS880 supplying the asynchronous exciter. The same AC500 is also used to control the rotational speed of the asynchronous motor rotating the system. The both

ACS880s have been equipped with FECA-01 EtherCAT adapter modules to make communication through EtherCAT fieldbus possible. The more detailed list of the devices used in the measurements is presented in the Appendix III.

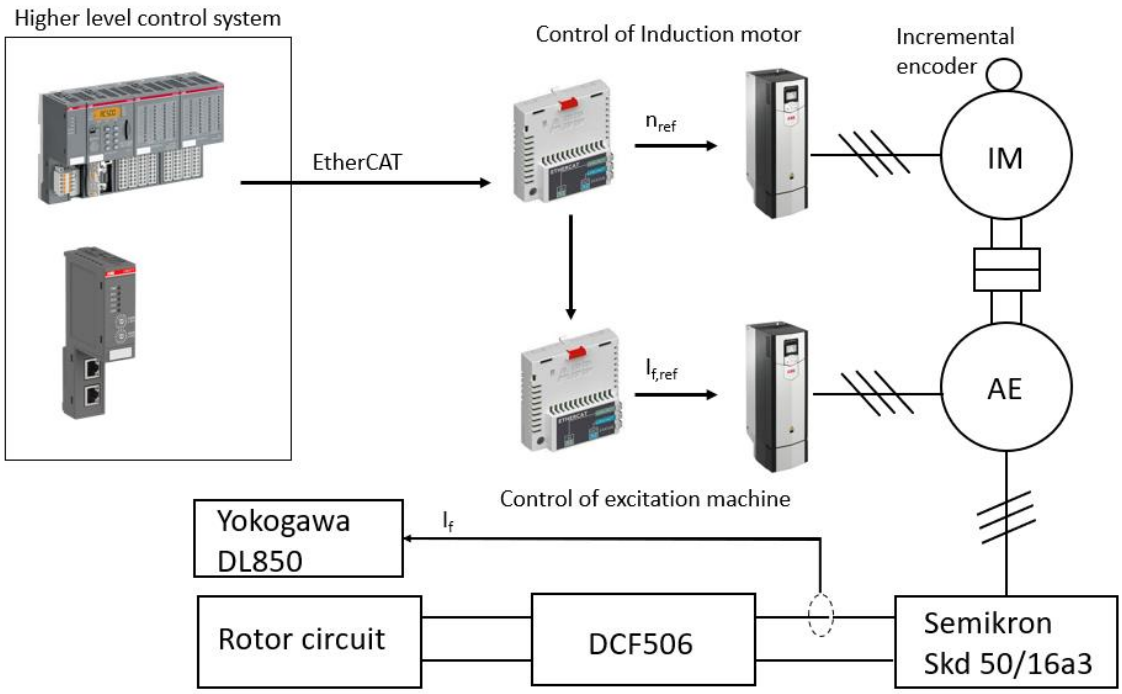

Figure 5.2 Illustration from the measurement system where AC500 is used to send references for ACS880 frequency converters. The rotor of the asynchronous exciter (AE) has been connected to diode bridge. Between the rotor circuit and diode bridge DCF506 overvoltage protection has been installed to protect the rotor from large voltage spikes of the rectified voltage. Yokogawa DL850 is used to measure the DC current of the field circuit.

Figure 5.3 The overview of the measurement system built into the laboratory. In right side picture the larger ACS880 is supplying the rotating machine. The smaller ACS880 is the supply unit for the asynchronous exciter.

5.1.1. Drive application programming (IEC 61131-3)

ABB ACS880 frequency converters have a build in PLC functionality which can be used to execute custom application specific control programs in parallel with the drive firmware. The application programming can be used with the drives equipped with N8010 application programming license and ZCU or BCU control units. The application programming environment allows the user to create own programs using ABB automation builder which is based on the Codesys environment developed by the 3S-Smart Software Solutions. The custom programs can be created with IEC 61131-3 defined programming languages such as

- Ladder diagram (LD)
- Function block diagram (FBD)
- Structured text (ST)
- Instruction list (IL)
- Sequential function chart (SFC)

There is also possibility to use continuous function chart (CFD). The figure 5.4 presents the system diagram of the ACS880 firmware and application programming environment. In the drive application programming the user can create own parameter groups and parameters. The application program also makes it possible to utilize the parameters of the frequency converter as an input through the DriveInterface.

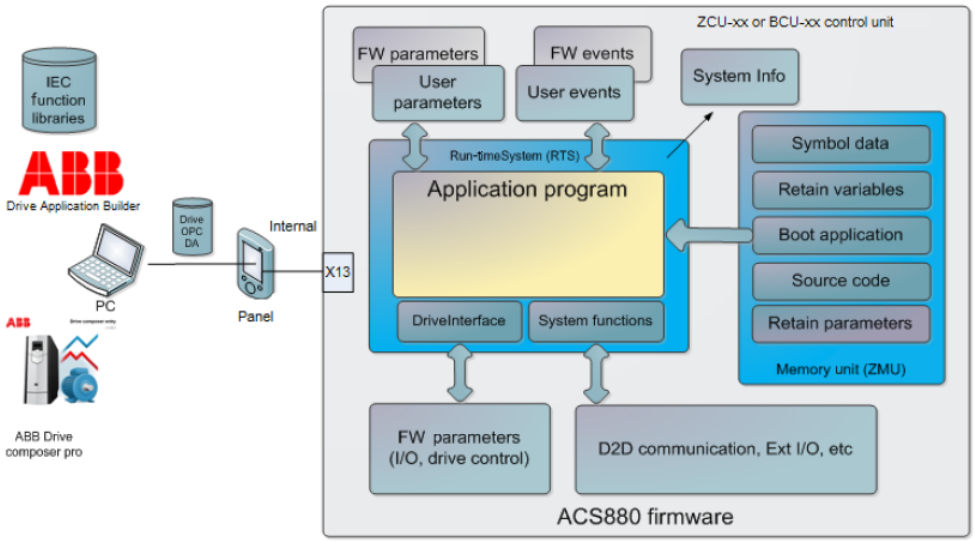

Figure 5.4 System diagram from the ACS880 firmware and the drive application program which can be programmed based on the application by the user. (ABB 2019)

5.2. Model verification

The simulation models and reality have their differences because the simulation model is just an approximation of the real system based on different assumptions and simplifications. To verify the machine model, the results of the simulation and actual measurements are compared in this section. The verification of the machine model is done with both sinusoidal supply and frequency converter supply. The comparison of the dynamics between the actual system and simulation model is also done.

5.2.1. Verification of the asynchronous exciter model

The comparison between the simulated asynchronous exciter model and the actual system with sinusoidal supply is done first. Figure 5.5 and table 5-1 present the results gathered from steady state measurements. Verification measurements for the asynchronous exciter

model at the steady state were done with three different voltage levels varying the slip between the field of the asynchronous exciter and the frequency of the rotor. In the figure 5.5 the field current is presented as a function of slip and frequency of synchronous machine. The field current behaves in similar manner as in the measured data. The nonlinear relation of field current at slip values lower than 2 is clearly reconcilable from both simulated and measured results.

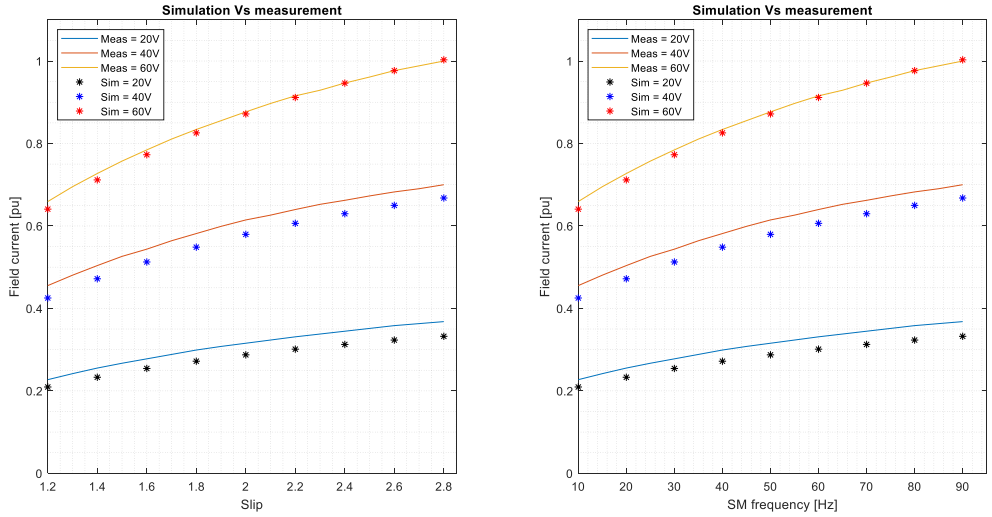

Figure 5.5 Comparison of the measured and simulated results as a function of slip and frequency of the synchronous machine. The frequency of the asynchronous exciter in this comparison is constant 50 Hz and rotating in opposite direction from the field of the synchronous machine.

The accuracy of the simulation model varies between different voltage levels and it seems that when supply voltage is higher the accuracy is slightly better. In the table 5-1, the same information as presented in the figure 5.5, is presented in numbers. The maximum error based on the calculation is between 9 to 10% which can be accepted since the model always includes uncertainty factors. Some uncertainty comes from the equivalent circuit parameters for the machine and rotor circuit. The simulation model does not include any information about the stator and rotor winding and build in magnetic saturation representation were not used in this study. Because of that some difference between the reality and simulation naturally occurs. Also, the measured data used in this comparison includes some error because the measured data also has some uncertainty.

Table 5-1 The results from the verification of the asynchronous exciter model with sinusoidal supply. The error is calculated comparing the simulated field current to the measured value of the field current.

Slip	U_{ph} = 20 [V]			U_{ph} = 40 [V]			U_{ph} = 60 [V]		
	Meas [A]	Sim [A]	Error [%]	Meas [A]	Sim [A]	Error [%]	Meas [A]	Sim [A]	Error [%]
1.2	2.34	2.157	7.82	4.69	4.38	6.61	6.79	6.6	2.80
1.4	2.63	2.4	8.75	5.19	4.86	6.36	7.49	7.33	2.14
1.6	2.86	2.62	8.39	5.6	5.28	5.71	8.08	7.959	1.50
1.8	3.08	2.801	9.06	5.99	5.65	5.68	8.59	8.505	0.99
2	3.25	2.96	8.92	6.33	5.97	5.69	9.03	8.978	0.58
2.2	3.41	3.102	9.03	6.59	6.245	5.24	9.43	9.389	0.43
2.4	3.55	3.22	9.30	6.82	6.485	4.91	9.75	9.747	0.03
2.6	3.69	3.329	9.78	7.03	6.694	4.78	10.06	10.06	0.00
2.8	3.79	3.423	9.68	7.21	6.878	4.60	10.3	10.33	-0.29

Figures 5.6 and 5.7 are presented to study the difference in the waveforms of the simulation model and actual system. The measured rotor current is presented in the figure 5.6. The comparison of the simulated and measured rotor currents reveal that the waveforms are similar and that the simulation can present the behaviour of the actual system at steady state accurately with sinusoidal supply.

The figures 5.6 and 5.7 also illustrate that the machine model is done assuming that the machine is well designed, and that the stator side does not introduce extra harmonics to the airgap. The same spikes which should be visible at the current waveform should also be visible at the voltage waveform. The simulation model containing the exciter machine and rotor circuit can be said to be accurate enough presentation from the actual asynchronous exciter at the steady state for this study if the errors due measurements, equivalent circuit parameters and simplifications in the model are taken into account in the evaluation.

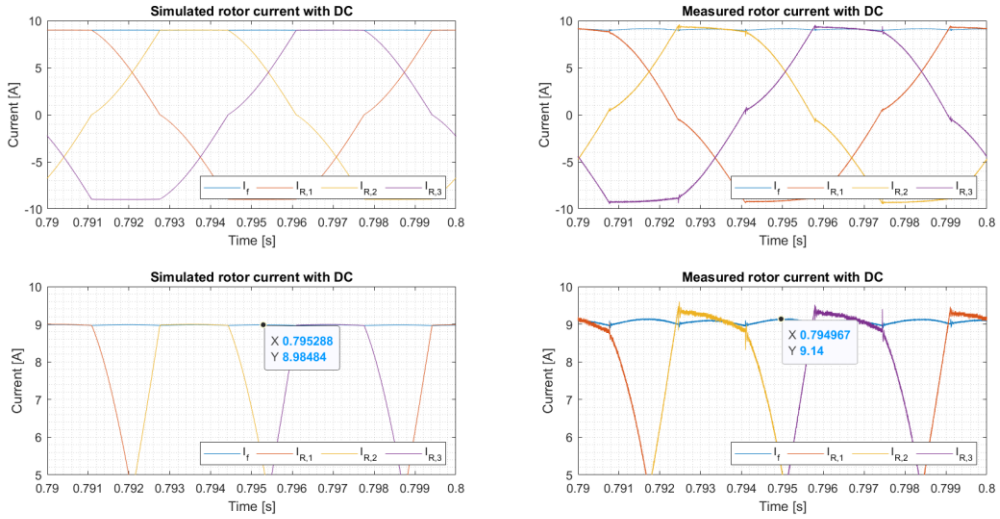

Figure 5.6 The comparison of the rotor current waveforms between the simulation model and measurements conducted with the actual system. The supplied phase voltage in this comparison was 60 Volts 50 Hz. The rotor of the asynchronous exciter was driven in opposite direction at 1500 rpm.

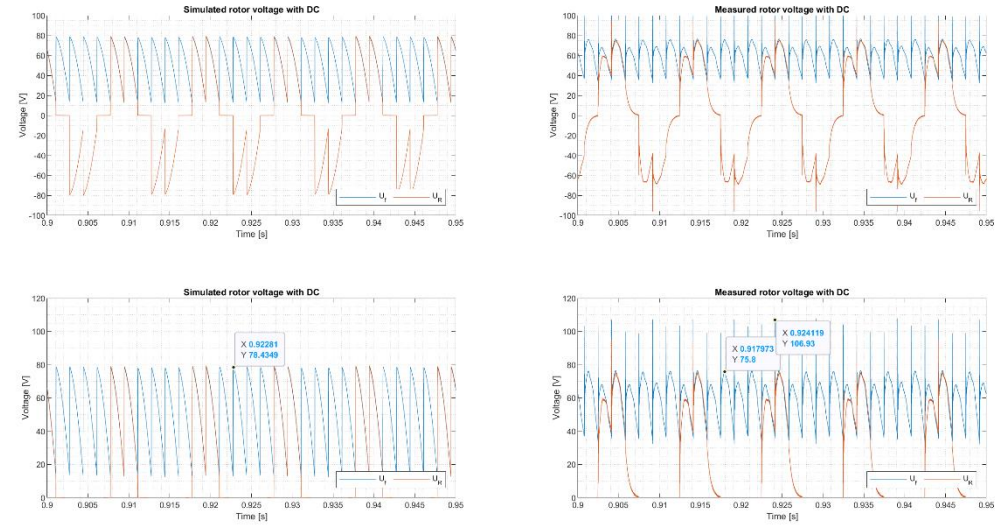

Figure 5.7 The comparison of the rotor voltage waveforms between the simulation model and measurements conducted with the actual system. The supplied phase voltage in this comparison was 60 Volts 50 Hz. The rotor of the asynchronous exciter was driven in opposite direction at 1500 rpm.

5.2.2. Verification with the frequency converter model

In the verification of the asynchronous exciter the variable frequency supply is also used to test how the model works while the supply is not sinusoidal. As with the sinusoidal supply the asynchronous exciter is supplied with different voltage levels at the steady state. The comparison between the simulation and actual system is presented in the figure 5.8 and table 5-2. With the ACS880 the control of the output voltage cannot be done independently from the frequency or the flux of the machine. For this reason, the comparison is done so that the different flux levels are given to the frequency converter and the frequency is kept constant. At each flux level the estimated output voltage from frequency converter is taken and used as an input for the simulation model. The results of the comparison are not exactly comparable to the sinusoidal measurement. The flux references were chosen so that the measurement points are similar so that the two supply methods are as comparable as possible.

In the figure 5.8 the same phenomenon continues. As with the sinusoidal supply, the nonlinear behaviour of the field current as a function of slip, is clearly visible. The error between the measured and the simulated values on the other hand does not seem to get smaller as clearly as the supply voltage is increased. The results presented in the table 5-2 show that the average error between the measured and simulated values is below 10 %. This accuracy is high enough for these research purposes. However, the error is continuously over 4 % which suggest that the model is not as accurate as with the sinusoidal measurement. This can be a result from the use of estimated supply voltage as an input for the simulation or from another error during the measurement. The error between these two supply methods is not big and can be negligible in this case.

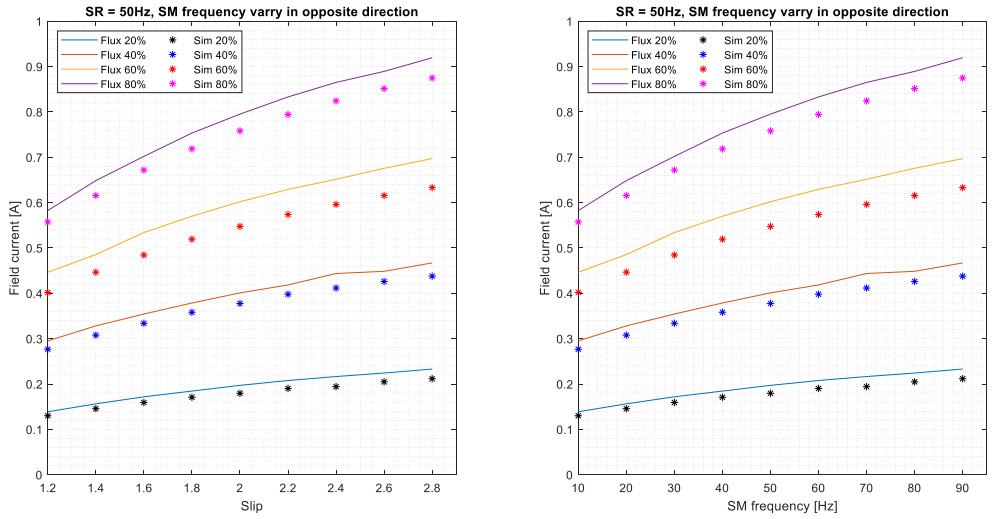

Figure 5.8 Comparison of the measured and simulated results as a function of slip and frequency of the synchronous machine. The frequency of the asynchronous exciter in this comparison is constant 50 Hz and rotating in opposite direction from the field of the synchronous machine. The voltage of the frequency converter supply was changed varying flux reference. The flux reference 20% = 23 V line-to-line, The flux reference 40% = 45 V line-to-line, The flux reference 60% = 68 V line-to-line, The flux reference 80% = 91 V line-to-line.

Table 5-2 The results from the verification of the asynchronous exciter model with sinusoidal supply. The error is calculated comparing the simulated field current to the measured value of the field current.

Slip	Flux = 20 %			Flux = 40% [V]			Flux = 60 %			Flux = 80 %		
	Meas [A]	Sim [A]	Error [%]	Meas [A]	Sim [A]	Error [%]	Meas [A]	Sim [A]	Error [%]	Meas [A]	Sim [A]	Error [%]
1.2	1.43	1.34	6.29	3.04	2.85	6.25	4.6	4.14	10.00	6	5.74	4.33
1.4	1.61	1.5	6.83	3.38	3.17	6.21	5	4.6	8.00	6.68	6.37	4.64
1.6	1.77	1.64	7.34	3.65	3.44	5.75	5.5	4.99	9.27	7.23	6.92	4.29
1.8	1.9	1.76	7.37	3.9	3.69	5.38	5.87	5.35	8.86	7.76	7.4	4.64
2	2.03	1.85	8.87	4.13	3.89	5.81	6.2	5.64	9.03	8.19	7.81	4.64
2.2	2.14	1.96	8.41	4.31	4.1	4.87	6.48	5.91	8.80	8.58	8.18	4.66
2.4	2.23	2	10.31	4.57	4.24	7.22	6.71	6.14	8.49	8.91	8.49	4.71
2.6	2.31	2.11	8.66	4.62	4.39	4.98	6.96	6.34	8.91	9.16	8.77	4.26
2.8	2.4	2.18	9.17	4.81	4.51	6.24	7.18	6.52	9.19	9.47	9.01	4.86

The rotor current of the asynchronous exciter is presented in the figure 5.9. The same phenomenon can be observed with the frequency converter supply as with sinusoidal. The measured waveform contains a lot more harmonic components compared to the simulated waveform. The waveform of the simulation is identical to the sinusoidal supply.

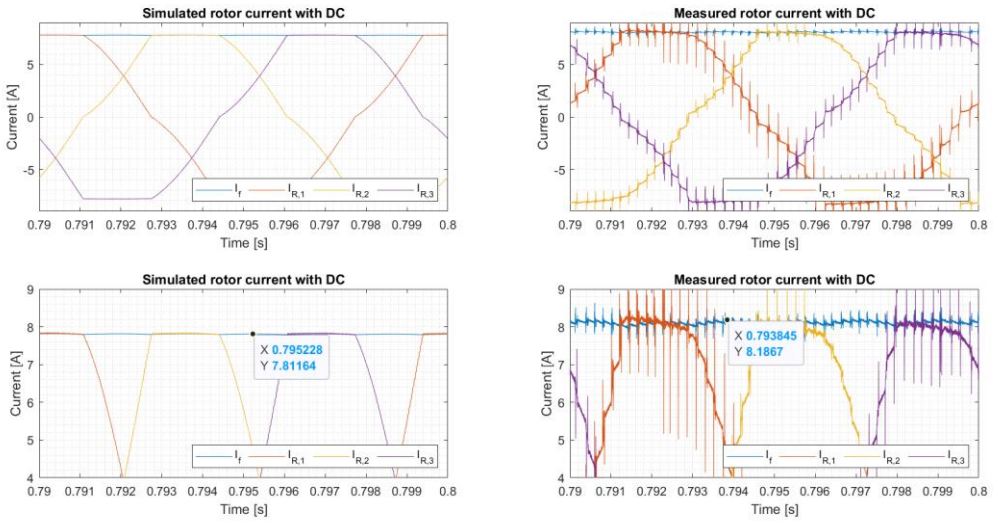

Figure 5.9 The comparison of the rotor current waveforms between the simulation model and measurements conducted with the actual system. The supplied line-to-line voltage in this comparison was 91 volts which is flux reference 80 % with frequency reference 50 Hz. The rotor of the asynchronous exciter was driven in opposite direction at 1500 rpm.

The voltage waveform of the rotor is presented in the figure 5.10. The voltage waveform of the rotor from the simulation model is not that similar compared to the measured waveform. The simulation does not take into account the nonlinear or nonideal behaviour of the actual circuit. The simulation model seems to assume that the voltage can be changed like an ideal step when voltage waveform goes from positive to negative half cycle or vice versa. The same observation can be made from figure 5.7. In real machine the voltage cannot be changed like an ideal step. The rotor leakage inductance induces voltage to oppose the change, when flux penetrating the rotor winding changes, slowing the voltage rise time in the rotor circuit.

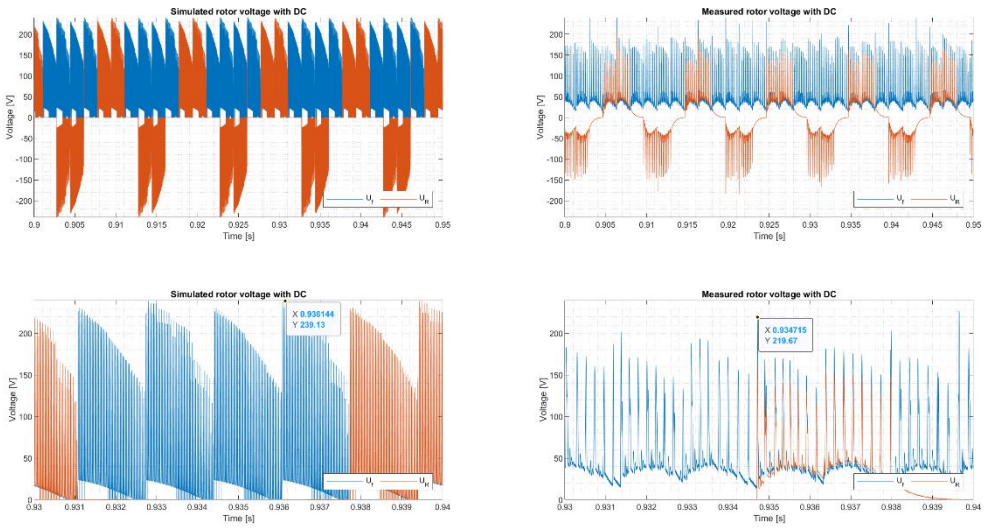

Figure 5.10 The comparison of the rotor voltage waveforms between the simulation model and measurements conducted with the actual system. The supplied line-to-line voltage in this comparison was 91 volts which is flux reference 80 % with frequency reference 50 Hz. The rotor of the asynchronous exciter was driven in opposite direction at 1500 rpm.

To evaluate how well the simulation model copes with transient situation compared to the real system, decay test was done to the system. The decay test was done by raising the field current to 9.38 amperes and by cutting off the supply of the asynchronous exciter. In the laboratory measurement the frequency converter was given command to stop modulating.

The results from the measured and simulated tests are presented in the figure 5.11. The time constant for the system calculated from the measured responses was from 100 to 105 milliseconds. The time constant calculated from the simulated result was around 120 milliseconds, which is almost exactly the time constant that can be calculated from parameters of field winding using equation 2.1. The difference between these two is around 20 milliseconds, which is large. Some of the difference could come from parameters such as resistances. In this thesis the root cause cannot be determined and it requires further study.

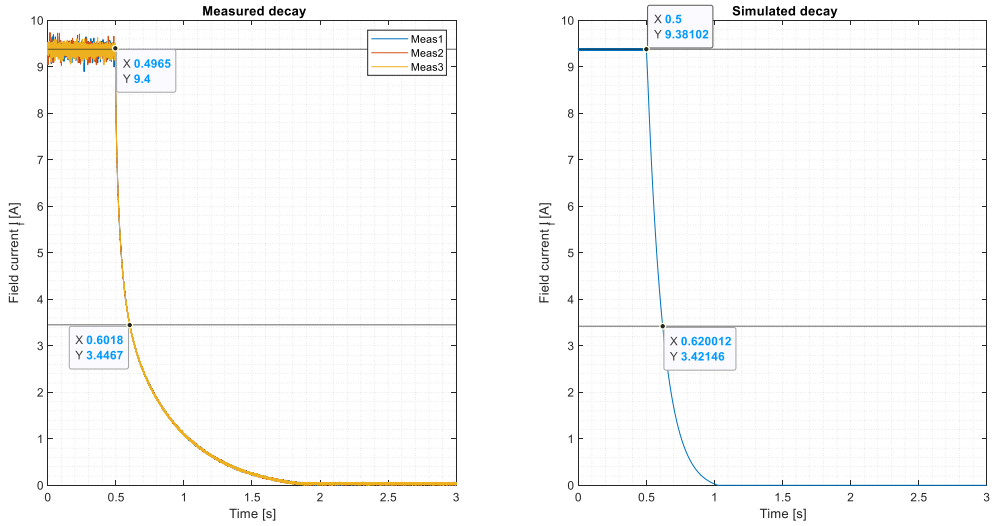

Figure 5.11 The comparison between measured and simulated current decays from frequency converter supplied system. The field current was set to 9.38 amperes and the supply was stopped while the rotor rotates at 1500 rpm.

If the decay curve is inspected visually, it is clear that the current in the actual field winding takes more time to reach zero compared to the simulation. This means that the actual system has more energy stored at the inductances. Because this decay relays on the natural fall of the current, it does not fall to zero as quickly. As it was mentioned earlier with the rotor voltage waveform the behaviour of the leakage inductances does not match with the actual system. This could be the reason explaining the difference in the behaviour of the field winding and rotor.

5.3. Implementation of control methods with ACS880

The control methods chosen to the implementation based on the simulation results use constant current transformation ratio between stator and field current of the main machine to estimate the field current. Both control methods use flux control as in the study of Ahonen et al. (2013), the algorithm is the same from that perspective. Algorithm with constant frequency and constant slip frequency were built into ACS880 frequency converter using drive application programming. The program has been presented in the figure 5.12.

```
PROGRAM PLC_PRG
VAR
    (* General variables and constants*)
    IF_ref      : REAL;         (* Current reference from system above *)
    Fslip       : REAL := 100;  (* Constant slip frequency *)
    MainField   : REAL;         (* Frequency of the rotor *)
    Is          : REAL;         (* Stator current*)
    pole        : INT := 2;     (* Number of pole pairs *)
    In          : REAL := 4.5;  (* Nominal stator current *)
    IfTOIs      : REAL := 2.58; (* Current transformation ratio*)

    (* Parameters for PID controller *)
    Controller  : PID;
    P           : REAL := 10;   (* Proportional gain *)
    I           : REAL := 0.5;  (* Reset time I in sec *)
    D           : REAL := 0;    (* Derivation time in sec *)
    LimitHIGH   : REAL := 1.5;
    LimitLOW    : REAL := 0.05;
END_VAR
```

```

FreqRef := 50;

(*MainField := pole*Device_Encoder_1_speed_filtered_1_4/60;
FreqRef := Mainfield + Fslip;*)

IF_ref := ((Device_FB_A_reference_1_3_5)/IfTOIs)/In;
Is := Device_Motor_current_1_7/In;

(* Current controller *)
Controller(
    ACTUAL := Is,
    SET_POINT := IF_ref,
    KP := P,
    TN := I,
    TV := D,
    Y_MANUAL := 0,
    Y_OFFSET := 0,
    Y_MIN := LimitLOW,
    Y_MAX := LimitHIGH,
    MANUAL := FALSE,
    RESET := FALSE,
);
FluxRef := Controller.Y*100;

```

Figure 5.12 Implementation of control methods with Drive application programming. The control method is changed by changing the way how the FreqRef variable is getting its value.

The basic principle of this program is that the PI-controller calculates flux reference to the scalar control of the frequency converter based on current feedback measured by the ACS880. The supply frequency is kept at constant 50 Hz or controlled based on the speed feedback as in simulation model presented in section 4.3.1. The field current reference is given to the algorithm through EtherCAT fieldbus, and that reference has been converted to stator current dividing with current transformation ratio of 2.58. An example of determining the current transformation ratio is given in Appendix VI. Before current reference is fed to the PI-controller, it is transformed into per-unit values as is done to the measured stator current. The output of the PI-controller is multiplied with 100 to convert the output into percentages.

5.3.1. Parameterization of ACS880

The ACS880 frequency converter must be parametrized to carry on field current control. The parameter list of ACS880 can be found from ACS880 firmware manual ABB (2012). For the parametrization of the ACS880 supplying the asynchronous exciter, custom parameter group 9 was created to act as a link between the drive application program and internal control of the ACS880. In this parameter group two parameters FluxRef and FreqRef were created. User motor model was not used in the parameter group 98 User motor parameters.

The parametrization of the slip ring machine is presented in the table 5-3. The machine parameters are the same as presented in the nameplate at Appendix I, except the nominal voltage of the machine. The nominal voltage is reduced because this allows the use of whole flux reference scale of the frequency converter 0-100 %. If the real nominal voltage is given, the range is from 0-30 % where 30 % means that at nominal frequency, rotated at 1500 rpm, the field current gets its nominal value. With the rotor circuit connected to the rotor of the slip ring machine, the nominal current 4.5 amperes of the slip ring machine is not reached, because the nominal current of the load is reached around 4-4.1 amperes in the slip ring machines stator.

In the table 5-4 the key parameters used to link the control implemented with application programming and internal control trees of the ACS880 basic firmware are presented. The flux reference and frequency references written in the parameter group 9 must be linked with

the Motor control, frequency and speed reference chains. The final table 5-5 presents the configuration of the EtherCAT fieldbus from the frequency converter side.

Table 5-3 Motor parameters given to ACS880 frequency converter which it uses to determine U/f curve and bases the control when scalar control is used.

Parameter group 99. Motor data	
99.03 Motor type	Asynchronous motor
99.04 Motor control mode	Scalar
99.06 Motor nominal current	4.5 A
99.07 Motor nominal voltage	113 V
99.08 Motor nominal frequency	50 Hz
99.09 Motor nominal speed	1400 rpm
99.10 Motor nominal power	1.8 kW
99.11 Motor nominal cos φ	0.8
Parameter group 30. Limits	
30.11 Minimum speed	-3000 rpm
30.12 Maximum speed	3000 rpm
30.13 Minimum frequency	-300 Hz
30.14 Maximum frequency	300 Hz

Table 5-4 Linking the control trees of the ACS880 basic firmware and the parameters of application programming.

Parameter group 97. Motor control	
97.06 Flux reference select	User flux reference
97.07 User flux reference (min = 0, max 200%)	P.9.1 (FluxRef)
Parameter group 19. Operation mode	
19.20 Scalar control reference unit	Hz
Parameter group 28. Frequency reference chain	
28.11 Frequency ref1 source	P.9.2 (FreqRef)
Parameter group 22. Speed reference selection	
22.11 Speed ref1 source	P.9.2 (FreqRef)

Table 5-5 Parameter configuration to establish EtherCAT fieldbus communication with AC500.

Parameter group 50. Fieldbus adapter (FBA)	
50.04 FBA ref1 type	General
50.05 FBA ref2 type	General
50.07 FBA A 1 actual type	Transparent
Parameter group 51. FBA A settings	
51.01 FBA A type	EtherCAT
51.02 Profile	ABB Drives

5.4. Algorithm testing, results and analysis

The step response test was conducted by giving the ACS880, supplying the slip ring motor, field current references from 0 to 1 p.u with 0.1 p.u step, using AC500 PLC as presented in figure 5.2. The AC500 also gave signal to trigger the digital input/output (DIO) port of the ACS880 to pinpoint that the field current reference was changed at a certain moment. The DIO port was connected to the Yokogawa DL850 and the signal was monitored during whole test. The frequency reference given to the ACS880 was constant 50 Hz. The shaft of the asynchronous exciter was rotated at nominal speed of the emulating asynchronous machine, 1500 rpm, in opposite direction than the stator field of the asynchronous exciter. The sample rate of Yokogawa was set to 2 kHz. This sample frequency is sufficient to study phenomena to nearest millisecond.

The accuracy test was performed so that the speed ramp of ACS880 controlling the rotating asynchronous machine was set to 450 seconds. When tested, this ramp accelerated the shaft into 1500 rpm in 225 seconds, which was close enough to simulation and real application to do this accuracy test. The angular velocity of the rotor was monitored with ABB drive composer software, using incremental encoder connected to the ACS880 supplying the exciter machine. The monitored rotational speed and the field current were synchronized using DIO ports of the ACS880 frequency converters. When AC500 gave start command for the ACS880 supplying the emulator machine, the DIO port of the ACS880 gave trigger signal for the Yokogawa DL850 which was monitored at the scope view of the measurement device as well as the current. The same trigger signal was also sent to DIO port of the ACS880 supplying the excitation machine. The DIO port was then monitored with drive

composer so that the two datasets could be synchronized. Sample frequency in this study is set to 200 Hz, because the phenomena studied are slow.

The measured field current is noisy and before any calculation and analysis the noise is removed from the data. The removal is performed by Smooth function of MATLAB®. The smoothing method used in the data processing, uses local regression with linear least squares and a polynomial model of 2nd degree. In the step response test the smoothing was done with 5 % span and in the accuracy test span was 10 % of the total number of data points.

5.4.1. Step response test: Flux control with constant frequency

In the first step response test the parameter LimitHigh of the current controller presented in figure 5.12, was set to 10 = 1000 %. Other parameters of the controller are kept as in the figure 5.12. This limit is higher than the maximum allowed flux reference in the ACS880 as presented in table 5-4. The limit is high to study if ACS880 limits the response when controller is parameterized as in figure 5.12. The results of the step response test are presented in the table 5-6 and couple of field current waveforms are presented in the figure 5.13.

The three measurements conducted indicate that the test was successful and repeatable, the results of each test at same operational points were similar. The rise times and overshoot percentages between measurements at same measurement points are close to each other. The average rise time for the excitation system, presented in figure 5.2, is around 145 milliseconds and overshoot at its maximum is 27.4 %. These results show that the flux control fulfils the set performance objective for a rise time of 0.2-0.5 seconds.

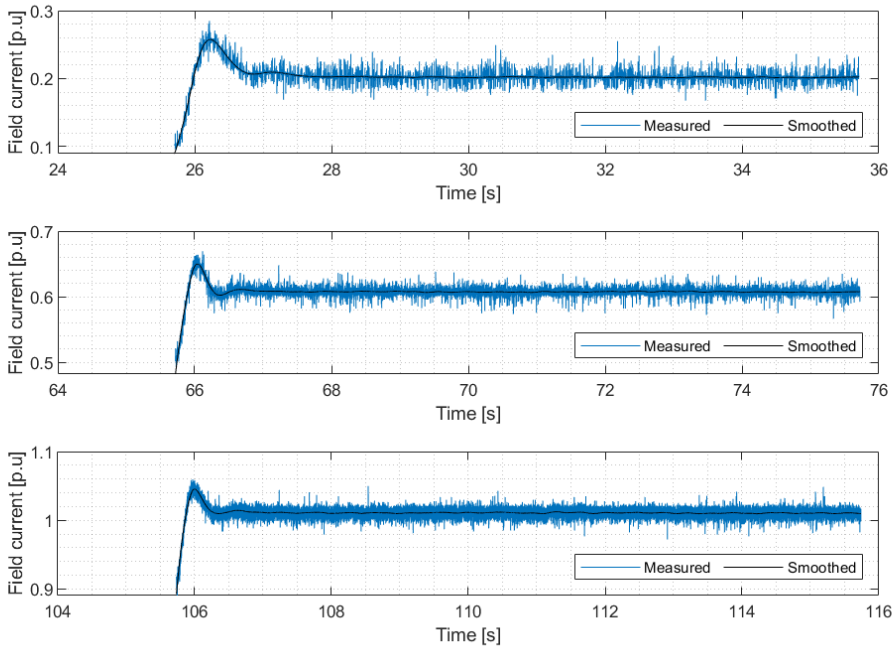

Figure 5.13 The smoothed waveform calculated from the measured waveform. Measurement points presented are steps from 0.1 to 0.2, 0.5 to 0.6 and 0.9 to 1 p.u.

Table 5-6 Rise times and overshoot percentage of the measured field current response during staircase step response test, while LimitHigh is set to 10. The results of the three step response tests are presented and average of the nine steps are presented. Example calculation is presented at Appendix IV.

Step [p.u]	Measurement 1		Measurement 2		Measurement 3	
	Rise time [ms]	Overshoot [%]	Rise time [ms]	Overshoot [%]	Rise time [ms]	Overshoot [%]
0.1 to 0.2	197	27.4	197	26.6	197	27.2
0.2 to 0.3	192	17.7	188	17.8	189	17.4
0.3 to 0.4	169	12.9	167	13.3	167	13.1
0.4 to 0.5	145	9.3	147	8.9	148	9.1
0.5 to0.6	133	7.2	131	7.0	131	7.0
0.6 to 0.7	122	5.5	123	5.3	123	5.6
0.7 to 0.8	118	4.9	121	4.7	115	4.5
0.8 to 0.9	115	4.1	115	4.1	115	3.8
0.9 to 1	113	3.3	117	3.3	111	3.5
AVG	144.7		145.1		144	

From the step response data, the time constant of the excitation system was determined at each measurement point. The results are presented in the table 5-7. There is no major variation in the time constants between different measurements, the average time constant of all measurements is close to 110 milliseconds. The time constant determined from the decay test was 5 to 10 milliseconds smaller. In the step response test the time constants between measurement points vary a lot and decrease while the field current increases. The averaged time constant from the forced step responses can be considered as a reliable estimate because the difference between result of decay test is not large.

Table 5-7 Time constants calculated of the measured field current response during staircase step response test, while LimitHigh is set to 10. The results of the three step response tests are presented and average of the nine steps are presented. Example calculation is presented at Appendix IV.

Step [p.u]	Measurement 1	Measurement 2	Measurement 3
	τ'_{d0} [ms]	τ'_{d0} [ms]	τ'_{d0} [ms]
0.1 to 0.2	169	171.5	168.5
0.2 to 0.3	160	159.5	158
0.3 to 0.4	136	133	132
0.4 to 0.5	108	110.5	110.5
0.5 to0.6	96	95.5	94.5
0.6 to 0.7	87	88	87
0.7 to 0.8	84	86	81.5
0.8 to 0.9	81	81	80.5
0.9 to 1	79	81	77
AVG.	110.8	111.8	109.9

The same measurement was repeated and in the second test the LimitHigh was set to 1.5 = 150 %. The limiting component in this measurement was the current controller. Results of this measurement are presented in tables 5-8 and 5-9. The average rise time of the system was around 165 milliseconds and the average time constant between 122-135 milliseconds. Even though the system becomes 20 milliseconds slower, the performance objective was reached.

Table 5-8 Rise times and overshoot percentage of the measured field current response during staircase step response test, while LimitHigh is set to 1.5. The results of the three step response tests are presented and average of the nine steps are presented. Example calculation is presented at Appendix IV.

Step [p.u]	Measurement 1		Measurement 2		Measurement 3	
	Rise time [ms]	Overshoot [%]	Rise time [ms]	Overshoot [%]	Rise time [ms]	Overshoot [%]
0.1 to 0.2	195	27.2	185.5	27.3	194.5	27.7
0.2 to 0.3	190	18.0	180	17.6	188.5	17.1
0.3 to 0.4	169	13.2	164	13.1	164.5	13.1
0.4 to 0.5	145	9.0	147.5	9.4	144.5	9.3
0.5 to0.6	132	6.7	135.5	7.1	134	6.7
0.6 to 0.7	132	4.7	140	4.3	131.5	4.7
0.7 to 0.8	147	2.1	151	2.1	146.5	2.5
0.8 to 0.9	168	0.6	171	0.6	173	0.3
0.9 to 1	201	0.1	212	0.1	212.5	0.2
AVG	164.3		165.2		165.5	

Table 5-9 Time constants calculated of the measured field current response during staircase step response test, while LimitHigh is set to 1.5. The results of the three step response tests are presented and average of the nine steps are presented. Example calculation is presented at Appendix IV.

Step [p.u]	Measurement 1	Measurement 2	Measurement 3
	τ'_{d0} [ms]	τ'_{d0} [ms]	τ'_{d0} [ms]
0.1 to 0.2	168	175	169
0.2 to 0.3	159	166	159
0.3 to 0.4	136	148	131
0.4 to 0.5	108.5	125	109
0.5 to0.6	96	108	97
0.6 to 0.7	94	102	93
0.7 to 0.8	101.5	114	100
0.8 to 0.9	111.5	128	114
0.9 to 1	126	148	131
AVG.	122.3	135.1	122.5

Figure 5.14 presents the flux references calculated by the current controller, during the step response test. Figure 5.14 shows the reason for the slower response when output of the current controller was limited to 150 %. In tables 5-6 and 5-8 the rise time is almost the same

before step from 0.5 to 0.6. After this point the current controller reaches the limit and as a result the rise time becomes slower. When LimitHigh was set to 10, flux reference rises over the 150 % at higher field current references, enabling smaller rise time. The flux reference limit of the ACS880 is not reached at any measurement point. The field current waveforms from the measurements are presented in figure 5.15. Field current waveforms are similar. Figures 5.14 and 5.15 show that the system is stable. The excitation system produces a bounded output for a given bounded input, with flux control method.

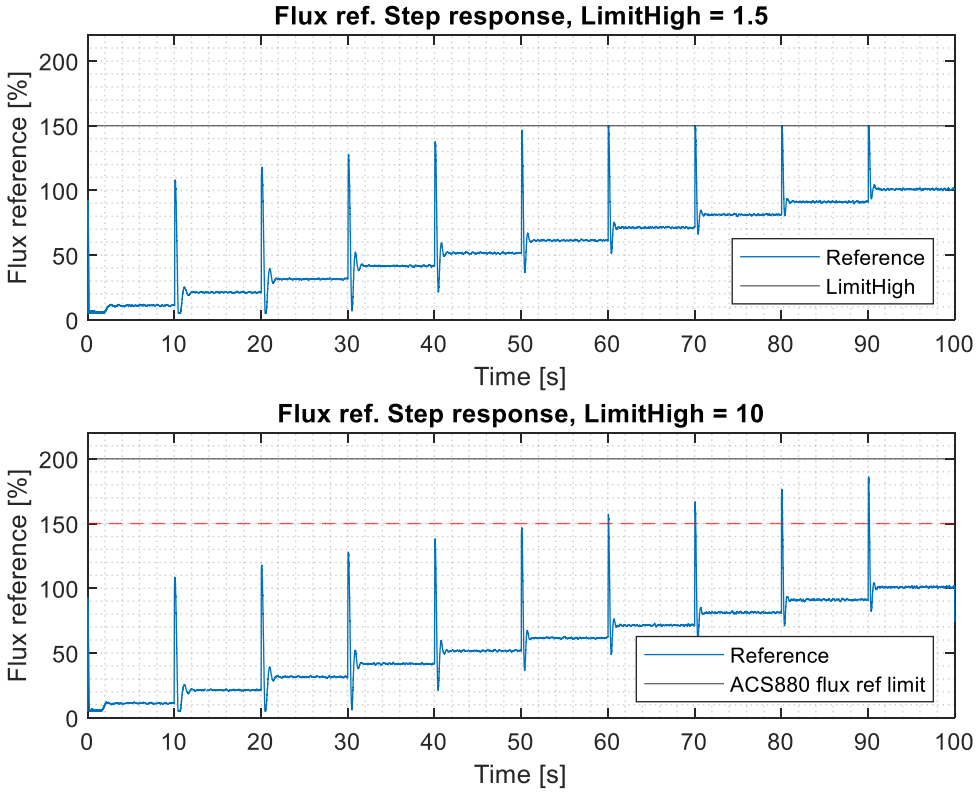

Figure 5.14 Flux reference calculated by the current controller. When current controller is limited below the limit of ACS880, the limit is reached and output of the controller is reduced. The flux reference limit of ACS880 is high enough that it is not reached during these measurements.

When the LimitHigh was 1.5 the current spike during start of the asynchronous exciter was reduced from 1.7 p.u to 1.3 p.u. Because the current spike was reduced significantly and performance criteria was met by limiting the output of the current controller, the LimitHigh was kept at 1.5 during the acceleration test.

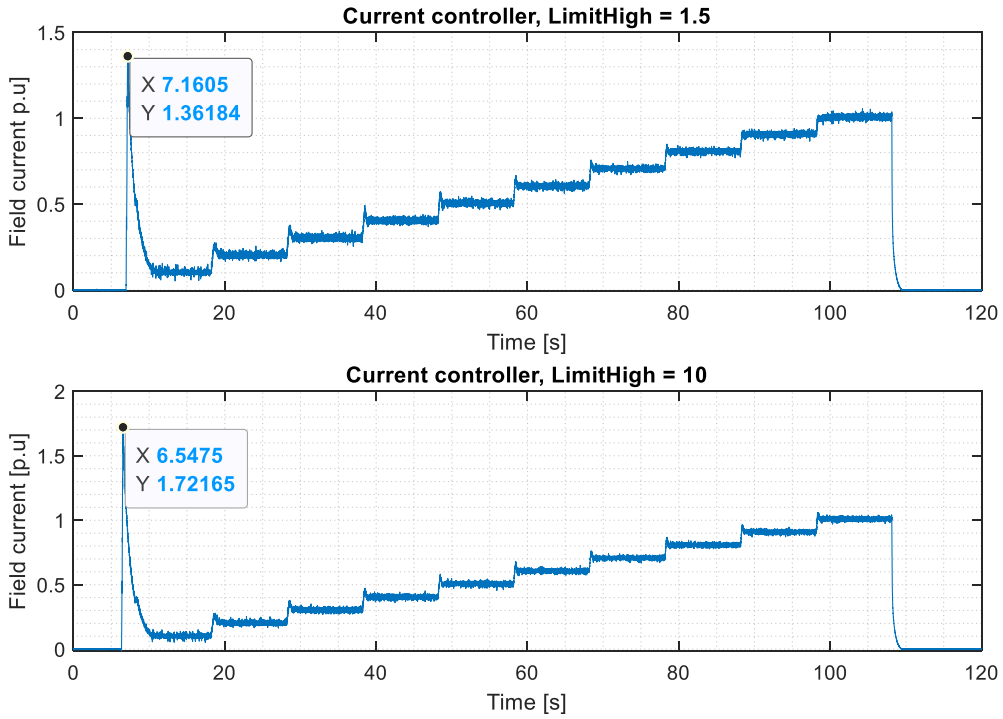

Figure 5.15 Field current waveforms from step response test with LimitHigh as 1.5 and 10.

The results from step response measurements are entirely different than those which were gathered from the simulation. The time constant of the system is almost 100 milliseconds longer in the actual system compared to the simulation. The average rise time is almost 120 milliseconds longer in the real system. Differences between the actual system and simulation models are expected, but these differences are so vast that this could not be explained just with minor inaccuracies between the parameters of simulation model and actual system. The control of flux and frequency in the ACS880 contains much more nuanced control loops which are embedded to the drive software. Those loops were not built into simulation model. This could be one reason for the difference in measured and simulated results. As discussed during the model verification, the most probable cause is the modelling of effects from leakage fluxes.

5.4.2. Accuracy test: Flux control with constant frequency

The flux control algorithm with constant frequency is the first algorithm which accuracy is tested. The current controller was parametrized as in the figure 5.12. The tests are conducted

with the same current reference levels as was done in the simulation at section 4.4.2. The results of each test are illustrated in the figures 5.17 to 5.19. The field current at different rotational speeds are presented in the tables 5-10 to 5-12.

From each of the figures the same behaviour can be observed. The current in the field winding increases as the rotor accelerates. The increase happens due steadily increasing slip during acceleration. With the current references 0.2 p.u and 0.5 p.u the control system can follow the current reference with sufficient accuracy. The measurement with smaller current reference had more inaccuracy and the error at the end of the ramp was around 3 % compared to the 2 % of the 0.5 reference. These errors are minor and negligible.

With the current reference 1 p.u the system was able to follow the field current reference accurately around 1 % at every other point except with zero speed. At zero speed the difference was in the range of 12 to 14 %. The behaviour of the current controller during acceleration at 1 p.u reference is presented at figure 5.16.

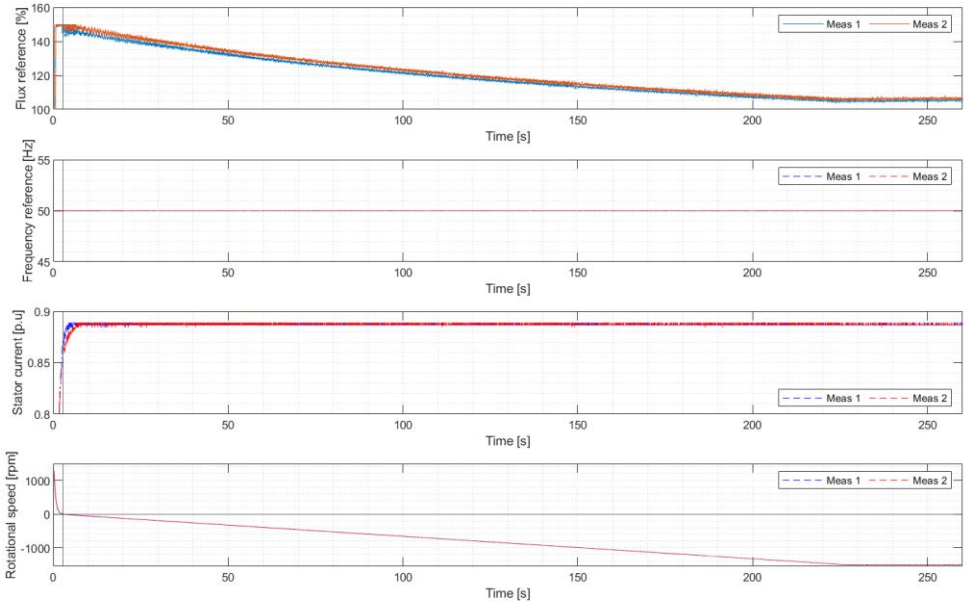

Figure 5.16 The flux reference, supply frequency and stator current during the acceleration. The field current reference during acceleration was 1 p.u and frequency reference was 50 Hz. Black line marks the time when rotational speed is zero. The flux reference hits the limiter when main machine is started and stops the shaft.

The current control loop can keep the stator current supplied to the asynchronous exciter constant during the acceleration. At zero speed the stator current does not reach the constant value of 0.89 p.u which is kept during the acceleration. While the rotor accelerates, the current controller decreases the flux reference to keep the stator current constant. The current control loop cannot compensate the effects of increasing slip and slip frequency, because there is no estimator that would help to compensate the effects of slip and slip frequency from the estimated field current. Nevertheless, this method can still control the field current with good accuracy. The flux reference reaches the limit of 150 % at zero speed. Limiting the current controller output affected the capability to supply field current at zero speed. Appendix V presents the result of the same measurement with LimitHigh at 10. The error at zero speed was reduced to around 5 %, but still the field current supplied was not high enough to remove the error.

In these measurements the slip ring machine can rotate the shaft before the asynchronous machine is started. During the data processing the value of the field current is taken at the point where rotational speed is zero. In the tests with 0.5 p.u and 1 p.u reference, at zero speed field current cannot be entirely trusted because the current is still decreasing from the inrush which happens when main machine starts to rotate in different direction. All in all, the results prove that this control method would be suitable for the application where direct online synchronous motors are started with load commutating inverter. Only possible weakness is the nominal field current at zero speed.

When the measured and simulated results are compared, same kind of phenomena can be observed from the calculated results and waveforms. The error between the reference and actual value are in the same range except in real system, where the field current was continuously higher than the reference unlike in the case of simulation it was under. The only major difference with the simulation and measurement was the zero speed with 1 p.u reference. At this point the simulation had 5 % error and in actual system almost 12-14 %. The simulation model was good enough to calculate similar results as in these measurements. The model has its shortcomings and it should be developed if more accurate results are needed. For this study it gave sufficiently accurate information about the accuracy and behaviour of this control method.

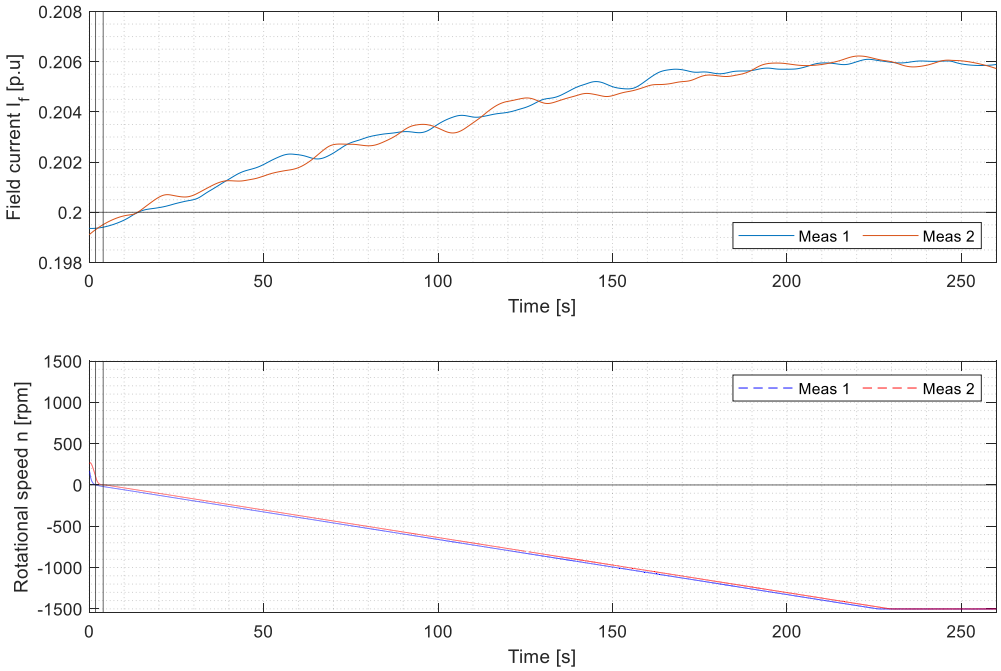

Figure 5.17 Behaviour of the field current with flux control with constant frequency as the main machine accelerates and field current reference is 0.2 p.u. The rotational speed is negative because the rotor is rotating at different direction than the stator field of exciter machine.

Table 5-10 The results from the accuracy test of flux control with constant frequency with field current reference 0.2 p.u. The test was done twice. From both measurements actual field current in p.u values has been presented as well as error to the reference.

	Measurement 1		Measurement 2	
Ref [p.u]	0.2		0.2	
Speed [rpm]	Actual [p.u]	Error [%]	Actual [p.u]	Error [%]
0	0.199	0.32	0.200	0.22
250	0.212	-5.99	0.201	-0.62
500	0.203	-1.41	0.203	-1.33
750	0.204	-1.92	0.204	-2.14
1000	0.205	-2.48	0.205	-2.41
1250	0.206	-2.82	0.206	-2.91
1500	0.206	-3.02	0.206	-3.00

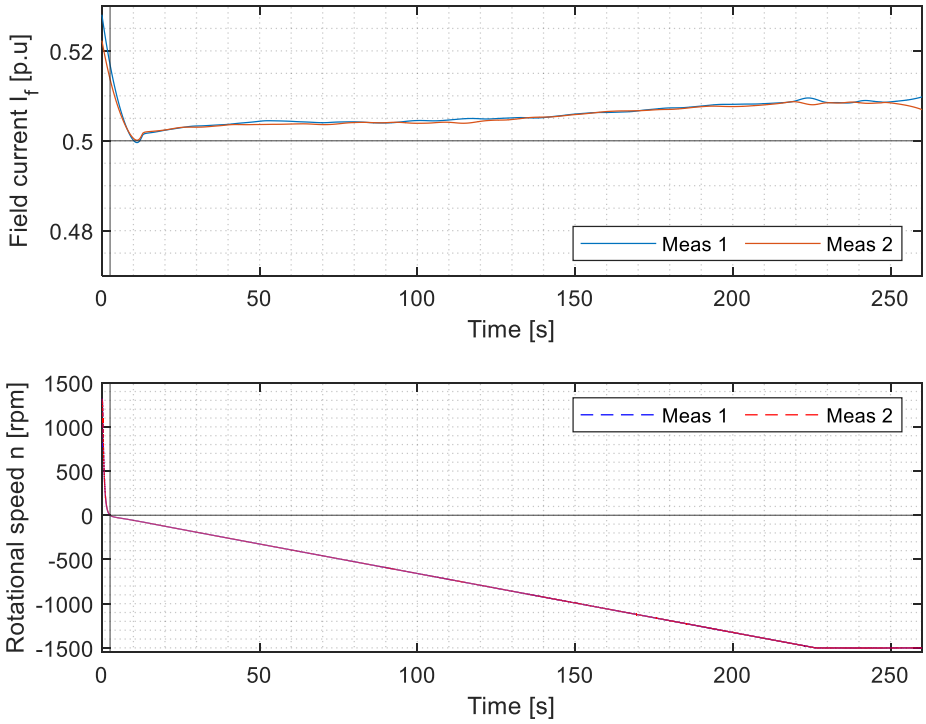

Figure 5.18 Behaviour of the field current with flux control with constant frequency, as the main machine accelerates and field current reference is 0.5 p.u. The rotational speed is negative because the rotor is rotating at different direction than the stator field of exciter machine. Black line marks the time when zero speed is reached.

Table 5-11 The results from the accuracy test of flux control with constant frequency with field current reference 0.5 p.u. The test was done twice. From both measurements actual field current in p.u values has been presented as well as error to the reference.

	Measurement 1		Measurement 2	
Ref [p.u]	0.5		0.5	
Speed [rpm]	Actual [p.u]	Error [%]	Actual [p.u]	Error [%]
0	0.517	-3.38	0.514	-2.71
250	0.504	-0.72	0.503	-0.69
500	0.504	-0.84	0.504	-0.77
750	0.505	-0.97	0.504	-0.78
1000	0.506	-1.20	0.506	-1.18
1250	0.508	-1.53	0.508	-1.50
1500	0.509	-1.83	0.508	-1.62

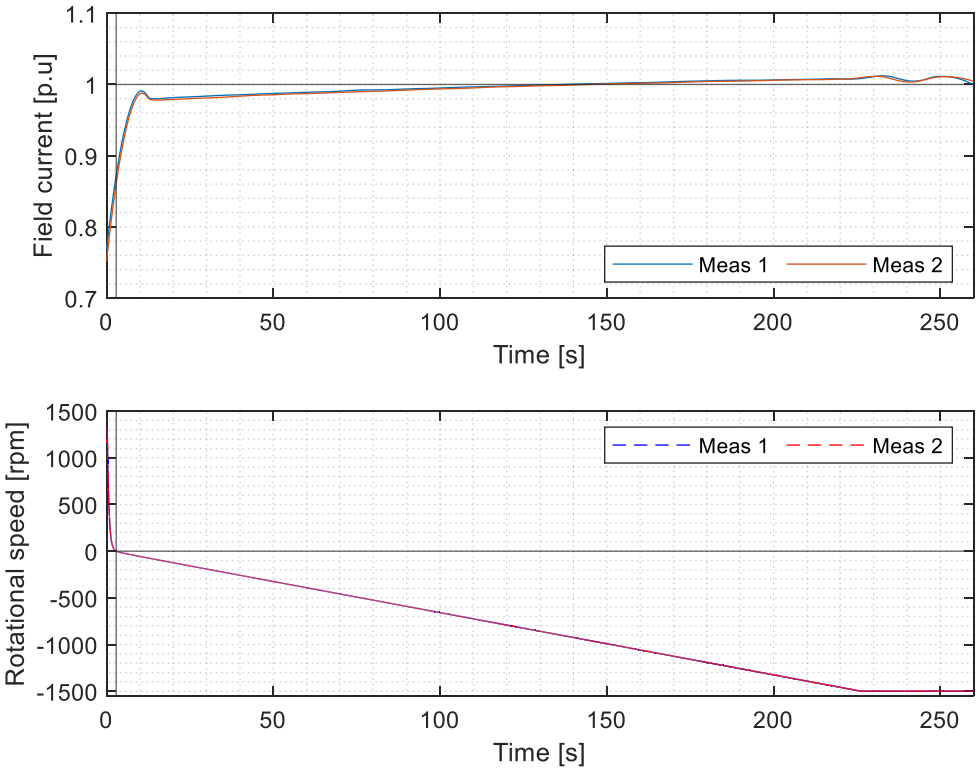

Figure 5.19 Behaviour of the field current with flux control with constant frequency as the main machine accelerates and field current reference is 1 p.u. Black line marks the time instant when zero speed is reached. The rotational speed is negative because the rotor is rotating at different direction than the stator field of exciter machine.

Table 5-12 The results from the accuracy test of flux control with constant frequency with field current reference 1 p.u. The test was done twice. From both measurements actual field current in p.u values has been presented as well as error to the reference

	Measurement 1		Measurement 2	
Ref [p.u]	1		1	
Speed [rpm]	Actual [p.u]	Error [%]	Actual [p.u]	Error [%]
0	0.878	12.17	0.861	13.90
250	0.986	1.42	0.983	1.74
500	0.992	0.79	0.988	1.16
750	0.997	0.28	0.995	0.54
1000	1.001	-0.12	0.999	0.05
1250	1.005	-0.49	1.004	-0.37
1500	1.004	-0.43	1.002	-0.22

5.4.3. Accuracy test: Flux and constant slip frequency control

The second control algorithm tested was the flux control with constant slip frequency. In this acceleration test the reference for the slip frequency was set at 100 Hz as was done with the simulation. The current controller was parametrized as in the figure 5.12. The tests were conducted with the same current reference levels as was done in the simulation and test of flux control with constant frequency. The results of each test are illustrated in the figures 5.21 to 5.23. The field current at different rotational speeds are presented in the tables 5-13 to 5-15.

If the results of the measurement with the field current reference 0.2 p.u and 0.5 p.u are observed, it is clear that the error in both cases is reducing while the machine accelerates. At the end of the acceleration the error is small, between 1 to 3 %. The maximum error with this method is almost 6 % at small rotational speeds and current references at zero speed. The measurement with field current reference 1 p.u has similar results as with smaller field current references: at zero speed the error is from 3 to 5.4 %, at the end of the acceleration the error is around 1 %. At zero speed results are not entirely reliable, because the asynchronous exciter was able to rotate the shaft before the main machine was started, although it gives an indication that the accuracy at zero speed is increased compared to the section 5.4.1, which suffered from the same problem. If tables 5-10, 5-11, 5-13 and 5-14 are compared, the results are similar at every measurement point. The results suggest that the current control with constant supply frequency is even more accurate with field current references 0.2 p.u and 0.5 p.u. The difference in accuracy is small and almost negligible.

The behaviour of the current control and frequency control loops is presented in the figure 5.20. Current control loop can follow the current reference as accurately at the zero speed as in section 5.4.1. The stator current supplied to the asynchronous exciter stays at constant 0.89 p.u, during the acceleration. The notable difference is that the stator current at zero speed reaches the value of 0.89 p.u. The frequency control loop decreases the supply frequency linearly during the acceleration. The current controller increases the flux reference to keep the stator current constant, while the output frequency decreases. The decrease of the field current during acceleration comes from the decreasing supply frequency because the slip increases during the ramp and stator current is kept constant.

This control method does not eliminate the error but reduces its effects at 1 p.u field current reference and at zero speed due higher supply frequency, as can be observed from the figure 5.23. The error could be compensated if the current control loop and frequency control loop would work together. In this study those control loops are individual loops without connection to each other and some error always occurs.

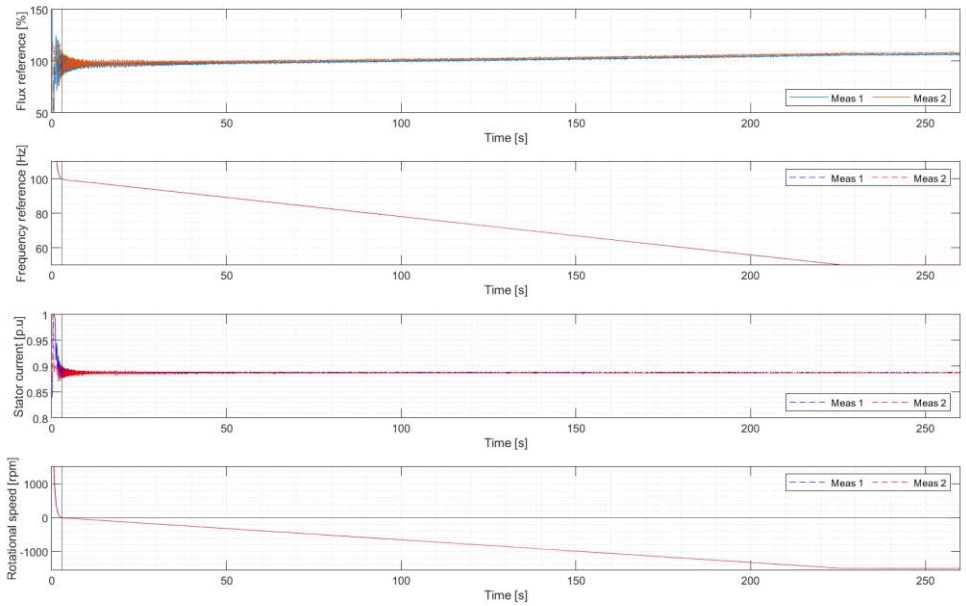

Figure 5.20 The flux reference, supply frequency and stator current are presented during the acceleration. The field current reference during acceleration was 1 p.u and slip frequency reference was 100 Hz. Black line marks the time instant when zero speed is reached. The rotational speed is negative because the rotor is rotating at different direction than the stator field of exciter machine.

While the rotor accelerates, the frequency of the asynchronous exciter supply is decreasing to keep the slip frequency as a constant based on the equation 3.3. According to simulation the field current should be at its highest value at zero speed and it should slowly reduce towards the end of the acceleration due lower supply frequency. The reduction of the field current is clearly visible from all the measurements at figures 5.21 to 5.23. This result suggest that the simulation model was able to describe the behaviour of the system during acceleration even though the model was not performing optimally and had some errors. The measurements done for the system gave constantly field current values which were higher

than the actual reference in contrast to the simulation which gave smaller values. This can be result of inaccuracies between the model and actual system.

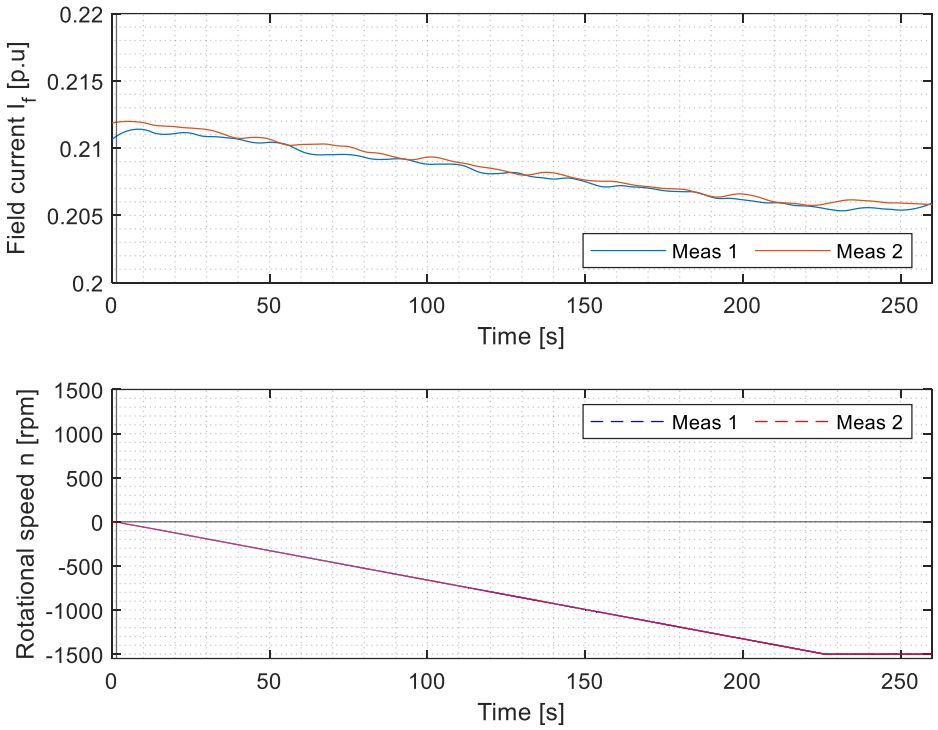

Figure 5.21 Behaviour of the field current with flux control with constant slip frequency, as the main machine accelerates and field current reference is 0.2 p.u. The waveforms of two measurements are presented. Black line marks the time instant when zero speed is reached. The rotational speed is negative because the rotor is rotating at different direction than the stator field of exciter machine.

Table 5-13 The results from the accuracy test of flux control with constant slip frequency with field current reference 0.2 p.u. The test was done twice. From both measurements actual field current in p.u values has been presented as well as error to the reference.

	Measurement 1		Measurement 2	
Ref [p.u]	0.2		0.2	
Speed [rpm]	Actual [p.u]	Error [%]	Actual [p.u]	Error [%]
0	0.211	-5.44	0.212	-5.95
250	0.211	-5.36	0.211	-5.40
500	0.209	-4.75	0.210	-5.03
750	0.209	-4.25	0.209	-4.39
1000	0.207	-3.72	0.208	-3.80
1250	0.206	-3.24	0.206	-3.25
1500	0.205	-2.74	0.206	-2.94

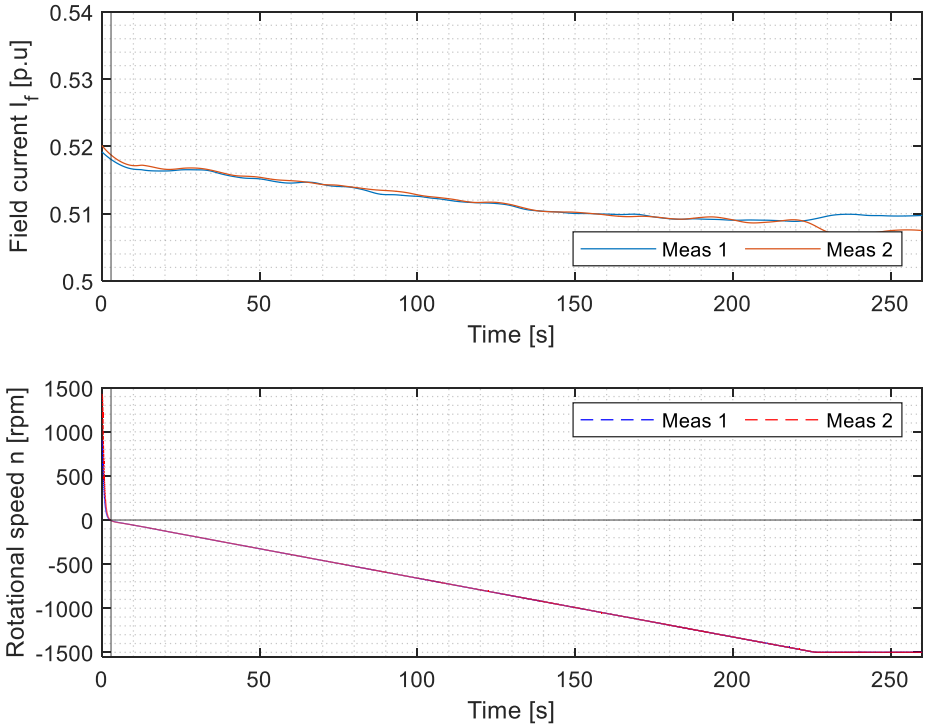

Figure 5.22 Behaviour of the field current with flux control with constant slip frequency, as the main machine accelerates and field current reference is 0.5 p.u. The waveforms of two measurements are presented. Black line marks the time instant when zero speed is reached. The rotational speed is negative because the rotor is rotating at different direction than the stator field of exciter machine.

Table 5-14 The results from the accuracy test of flux control with constant slip frequency with field current reference 0.5 p.u. The test was done twice. From both measurements actual field current in p.u values has been presented as well as error to the reference.

	Measurement 1		Measurement 2	
Ref [p.u]	0.5		0.5	
Speed [rpm]	Actual [p.u]	Error [%]	Actual [p.u]	Error [%]
0	0.518	-3.63	0.519	-3.76
250	0.516	-3.16	0.516	-3.20
500	0.514	-2.80	0.514	-2.83
750	0.512	-2.35	0.512	-2.38
1000	0.510	-2.00	0.510	-2.03
1250	0.509	-1.84	0.509	-1.87
1500	0.509	-1.83	0.508	-1.61

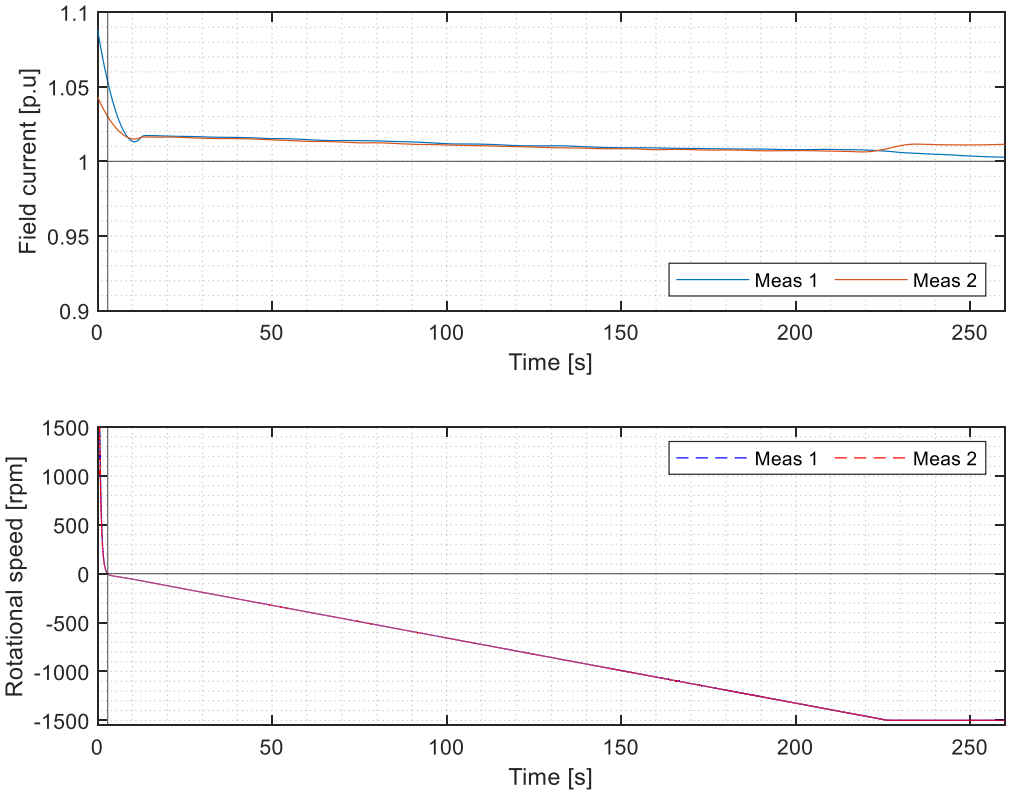

Figure 5.23 Behaviour of the field current with flux control with constant slip frequency, as the main machine accelerates and field current reference is 1 p.u. The waveforms of two measurements are presented. Black line marks the time instant when zero speed is reached. The rotational speed is negative because the rotor is rotating at different direction than the stator field of exciter machine.

Table 5-15 The results from the accuracy test of flux control with constant slip frequency with field current reference 1 p.u. The test was done twice. From both measurements, actual field current in p.u values is presented as well as error to the reference value.

	Measurement 1		Measurement 2	
Ref [p.u]	1		1	
Speed [rpm]	Actual [p.u]	Error [%]	Actual [p.u]	Error [%]
0	1.054	-5.35	1.030	-3.01
250	1.016	-1.61	1.015	-1.53
500	1.014	-1.39	1.012	-1.24
750	1.011	-1.13	1.010	-1.03
1000	1.009	-0.91	1.008	-0.85
1250	1.008	-0.83	1.007	-0.72
1500	1.005	-0.54	1.012	-1.16

5.4.4. Summary from algorithm testing

The observations and key results from the laboratory measurements can be summarised as follows:

- The flux control method of asynchronous exciter can provide stable and fast response time for brushless direct online synchronous motor. The fastest rise time achieved in this study was around 111 ms and the average was 145 ms, which are notable faster than the requirement of 0.2 seconds.

- Measurements performed do not indicate which control method is the most beneficial. When the slip frequency is controlled, the major benefit is the supply capability at zero speed. Both control methods were accurate and the error was generally under 5 %.

- The accuracy of the current control could be improved by including the effect of actual slip and supply frequency values to the current reference

- If the supply frequency of the constant frequency method is increased, the accuracy at zero speed should improve. The accuracy and ability to supply field current at zero speed can also be improved by giving ACS880 higher flux reference at zero speed.

- The major disadvantage of the constant slip frequency control method is that it requires speed feedback from pulse encoder which exposes the system to malfunction due loss of feedback signal due error or damaging of the encoder module.

- The actual synchronous machine is controlled by higher level automation system and it would probably make the minor accuracy differences between these control methods negligible.

6. SUMMARY AND FINAL CONCLUSION

The control of the direct online brushless synchronous motor field current was studied and evaluated in the context of starting it with the load commutating inverter. Two different control methods were successfully implemented to ACS880 frequency converter:

1. Flux control with constant supply frequency
2. Flux control with constant slip frequency.

Concepts were verified in small scale test set-up to be suitable for the intended application. Both control methods were stable and able to follow the field current references accurately. The flux control method was able to comply with the specified dynamical requirements. The most beneficial control method was not determined because it should be considered with application specific requirements at hand.

The use of simulation as an approach to the evaluate performance of different control systems with asynchronous exciter was partly successful and similar trends were gathered from the acceleration simulations and measurements. The intent of using the simulation model in the step response test turned out to be unsuccessful because of the shortcomings of the machine model.

As a further action the concept should be tested in real scale and control software could be developed more to include estimator which corrects the effects of slip frequency in the current control loop. Also, the effect of inner control loops of the ACS880 could be studied to gather information whether there are some factors which have a negative effect on the performance of the system.

The simulation model should be developed so that it works more accurately with dynamical simulations. Preferably the new machine model would be constructed so that whole model is more detailed, perhaps in the same kind of manner as was done by Ruuskanen et al. (2008). In this way more parameters can be defined and error, based on the how model calculates, can be more accurately evaluated and managed.

REFERENCES

ABB 2012, “ABB industrial drives, Firmware manual ACS880 primary control program.”. [Online]. [Accessed 3 April 2021]. Available at: https://library.e.abb.com/public/6b0e2b9eba86e68bc1257b0c0053dab2/EN_ACS880_FW_Man_C.pdf

ABB 2017, “Synchronized bypass unit Engineering Guideline” ABB special purpose drives Synchronized bypass unit. [Internal document]

ABB 2019, “ABB INDUSTRIAL DRIVES, Drive application programming (IEC 61131-3) Programming manual.”. [Online]. [Accessed 3 April 2021]. Available at: https://library.e.abb.com/public/4c933ef3c3494fea85597cdeb8ebc031/EN_Drive_application_PM_F.pdf

ABB 2020, “UNITROL 1020 User Manual.”. [Online]. [Accessed 2 March 2021]. [Limited access document]

ABB 2021, Memo from meeting at 9.2.2021 with Liukkonen O., Kivioja J. P, Karttunen S., Ketola P & Holopainen A. [Internal document]

ABB a2021, Memo from meeting at 1.3.2021 with Liukkonen O., Westerlund J., Janhunen T. Rauhala T., Ketola P., Niemelä M. & Holopainen A. [Internal document]

ABB b2021, Memo from meeting at 12.5.2021 with Ketola P., Liukkonen O., Seppälä P. & Holopainen A. [Internal document]

Ahonen, T. Potinkara, A. & Tahvainenen, A. 2013 “Saimaa follow-up Project: Brushless Excitation with Slip Ring Motor”. [Internal document]

ANS/NEMA MG 1-2016, *Motors and generators*, Rosslyn, Virginia, USA: National Electrical Manufacturers Association, 2018.

API 546, *Brushless Synchronous Machines 500 kVA and Larger*, 3. edition, Washington, DC, USA: American Petroleum Institute, 2008.

Arnsten E., Lindström J. & Tervaskanto J. 2018. ” Motor Control Panels for ABB Synchronous Motors”, ABB Large Motors and generators. [Internal document]

Aura, L. & Tonteri, A. J. 1986. Sähkömiehen käsikirja, osa 2: Sähkökoneet. Porvoo: WSOY. 373 s. ISBN 951-0-13479-1

Berry, P. J. & Hamdi, E. S. 2015. "An investigation into damper winding failure in a large synchronous motor" *2015 50th International Universities Power Engineering Conference (UPEC)*. pp. 1-4, doi: 10.1109/UPEC.2015.7339924.

Eichenberg, J.P., Hennenfent, H. & Liljestrand, L. 1998. "Multiple re-strikes phenomenon when using vacuum circuit breakers to start refiner motors" *Conference Record of 1998 Annual Pulp and Paper Industry Technical Conference (Cat. No.98CH36219)*, pp. 266–273. doi 10.1109/PAPCON.1998.685530

Fingrid 2018, "Grid Code Specifications for Power Generating Facilities VJV2018" [Online]. [Accessed 5 March 2021]. Available at: https://www.fingrid.fi/globalassets/dokumentit/en/customers/grid-connection/grid-code-specifications-for-power-generating-facilities-vjv2018-.pdf

IEC 60034-1, *Rotating electrical machines – Part 1: Rating and performance*., 13.0 edition, Geneva, Switzerland International Electrotechnical Commission, 2017.

IEC 60034-3, *Rotating electrical machines –Part 3: Specific requirements for synchronous generators driven by steam turbines or combustion gas turbines and for synchronous compensators*., 7.0 edition, Geneva, Switzerland International Electrotechnical Commission, 2020.

IEC 60034-16-1, *Rotating electrical machines – Part 16-1: Excitation systems for synchronous machines – Definitions*, 2.0 edition, Geneva, Switzerland International Electrotechnical Commission, 2011.

Ilic, I., Viskovic, A. & Vrazic, M. 2011. "User P-Q diagram as a tool in reactive power trade," 2011 8th International Conference on the European Energy Market (EEM), 2011, pp. 580-584, doi: 10.1109/EEM.2011.5953078.

Kjaer, P. C., Kjellqvist, T. & Delaloye, C. 2005. "Estimation of field current in vector-controlled synchronous machine variable-speed drives employing brushless asynchronous exciters" *IEEE Transactions on Industry Applications.*, vol. 41, No, 3, pp. 843–840. doi 10.1109/TIA.2005.847290

LeDoux, K., Visser, P.W., Hulin, J.D. & Nguyen, H. 2015. “Starting Large Synchronous Motors in Weak Power Systems” *IEEE Transactions on Industry Applications.*, vol. 51, No, 3, pp. 2676–2682. doi 10.1109/TIA.2014.2373820

Luomi, J. 1982. Sähkökoneiden muutosilmiöt. Espoo: Otakustantamo. 206 s. ISBN 951-671-319-x

Nevelsteen, J. & Aragon, H. 1989. “Starting of large motors-methods and economics” *IEEE Transactions on Industry Applications.*, vol. 25, No, 6, pp. 1012–1018. doi 10.1109/28.44236

Jatskevich, J., Pekarek, S. D. & Davoudi, A. 2006. “Parametric average-value model of synchronous machine-rectifier systems” *IEEE Transactions on Energy Conversion*, vol. 21, No, 1, pp. 9–18. doi 10.1109/TEC.2005.847974

Jiao, N., Liu, W., Zhang, Z., Meng, T., Peng, J. & Jiang, Y. 2017. “Field Current Estimation for Wound-Rotor Synchronous Starter–Generator With Asynchronous Brushless Exciters” *IEEE Transactions on Energy Conversion.*, vol. 32, No, 4, pp. 1554–1561. doi 10.1109/TEC.2017.2698599

Nøland, J. K., Giset, M., & Alves, E.F. 2018. *“Continuous Evolution and Modern Approaches of Excitation Systems for Synchronous Machines” 2018 XIII International Conference on Electrical Machines (ICEM)*, pp. 104–110. doi 10.1109/ICELMACH.2018.8507212

Nøland, J. K., Nuzzo, S., Tessarolo, A. & Alves, E. F. 2019. “Excitation System Technologies for Wound-Field Synchronous Machines: Survey of Solutions and Evolving Trends” *IEEE Access.*, vol. 7, pp. 109699–109718. doi 10.1109/ACCESS.2019.2933493

Platero, C. A., Blázquez, F., Rebollo, E., Blánquez, F. R., Martínez, J. A. & Redondo, M. 2015. “Enhancement of a high speed de-excitation system for brushless synchronous machines by large blocking voltage semiconductors” *2015 IEEE 10th International Symposium on Diagnostics for Electrical Machines, Power Electronics and Drives (SDEMPED)*, pp. 50–55. doi 10.1109/DEMPED.2015.7303668

Pyrhönen, J., Hrabovcová, V. & Semken, R.S. 2016. *Electrical machine drives control: An introduction.* Wiley & Sons Ltd. 504 p. ISBN 978-1-119-26045-5

Pyrhönen, J., Jokinen, T. & Hrabovcová, V. 2014. *Design of rotating electrical machines.* 2nd ed. Wiley & Sons Ltd. 584 p. ISBN 978-1-118-58157-5

E. A. Qasmi, W. Sun, J. Soomro, M. U. Tahir & F. A. Chachar, 2019 "Power Quality Analysis of Phase Controlled Bidirectional and Unidirectional AC Voltage Controllers and their impacts on input power system," 2019 2nd International Conference on Computing, Mathematics and Engineering Technologies (iCoMET), pp. 1-6, doi: 10.1109/ICOMET.2019.8673424.

Ritter, C., Kobi, H. & Morf, P. 2007, "Utilization of Soft-Starter VDF in Reciprocating Compressor A." *5th Conference of the EFRC* [Online]. [Accessed 6 February 2021]. Available at https://library.e.abb.com/public/d72037470e4b0924c12572b4003d3d62/Utilization%20of%20Soft-Starter%20VFD%20in%20Reciprocating%20Compressor%20Applications_EFRC07.pdf

Ristanovic, D., Taher, M., Getschmann, T. & Bhatia, N. 2020. "Large Synchronous Motors as Drivers for Centrifugal Compressors in LNG Liquefaction Plants" *IEEE Transactions on Industry Applications.*, vol. 56, No, 6, pp. 6083–6093. doi 10.1109/TIA.2020.3012616

Jiao, N., Liu, W., Meng, T., Peng, J. & Mao, S. 2017. "Detailed Excitation Control Methods for Two-Phase Brushless Exciter of the Wound-Rotor Synchronous Starter/Generator in the Starting Mode" *IEEE Transactions on Industry Applications.*, vol. 53, No, 1, pp. 115–123. doi 10.1109/TIA.2016.2607149

Jiao, N., Liu, W., Meng, T., Sun, C. & Jiang, Y. 2019. "Decoupling start control method for aircraft wound-rotor synchronous starter-generator based on main field current estimation" *IET Electronic power applications.*, vol. 13, No, 7, pp. 863–870. doi 10.1049/iet-epa.2018.5140

Tervaskanto, J. 2018. *"ABB Motor control panel: 300-series". Technical description.* ABB Oy. [Internal document]

Trzynadlowski, A. M. 2016. *Introduction to modern power electronics.* 3rd edition. Wiley & Sons Ltd. 452 p. ISBN 978-1-119-00321-2

Rashid, M. H. 2018. “Power Electronics Handbook (4th Edition) - 14.3.1 Phase-Controlled Three-Phase AC Voltage Controllers”. Elsevier. [Online] [Accessed February 2021] Retrieved from https://app.knovel.com/hotlink/pdf/id:kt00CXCY95/power-electronics-handbook/phase-controlled-three

Ruuskanen, V., Niemelä, M., Pyrhönen, J., Kanerva, S. & Kaukanen, J. 2009. “Modelling the brushless excitation system for a synchronous machine” *IET Electronic power applications.*, vol. 3, No, 3, pp. 231–239. doi: 10.1049/iet-epa.2008.0079

Shell 2007, *Technical specification synchronous ac machines (amendments/supplements to IEC 60034-1 and IEC 60034-14) – Design and engineering practice*, DEP 33.65.11.31-Gen.

Steigerwald, R. L. & Lipo, T. A. 1974. “Analysis of a Novel Forced-Commutation Starting Scheme for a Load-Commutated Synchronous Motor Drive” *IEEE Transactions on Industry Applications.*, vol. IA-15, No, 1, pp. 14–24. doi 10.1109/TIA.1979.4503608

Stemmler, H. 1994. “High-power industrial drives” *Proceedings of the IEEE.*, vol. 82, No, 8, pp. 1266–1286. doi 10.1109/5.301688

Zhang, Z., Liu, W., Mao, S., Peng, J., Sun, C., Meng, T. & Jiao, N. 2017. “Research on excitation control method for the three-phase brushless asynchronous excitation system of wound-field synchronous starter/generators” *2017 IEEE Energy Conversion Congress and Exposition (ECCE).*, pp. 2074-2078. doi 10.1109/ECCE.2017.8096413

Zhang, Z., Liu, W., Zhao, D., Mao, S., Meng, T. & Jiao, N. 2016. “Steady-state performance evaluations of three-phase brushless asynchronous excitation system for aircraft starter/generator” *IET Electronic power applications.*, vol. 10, No, 8, pp. 788–798. doi 10.1049/iet-epa.2016.0077

APPENDIX I. Machine nameplates

APPENDIX II. Simulink® block parameters.

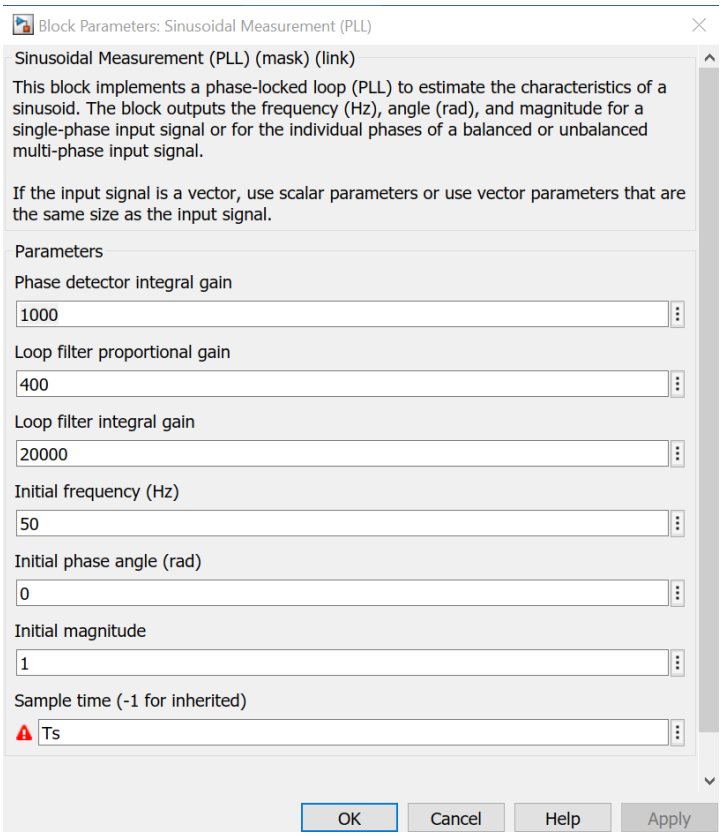

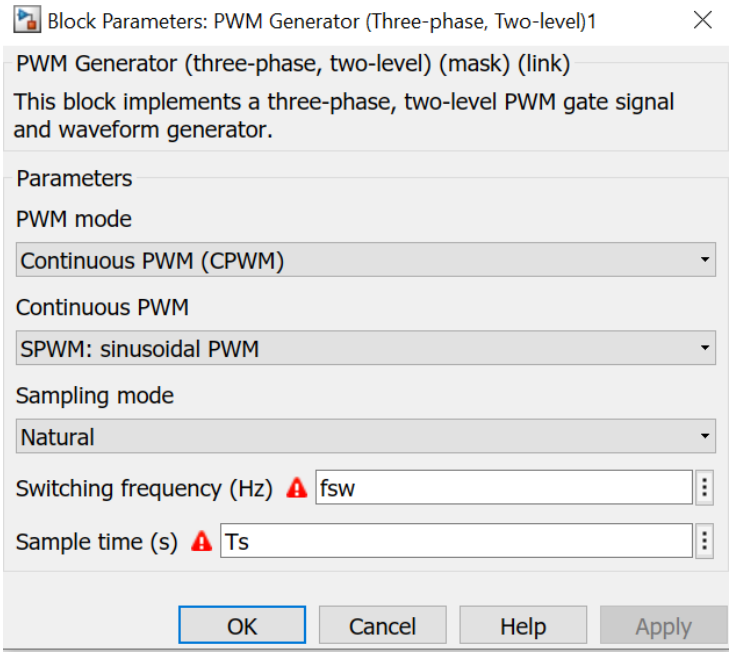

APPENDIX III. List of laboratory equipment and software used

Laboratory equipment	Additional information
Yokogawa DL850	-
Fluke 80i-110s AC/DC current probe	Rotor current AC
Fluke i30s AC/DC current clamp	DC current
Yokogawa 700929 Isolated passive probe 1000V/100MHz	Rotor voltage AC
Yokogawa 700929 Isolated passive probe 1000V/100MHz	DC voltage
AC500 PM583 PLC	V2 CPU
CM579-ETHCAT	-
FECA-01 EtherCAT adapter module	REV.
Leine & Linde encoder RHI 503	4096 ppr (TTL)
FEN-11 absolute encoder interface module	TTL IN
ABB ACS880-01-017A-3 (SR machine)	Optional licenses k473 + N7502 + N8010 Firmware: AINFC v.2.72.
ABB ACS880-11-025A-3 (Siemens induction machine)	

Software	
ABB Automation builder	Version 2.1 (Premium licence)
Drive composer pro	Version 2.2
Codesys	Version 2.3.9.55

APPENDIX IV. Rise time and time constant example

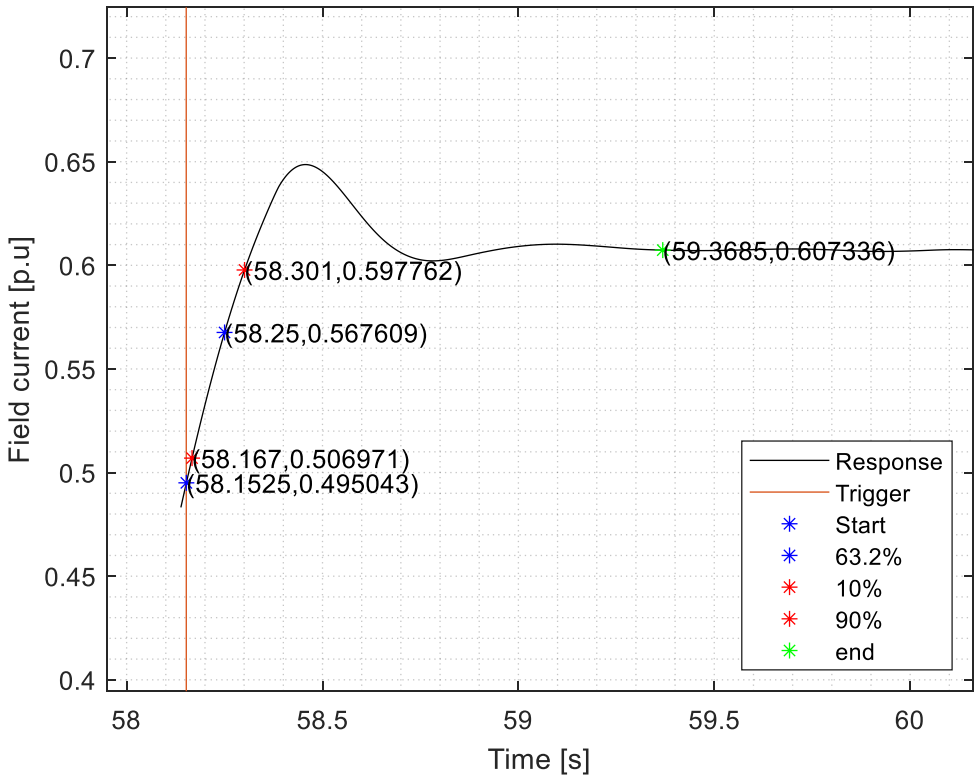

Figure 1 Step response from test 3, when parameter LimitHigh is 1.5. Time instances that are used to calculate the rise time and time constant.

Time constant:

$$\tau'_{\mathrm{d0}} = t_{63.2\%} - t_{start} = 58.25\ s - 58.1525\ s = 97.5\ ms$$

Rise time:

$$Rise\ time = t_{90\,\%} - t_{10\,\%} = 58.301\ s - 58.167\ s = 134\ ms$$

APPENDIX V. Acceleration test 1 p.u, flux control with constant frequency.

The acceleration test performed in the section 5.4.2 showed that the flux reference at zero speed is limited. The same test was repeated and parameter LimitHigh was set to 10, to study if limiting the flux reference has an impact to the capability to supply field current at zero speed. The field current waveform from that measurement is presented in figure 2. The current waveform is almost identical to the waveform presented in section 5.4.2. Table 1 shows that the error at zero speed was reduced.

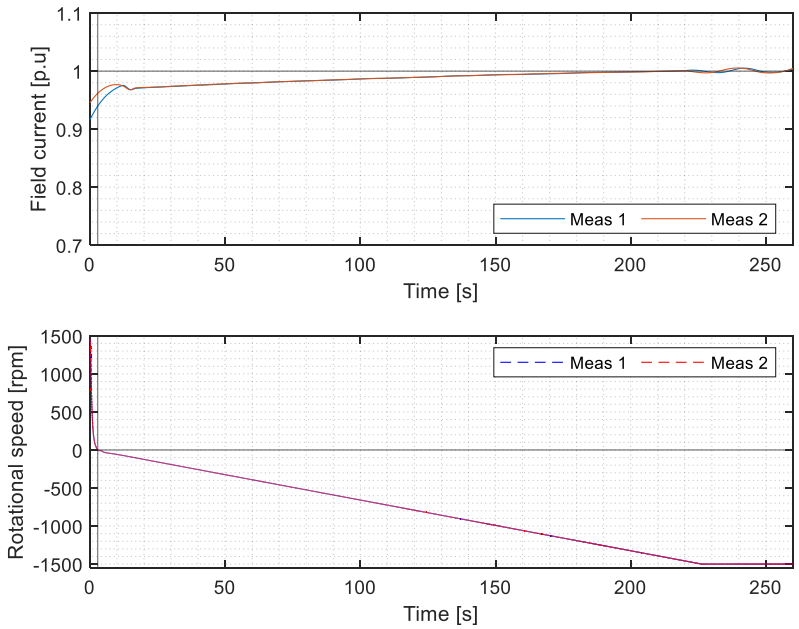

Figure 2 Behaviour of the field current when rotor accelerates, and LimitHigh is 10.

Table 1 Actual field current values and error compared to the reference, when LimitHigh was set 10.

	Measurement 1		Measurement 2	
Ref [p.u]	1		1	
Speed [rpm]	Actual [p.u]	Error [%]	Actual [p.u]	Error [%]
0	0.939	6.05	0.962	3.83
250	0.976	2.45	0.976	2.43
500	0.983	1.74	0.983	1.73
750	0.988	1.18	0.988	1.17
1000	0.994	0.64	0.994	0.60
1250	0.998	0.21	0.998	0.24
1500	0.999	0.06	0.997	0.30

Figure 3 clearly shows that the reduction in the error at zero speed comes from the ability to supply more stator current to the asynchronous exciter.

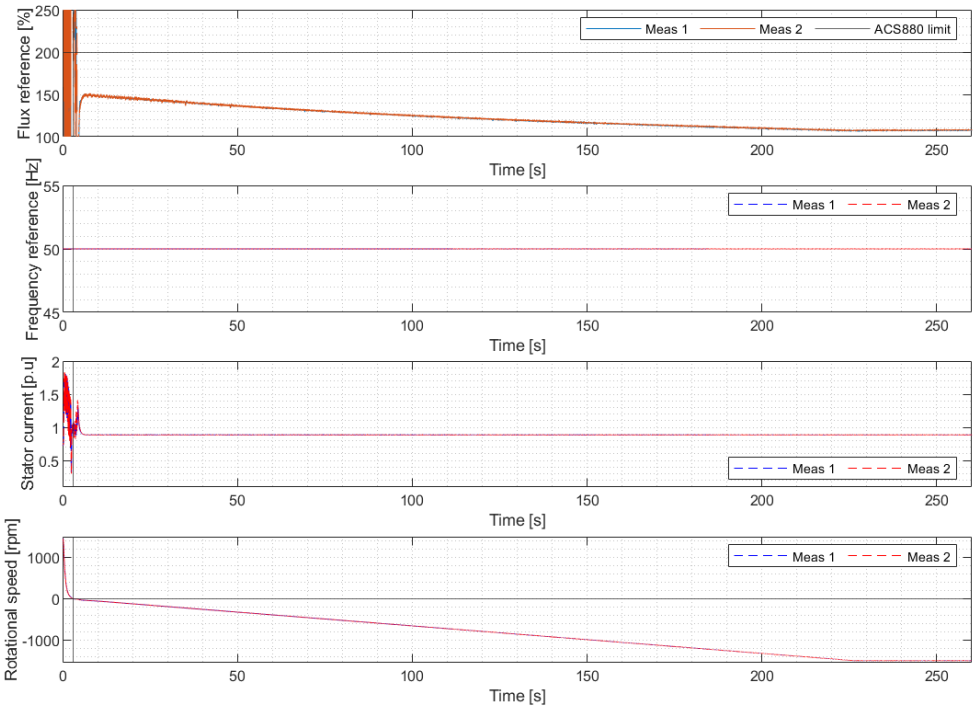

Figure 3 The flux reference, supply frequency and stator current during the acceleration. The field current reference during acceleration was 1 p.u and frequency reference was 50 Hz. Black line marks the time when rotational speed is zero.

APPENDIX VI. Current transformation ratio

The current transformation ratio was determined by measuring the field current and stator current of the slip ring machine at different flux references given to the ACS880. Table 2 contains the results of these measurements. During measurement, the slip ring machine was rotated 1500 rpm in opposite direction than its stator field.

Table 2 Field and stator currents at different flux references when shaft is rotated at 1500 rpm in opposite direction than the field of the asynchronous exciter.

Flux reference [%]	Field current If [A]	Stator current Is [A]	If/Is
10	0.9	0.43	2.09
20	1.9	0.81	2.35
30	2.99	1.2	2.49
40	3.9	1.58	2.47
50	5	1.97	2.54
60	6	2.37	2.53
70	7.1	2.77	2.56
80	8.1	3.168	2.56
90	9.1	3.55	2.56
100	10.2	3.93	2.60
		AVG.	2.47

The current transformation ratio at different measurement points was calculated by dividing field current with stator current. Average was taken from all the measurement points and used as a current transformation ratio. The current transformation ratio was then tested and adjusted to give nominal field current at 1500 rpm and 100% flux reference. In this thesis final value was 2.58.